Nanomaterials

Mechanics and Mechanisms

K.T. Ramesh

Springer

Nanomaterials
Mechanics and Mechanisms

K.T. Ramesh

Nanomaterials

Mechanics and Mechanisms

Springer

K.T. Ramesh
The Johns Hopkins University
Baltimore, MD 21218
USA
ramesh@jhu.edu

ISBN 978-0-387-09782-4 e-ISBN 978-0-387-09783-1
DOI 10.1007/978-0-387-09783-1
Springer Dordrecht Heidelberg London New York

Library of Congress Control Number: 2008942797

To Arjun, Rohan and Priti, for your love and patience.

Preface

This book grew out of my desire to understand the mechanics of nanomaterials, and to be able to rationalize in my own mind the variety of topics on which the people around me were doing research at the time.

The field of nanomaterials has been growing rapidly since the early 1990s. Initially, the field was populated mostly by researchers working in the fields of synthesis and processing. These scientists were able to make new materials much faster than the rest of us could develop ways of looking at them (or understanding them). However, a confluence of interests and capabilities in the 1990s led to the explosive growth of papers in the characterization and modeling parts of the field. That confluence came from three primary directions: the rapid growth in our ability to make nanomaterials, a relatively newfound ability to characterize the nanomaterials at the appropriate length and time scales, and the rapid growth in our ability to model nanomaterials at atomistic and molecular scales.

Simultaneously, the commercial potential of nanotechnology has become apparent to most high-technology industries, as well as to some industries that are traditionally not viewed as high-technology (such as textiles). Much of the rapid growth came through the inventions of physicists and chemists who were able to develop nanotechnology products (nanomaterials) through a dizzying array of routes, and who began to interface directly with biological entities at the nanometer scale. That growth continues unabated.

What has also become apparent is that much of the engineering community continues to view nanomaterials as curiosities rather than as the potentially game-changing products that they can be. This book seeks to provide an entré into the field for mechanical engineers, material scientists, chemical and biomedical engineers and physicists. The objective is to provide the reader with the connections needed to understand the intense activity in the area of the mechanics of nanomaterials, and to develop ways of thinking about these new materials that could be useful to both research and application.

Note that the book does not cover the areas associated with soft nanomaterials (polymer-based or biologically-derived), simply because I am not knowledgeable about such systems (and the mechanics can be quite different). This is not intended to minimize the importance of soft nanomaterials or the potential of soft nanotechnology; the reader will simply have to go elsewhere to encounter those areas.

This book is intended to be read by senior undergraduates and first-year graduate students who have some background in mathematics, mechanics and materials science. It should also be of interest to scientists from outside the traditional fields of mechanical engineering and materials science who wish to develop core expertise in this area. Although senior undergraduates should be able to read this book

from cover to cover, they may find it somewhat heavy going as a textbook. First and second year graduate students should find this book challenging but accessible.

My intent has not been to provide a review of the field but rather to provide a basic understanding. If the reader puts the book down with an appreciation of the excitement of the field of nanomaterials and the potential applications in mechanical engineering, materials science and physics, this book will have achieved its objectives. My personal objective with this book is to provide a means for integrating the discussions that currently go on in the mechanics and materials communities, and at the same time to provide an accessible path to those from outside these disciplines who wish to get involved in one of the most exciting fields of our time.

While this book is intended to be read cover to cover, it can also be used as a reference work. The book should serve effectively as a textbook for a course in nanomaterials or nanomechanics as it relates to materials. It is possible that mechanical engineers using this book will also want to have a materials science reference available as they move through this volume, and conversely, material scientists using this book may want to have a basic mechanics of solids book as a companion volume. An effective scenario would be for graduate students who have taken courses in the mechanics of solids or the mechanical properties of materials to then take a course that uses this book as a text. The suggested reading at the ends of the chapter will be useful for those who wish to pursue a particular topic in greater depth than can be covered in a book such as this.

I am aware that the book in its current form does not have enough problems at the end of each chapter to make it ideal as a textbook. However, this is a field at the cutting edge of nanotechnology, rather than an established area with standard problems that can be given to students without considering their specific backgrounds. The problems that are provided at the ends of the chapters are intended to provoke discussion and further study, rather than to provide training in specific solution methods.

We are in the midst of a veritable explosion in nanotechnology, and nanomaterials are at the heart of it. I hope you put this book down as excited about the field as I have been in the writing of it.

The Johns Hopkins University *K.T. Ramesh*
Baltimore, MD

Acknowledgements

This book developed as a result of conversations with many students and colleagues working in the area of the mechanics of nanomaterials. What began as a simple attempt to rationalize my own thinking in this area became a concept for a book after discussions with Elaine Tham, my editor at Springer. Both she and her assistant, Lauren Denahy, deserve my thanks for their patience with me as I learned how to write a large document.

My thanks go also to my assistant, Libby Starnes, who has given me a great deal of help in organizing my materials for this volume, and in rearranging my schedule to make time for this book. Her resourcefulness and ability to handle details have been terrific.

I would like to give special thanks to the several anonymous reviewers of this book. Their suggestions have greatly improved the manuscript, and I appreciate all the effort involved.

My research group has been bearing the weight of my absentmindedness as I worked on this book for nearly a year now, and I would like to express my gratitude to all of them. They have helped me immeasurably by doing the research that I get to talk about, by being willing to critique ideas, and by helping me make up for the times that I was unavailable. During the writing of this book, the research group included Dr. Shailendra Joshi, Reuben Kraft, Bhasker Paliwal, Dr. Qiuming Wei, Dr. Fenghua Zhou, Jessica Meulbroek, Emily Huskins, Sarthak Misra, Dr. Jamie Kimberley, Dr. Krishna Jonnalagadda, Dr. Buyang Cao, Cindy Byer, Rika Wright, Guangli Hu, Cyril Williams, Brian Schuster, Dr. Bin Li, Dr. Nitin Daphalapurkar and Dr. George Zhang. My thanks to all! Several students have been involved in reviewing chapters of this book, and to them my special thanks: Guangli Hu, Cindy Byer, Justin Jones; Christian Murphy made up some of the illustrations.

My colleagues at Hopkins have been a big help, explaining (patiently) to me the physical concepts in nanomaterials and nanomaterial behavior. This is an exploding field, and my knowledge of it comes almost entirely through my interactions with the faculty and students around me at Johns Hopkins. Special thanks to Evan Ma, Kevin Hemker, Bill Sharpe, Jean-Francois Molinari and Todd Hufnagel.

Finally, this book would not have been possible without the love and support of my family, who had to put up with my occasional pre-occupation, my prolonged absences, and a lack of social interaction as I wrote. They kept me sane during the difficult times, and cheerfully stepped in to help when they could. Rohan reviewed some of the chapters, and everyone has been involved with the proofreading. Arjun has been a source of good cheer throughout the process, and Priti, I could not do this without you. To my family, my love and my thanks for all that you do!

Contents

Acronyms

There are several acronyms that are commonly used in the field of nanomaterials. Some of the primary acronyms are listed here for use throughout the book.

AFM	Atomic Force Microscopy
cg	coarse-grained
CNT	Carbon NanoTubes
DDD	Discrete Dislocation Dynamics
EAM	Embedded Atom Method
FEM	Finite Element Method
LEFM	Linear Elastic Fracture Mechanics
MD	Molecular Dynamics
MFM	Magnetic Force Microscopy
MWCNT	Multi-Walled Carbon NanoTube
nc	NanoCrystalline
ns	NanoStructured
OIM	Orientation Imaging Microscopy
QC	Quasi Continuum
SEM	Scanning Electron Microscopy
STEM	Scanning Transmission Electron Microscopy
STM	Scanning Tunneling Microscopy
SWCNT	Single-Walled Carbon NanoTube
TEM	Transmission Electron Microscopy
ufg	ultra fine grained
XRD	X-Ray Diffraction

List of Figures

List of Tables

There's plenty of room at the bottom.
Richard Feynman

1 Nanomaterials

1.1 Length Scales and Nanotechnology

Nanotechnology demands the ability to control features at the nanoscale (10^{-9} m), and a variety of techniques have been developed recently that give humanity this ability. From a fundamental science perspective, issues of physics and chemistry must be addressed at these scales. Surface and boundary effects can dominate the response. Many of the classical distinctions between mechanics, materials and physics disappear in this range of length scales, and a new kind of thinking emerges that is commonly called nanoscience (sometimes humorously interpreted as "very little science"). The recent rapid development of nanoscience is the result of a new-found ability to observe and control structure at small length and time scales, coupled with the development of computational capabilities that are most effective at small scales.

It is useful to develop a physical idea of length scale, and Figure 1.1 shows the range of length scales of common interest in mechanics and biology (the latter is included because it allows one to develop a human sense of scale). Beginning at small scales, features associated with atomic radii are on the order of 1 Å (one angstrom, 10^{-10} m) in size. The atomic lattice spacing in most crystals is of the order of 3 Å. The diameter of a carbon nanotube is about 2 nm or 20 Å, and this correlates well with the diameter of a double helix of DNA (which indicates, incidentally, that the nanotube is a good approach to handling DNA). A tobacco mosaic virus is about 50 nm across (this corresponds approximately in scale with the typical radii of curvature of the tips of nanomanipulators such as AFM probes). Grains in most polycrystalline metals have sizes that range from about 1 μm to about 20 μm (grain boundary thicknesses, to the extent that they can be defined, are typically <1 nm). A number of bacteria (living organisms) are also about 1 μm in size, a reminder of the remarkable sophistication of nature. Small-scale failure processes, such as the voids developed in spallation, are typically of the order of 10 μm in separation. Many cells in eukaryotic organisms are of this size-scale. Some of the most sophisticated small devices in engineering, integrated circuit chips, are of the order of 1 cm in size (the corresponding natural "device" might be a beetle). The author arrives on the scale at about 1.8 m, while an M1A1 Abrams tank is about four times bigger. Some of

K.T. Ramesh, *Nanomaterials*, DOI 10.1007/978-0-387-09783-1_1,

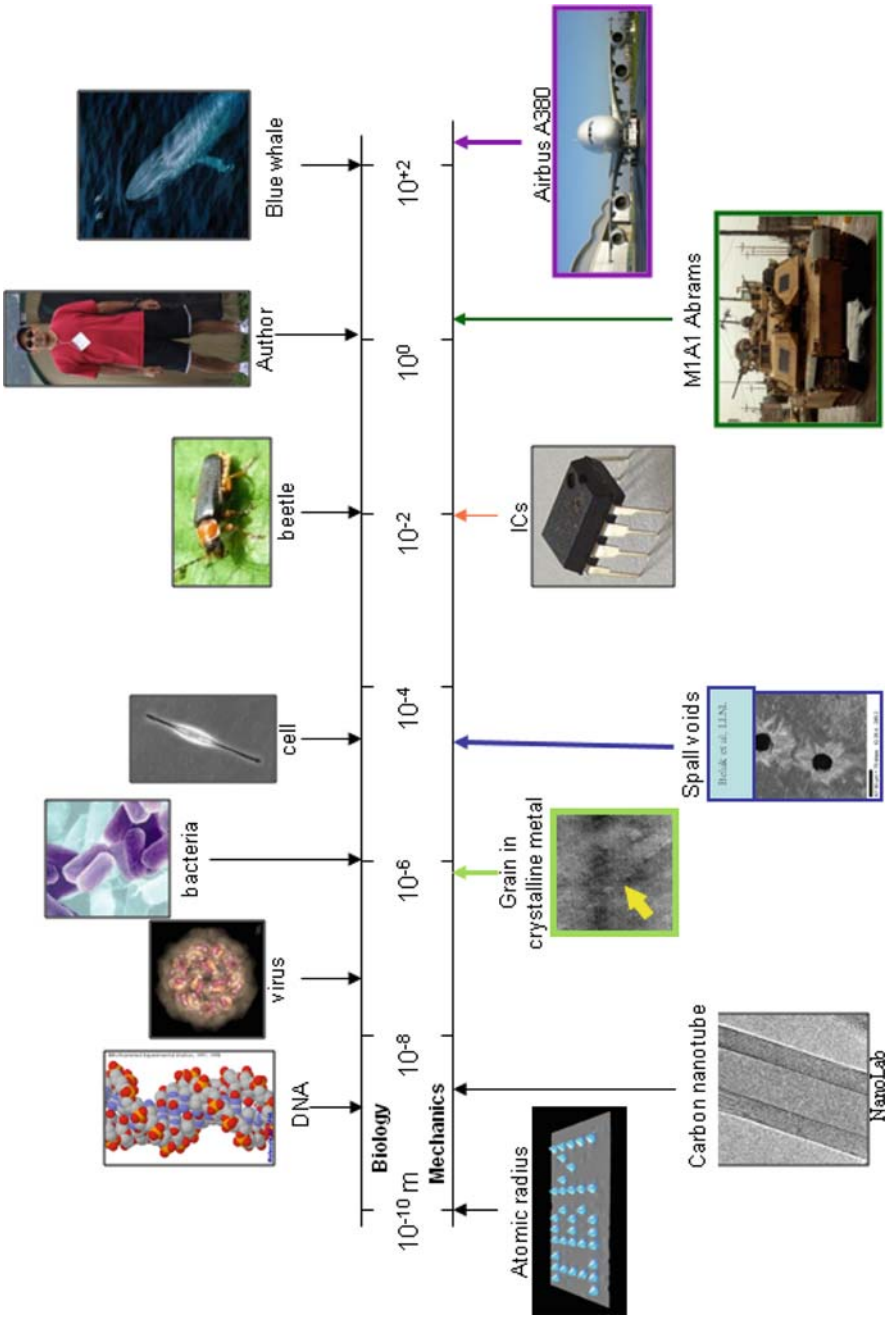

Fig. 1.1 Length scales in mechanics and materials and in nature. The topics of interest to this book cover a large part of this scale domain, but are controlled by features and phenomena at the *nm* scale. Note the sophistication of natural materials and systems at very small length scales.

the largest animals are blue whales, coming in at about 100 m, comparable in size to some aircraft. Phenomena and features at the nanoscale and microscale can dominate the behavior and performance of devices and structures in the centimeter to 100 m range. *Most of the behaviors of interest to this book arise from length scales of 0.1–100* nm*, and this will be our definition of "the nanoscale."*

One way to distinguish between nanotechnology and nanoscience is by distinguishing between what we can control and what we can understand. Most of what we interact with as humans has structure at the nanoscale, that is, there is a nanoscale substructure to most materials. Understanding what the nanoscale structure does (in terms of behavior or phenomena) is the core of nanoscience. Controlling nanoscale structure so as to achieve a desired end is the essence of nanotechnology. Nanotechnology cannot succeed without nanoscience, and the most efficient growth of nanotechnology (and growth with the smallest risk) occurs when the necessary nanoscience is already available.

The enabling science in much of nanotechnology today is the science of nanomaterials (indeed in the broadest sense, nanotechnology would not be possible without nanomaterials). From a disciplinary viewpoint, most nanoscale phenomena are either controlled or modulated by the mechanics at the nanoscale, and so mechanics plays a critical role in nanoscience. Nanomechanics controls phenomena as immediately obvious as the interaction of interfaces between nanosize crystals and as subtle as the folding of proteins (controlling and organizing the living cell). The mechanics of nanomaterials is therefore the focus of this book.

1.2 What are Nanomaterials?

A nanomaterial is a material where some controllable relevant dimension is of the order of 100 nm or less. The simple presence of nanoscale structure alone is not sufficient to define a nanomaterial, since most if not all materials have structure in this range. The ability to *control* the structure at this scale is essential. One could argue, in this sense, that many of the classical alloys and structural materials that contained nanoscale components by design (e.g., Oxide-Dispersion-Strengthened or ODS alloys) could be called nanomaterials. Conventionally, however, the modern usage of the term does not include the classical structural materials. In modern usage, nanomaterials are newly developed materials where the nanoscale structure that is being controlled has a dominant effect on the desired behavior of the material or device.

There are three different classes of nanomaterials: discrete nanomaterials, nanoscale device materials, and bulk nanomaterials. Discrete nanomaterials or *dn* materials are material elements that are freestanding and 1–10 nm in scale in at least one dimension (examples include nanoparticles and nanofibers such as carbon nanotubes). Nanoscale device materials or *nd* materials are nanoscale material elements that are contained within devices, usually as thin films (an example of an *nd* material would be the thin film of metal oxide used within some semiconductor fabrication).

Table 1.1 A broad classification of nanomaterials on the basis of dimensionality and morphology.

Type of nanomaterial	Dimensionality	Morphology	Characteristics	Remarks
Discrete nano (dn) materials	0D or 1D	Particles, fibers	Large surface functionalization	Potential health hazard
Nanoscale device (nd) materials	Usually 2D, occasionally 1D	Thin films, sometimes wires	Functionalization, electrical/thermal characteristics	Semiconductor fabrication
Bulk (nc or ns) nanomaterials	3D	Minimum mm^3	Mechanical and structural applications	May be built up from dn and nd materials

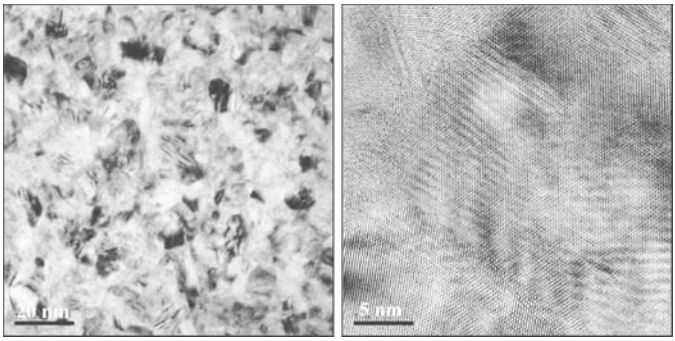

(a) (b)

Fig. 1.2 Transmission electron micrographs (see Chapter 3) of nanocrystalline nickel material produced by electrodeposition (Integran). (a) Conventional TEM micrograph showing the grain structure. The average grain size is about 20 nm. (b) High resolution electron microscopy image of the same material. Note that there is no additional or amorphous phase at the grain boundaries, although many models in the literature postulate the existence of such a phase. Micrographs by Qiuming Wei. Reprinted from Applied Physics Letters, 81(7): 1240–1242, 2002. Q. Wei, D. Jia, K.T. Ramesh and E. Ma, Evolution and microstructure of shear bands in nanostructured fe. With permission from American Institute of Physics.

Bulk nanomaterials are materials that are available in bulk quantities (defined here as at least mm^3 volumes) and yet have structure controlled at the nanoscale. Bulk nanomaterials may be built up of discrete nanomaterials or nanoscale device materials (for example one may construct a bulk nanomaterial that contains a large number of nanofibers). It is possible to view this classification approach (Table 1.1) in a mathematical light: discrete nanomaterials are either zero-dimensional (particles) or one-dimensional (fibers), nanoscale device materials are typically two-dimensional (thin films), and bulk nanomaterials are three-dimensional.

The vast majority of materials are polycrystalline, that is, they are made up of many crystals (which are also called grains within the materials community). Most conventional engineering materials have grain sizes of 10–100 μm. In this regard, we distinguish between two subclasses of bulk nanomaterials: nanocrystalline materials (*nc* materials) with crystal or grain sizes that are <100 nm, and nanostructured materials (*ns* materials) with mixtures of nanoscale and conventional crystal sizes. An example of a nanocrystalline material is shown in Figure 1.2. Polycrystalline materials with grain sizes between 100 nm and 1 μm are conventionally called ultrafine-grained or *ufg* materials. Note that some of the literature includes the range between 100 nm and 500 nm in the "nanocrystalline" domain.

1.3 Classes of Materials

There are three basic classes of materials categorized on the basis of atomic bond type and molecular structure: metals, ceramics and polymers. The character of polymers is typically determined by the interactions of large numbers of long-chain

molecules (typically more than 100 nm long). There are several discrete nanomaterials and nanostructured materials based on polymers, including microspheres and microballoons (hollow spheres), and some two-dimensional structures (such as lamellae) that can be used to build three-dimensional bulk nanostructured materials. Some composites consisting of a polymer matrix with clay nanoparticles or carbon nanotubes as reinforcements are also considered to be bulk nanomaterials. This book does not examine soft nanomaterials in any detail, simply because the author is not knowledgeable about the field. The book focuses on nanomaterials that are either metals or ceramics or composites of these two.

1.4 Making Nanomaterials

The ways in which nano materials are made vary widely, and there is not enough room in this book to discuss all of them. On the other hand, it is important to understand some features of the processes used in the synthesis of nanomaterials, because the processing route often dominates the behavior of any given material. The focus here is on processing issues in nanomaterials, rather than on the broader issues associated with processing nanotechnology – in particular, issues related to nanobiotechnology are ignored in this discussion.

The fundamental issue associated with the making of nanomaterials is that one is trying to *control* the structure of a material at a very fine scale. Stated differently, one is trying to introduce order into the material at a very fine scale (or equivalently, trying to reduce the entropy density all over this material). This attempt to reduce the local entropy density has two direct consequences. First, such processes will require a significant amount of energy and therefore may incur significant expense. Second, the material that is generated is often thermodynamically unstable, and may attempt to revert to a higher entropy state (for example through growth of features that were initially nanoscale). Some of the more creative processing techniques use this fact to their advantage: they begin by generating extremely disordered states, which on equilibration generate the desired nanostructured state.

In a broad sense, the approaches used to make materials can be put into two categories: *top-down* approaches, in which one begins with a bulk material that is then processed to make a nanomaterial, and *bottom-up* approaches, in which the nanomaterial is built up from finer scales (in the limit, building the nanomaterial up one atom at a time). It is evident that bottom-up approaches require control of processes at very fine scales, but this is not as difficult as it sounds, since chemical reactions essentially occur molecule by molecule (indeed, the nanomaterials made by nature are *grown* through bottom-up approaches).

1.4.1 Making dn *Materials*

The processes required to generate discrete nanomaterials are usually quite distinct from the processes required to generate bulk nanomaterials. Many bulk nanoma-

terials are created from *dn* materials using a second processing step (such bulk nanomaterials are said to have been created using a *two-step* process). Discrete nanomaterials themselves are often made using bottom-up approaches, sometimes relying on *self-assembly* to generate the desired nanoparticles or nanofibers. Under some conditions, a properly tuned bottom-up process (such as condensation from a vapor) can be used to generate significant quantities of discrete nanomaterials such as nanopowders. The majority of processing routes for *dn* materials rely on controlling the nucleation and growth process, since nucleation dominated processes tend to generate small sizes. Thus, one might nucleate nanoparticles by condensation from a vapor or precipitation from solution, and then intervene to control the growth of the particles, resulting in nanoparticles. Some of the typical approaches to creating discrete nanomaterials include:

- Condensation from a vapor phase (Birringer et al., 1984)
- Precipitation from solution (Meulenkamp, 1998)
- Chemical vapor deposition (Ren et al., 1998)
- Chemical reactions, particularly reduction or oxidation (Brust et al., 1994)
- Processes used to generate colloidal phases (Ahmadi et al., 1996)
- Self-assembly using surfaces (Li et al., 1999)
- Mechanical attrition (Nicoara et al., 1997)

A very large number of processes are used to generate discrete nanomaterials, using technologies borrowed from a variety of fields. Sometimes nanoparticles and nanotubes are byproducts of reactions that are already industrially relevant, and the usefulness of these byproducts has only recently been recognized. The characterization and transport of these dn materials are major issues in the development of nanotechnology. The definitive characterization of nanoparticle size and size distribution may require expensive high-resolution electron microscopy, and optical and X-ray techniques that obtain a reasonable measurement of the average size of nanoparticles over reasonably large volumes are of industrial interest.

1.4.2 Health Risks Associated with Nanoparticles

There is very little data on the interaction of nanoparticles with biological systems and the environment. Particles with nanoscale dimensions can easily pass through biological systems, and may accumulate in undesirable locations within cells, and so there are potential health risks associated with nanoparticles. Scientific study of these effects is only just beginning in the early twenty-first century, on two fronts: the potential health risks, and the potential use of nanoparticles for clinical treatments. Given the lack of data and the ease with which nanoparticles can be redistributed in the environment given their small sizes, it is wise to take precautions in handling nanoparticles. Industrial operations with nanoparticles should consider such particles to be a potential hazard, and develop handling protocols that are consistent with potential hazards. Bulk nanomaterials (fully dense nanomaterials) are

not likely to be a danger in themselves, but note that some nanoparticles may be generated during the fracture or failure of such materials.

1.4.3 Making Bulk Nanomaterials

There are two basic approaches to the production of bulk nanomaterials, commonly referred to as the bottom-up and top-down approaches. In bottom-up approaches, the material is built up one atom, molecule, particle or layer at a time, with the focus on precise control at this scale. While materials made in this way can have very clean microstructures, the approach is inherently expensive and is generally not suitable for making large quantities of material. In top-down approaches, on the other hand, the nanomaterial is made by the application of macroscale processes, with the nanoscale structure caused to develop afterwards. Such approaches generally do not generate a high-quality material, but are relatively inexpensive. There are also some approaches that defy such broad categorization.

1.4.3.1 Deposition Techniques

Deposition techniques used to generate nanocrystalline materials include electrodeposition (Elsherik and Erb, 1995), chemical (Bhattacharyya et al., 2001) and physical (Musil and Vlcek, 1998) vapor deposition (CVD and PVD), and a variety of techniques associated with semiconductor fabrication. These are typically slow processes used for the development of relatively thin films of material, with the best control of microstructure usually obtained if the film thickness is less than 1 μm (although some commercial electrodeposited nanocrystalline materials are now available with thicknesses up to 1 mm). These techniques are well adapted to the development of coatings, e.g., with mechanical applications in wear resistance and friction control. The major advantage of these techniques is that very precise control of the environment allows one to develop very precisely controlled microstructures, and so bulk materials produced in this way can be made in relatively reproducible fashion. Further, it is possible to generate microstructures with specific contaminants and specific doping (approaches that are particularly useful in sensor applications). Figure 1.2 shows the microstructure of a commercially developed electrodeposited nanocrystalline nickel film from Integran.

The substantial process control that is available does not, however, imply that the materials that are generated will be free of defects. The development of controlled fully dense nanocrystalline structures is not an easy task. Process optimization is expensive, and the classic business problem remains of defining a sufficiently large market to make process optimization economically viable. For most nanocrystalline materials, therefore, it remains difficult to obtain reproducible films through deposition techniques. Indeed, much of the early confusion about the properties of

nanocrystalline materials arose from the variability in material microstructures that are generated through these various processes (Agnew et al., 2000). Specific issues of concern include porosity, inhomogeneous microstructures and particularly columnar grains, and variable grain size distributions. This makes it difficult to compare the results obtained by one laboratory on a material that they have made with the results obtained by another laboratory on another nominally identical material that was made differently. As a consequence, both intensive and extensive characterization of a nanomaterial is essential if one is to understand the behavior. Intensive characterization procedures attempt to determine structure at a very fine scale, e.g., using TEM to determine local grain size. Such intensive procedures are incapable of providing information over large volumes. Extensive characterization procedures seek to determine the degree of variation of a structural feature (such as the grain size) with location over a larger length scale. Such procedures are usually incapable of resolving detail at the same fine scales as intensive procedures. We discuss some possible characterization procedures in chapter 3.

Deposition techniques such as those discussed in this section are typically only capable of making films of material. Thin films are the most common products, although the use of multiple layers may allow one to build up thicker two-dimensional structures, and occasionally up to the "bulk" mm thickness. These techniques, particularly those that have been optimized for semiconductor fabrication, have tremendous potential for making nanomaterials for applications within devices, i.e., *nd* materials. Since such devices represent a large fraction of the current commercial value of nanotechnology, these techniques have much to offer the nanotechnologist. The optimization of semiconductor fabrication processes for volume and cost allows one to develop relatively large films in terms of surface area, and thus the potential for volume production should not be minimized.

1.4.3.2 Consolidation of *dn* Materials

The second major approach to making bulk nanomaterials relies on the already well developed capacity for generating large volumes of nanoparticles or nanopowders. The idea is to take a large volume of nanoparticles and then consolidate this to generate a bulk nanomaterial. Many of the techniques used in the powder metallurgy and ceramics industries can be applied to these nanopowders – these industries have generated bulk materials from powders for decades. The primary difficulty faced in the direct application of these classical powder techniques results from the difference in powder size.

The typical steps in the consolidation of bulk materials from powders are:

1. Mixing of the powders, if necessary (it is sometimes advantageous to start with a variety of powder sizes, and different material powders might be used if a composite material is desired).
2. An initial consolidation step, typically *cold isostatic pressing* (CIPing) to generate a solid that can be handled, called a *green body*.

3. Further consolidation of the green body, either through *sintering* or *hot isostatic pressing* (HIPing) to obtain the desired density. This step usually involves a high temperature because it is usually controlled by diffusion mechanisms.
4. A *finish* machining process to remove regions of the material that have not been completely consolidated.

A variety of other steps are possible, including plastic deformation through rolling and forging, and the precise recipes used are often jealously guarded as proprietary information by laboratories and companies. The specific temperature histories and pressure histories used in a process have a major influence on the final microstructure. The relative instability of nanomaterials implies that grain growth is a major issue at high temperatures, and a compromise that must often be considered is between the desired final density and the desired final grain size.

Every group making materials by powder consolidation also appears to have a different definition of "full density," with some industries defining full density as 98% of the theoretical density (which is calculated using the known densities of the elements, compounds or phases involved and assuming no porosity). This is a major problem because the mechanical properties of the nanomaterial can be very strongly dependent on the presence of even small amounts of porosity. The properties of a material with 98% density can be very different from that of the same material with 99.5% density (particularly with regard to fracture and failure).

Part of the difficulty with density arises because the more traditional powder metals produced by the powder metallurgy industry are designed for applications where small amounts of porosity would be removed by subsequent processes such as forging, or the small porosity might even be beneficial (as in lubrication systems). Such finishing processes are often not used in the development of the nanomaterial, resulting in residual porosity. A related difficulty is that it can be very difficult to see the porosity within a nanomaterial, because unlike traditional powder processed materials the porosity might be very finely distributed as very small voids. The consequence is that lower final densities may be considered acceptable by a materials processing vendor in nanomaterials because the quality control step is not able to find significant pores.

An example of a bulk nanomaterial (nanocrystalline iron) made by the consolidation of powders is presented in Figure 1.3. First, nanostructured iron particles were generated by a mechanical attrition process: commercial iron powder with a purity of 99.9% and a range of powder sizes averaging around 5 μm was used as a starting material for ball milling. Ball milling (Malow and Koch, 1998) was conducted using a SPEX 8000 mill with a vial and balls made of stainless steel (SS440). The weight ratio of balls/powder was 4:1 and the milling time was 18 h. The vial was sealed in an argon atmosphere and cooled using a fan during milling. The powder particles after milling had internal grain sizes on the order of 10 nm (Malow and Koch, 1998) as revealed by X-ray diffraction line broadening. A two-step consolidation procedure was used to form bulk nanocrystalline iron with the desired grain size. In the first step, the powder was compacted at a pressure of 1.4 GPa at room temperature for about 10 h using a tungsten carbide (WC) die set. The resulting compact had a

Fig. 1.3 Transmission electron micrograph of nanocrystalline iron produced by consolidation of a nanocrystalline precursor made by ball milling. There is a range of grain sizes, and many of the grains show evidence of the prior plastic work produced by the ball-milling process. The width of the photograph represents 850 nm.

green density of 72–75% of the theoretical density. In the second step, the compact was transferred into a larger WC die set for hot consolidation in a hot press. A temperature of 753 K and a consolidation time of 30 min at a pressure of 850 MPa was used to obtain an average grain size of just less than 100 nm and a final density of 99.2% of the theoretical density.

One interesting feature of the nanocrystalline iron shown in this figure is that there are no visible voids in the material observable within the transmission electron microscope (TEM observations represent very small volumes), even though there must be 0.8% of porosity somewhere within the material. It is possible that the voids are very small and so not easily seen, or perhaps the porosity is eliminated by the TEM specimen preparation procedure. Another interesting feature of the nanocrystalline material shown in this figure is one that is to be expected from a consolidated material: many of the grains show evidence of the substantial prior plastic deformation involved in the consolidation process (there is extensive dislocation activity within the grains). This can make it difficult to decouple the effects of plastic deformation and the effects of the small grain size on the mechanical properties of the nanomaterial, and from a science viewpoint this can be viewed as one of the disadvantages of the consolidation process. From an engineering viewpoint, however, the consolidation process allows one to generate substantial quantities of bulk nanomaterials, and to take advantage of existing technologies in the powder metallurgy and ceramics industry. At the date of publication of this book, reproducibility of the quality of bulk nanomaterials made by the consolidation process remains a contentious issue.

1.4.3.3 Severe Plastic Deformation Processes

A variety of processing techniques for bulk nanomaterials fall under the rubric of severe plastic deformation (SPD) processes (Valiev et al., 2000; Valiev and Langdon, 2006). The primary idea in all of these is to develop very large plastic deformations within metals, with associated dislocation substructures, and then to use the processes of recovery, recrystallization and rearrangement of microstructure to develop the crystalline microstructures of interest. Recovery involves the thermally-enhanced motion of dislocations to reduce internal stresses through rearrangement and annihilation, while recrystallization involves the growth of new nearly strain-free crystals out of a collection of heavily-worked prior crystals. Large plastic deformations of metals have been known to develop patterned dislocation substructures for many years (Mughrabi, 1983), and the metalworking industry has used this extensively to their advantage. Large plastic deformations can result in dislocation structures that reorganize themselves to form cells, subgrains (regions with small angular misalignment, usually separated by dislocation walls), and eventually large angle grain boundaries (Hughes and Hansen, 1997), resulting in progressive grain refinement. The final grain size that is obtained in these processes depends strongly on the details of the thermomechanical processes involved – in general, larger strains develop finer grains, but the minimum grain size that can be obtained varies from material to material. Truly nanocrystalline grains ($\leq 100\,\text{nm}$) have been observed within the centers of adiabatic shear bands developed within some materials, and have also been developed during high-pressure torsion processes. However, most SPD processes result in ultra-fine-grain sizes in most materials.

1.4.3.4 Equal Channel Angular Processing

Equal channel angular processing or Equal Channel Angular Pressing, commonly known as ECAP, is a technique in which very large plastic deformations are developed by forcing a metal rod (the sample) through a die, with a die axis that changes direction suddenly (resulting in substantial shear deformation). Some variants of this technique are known as equal channel angular extrusion (ECAE) processes. A schematic diagram representing such a process is shown in Figure 1.4, with a hard plunger forcing a metal sample between two channels of equal size connected by an angular section (thus the name Equal Channel Angular). The magnitude of the shear strain that is developed in a single pass of the specimen through the die is determined by the die geometry, and particularly the included angle ϕ shown in the figure. The angle Φ subtended by the external radius is also an important parameter. Various obtuse die angles and dimensions may be used, and die design is a critical part of an effective ECAP process. Angles closer to 90° give larger shear strains, but require greater workability of the material. The metal specimen that is forced through the die is typically about 1 inch in diameter and several inches long and is made of conventional grain size materials. Substantial forces are required to develop these deformations, and so large presses must be used and particular care must be taken with die design for high-strength metals.

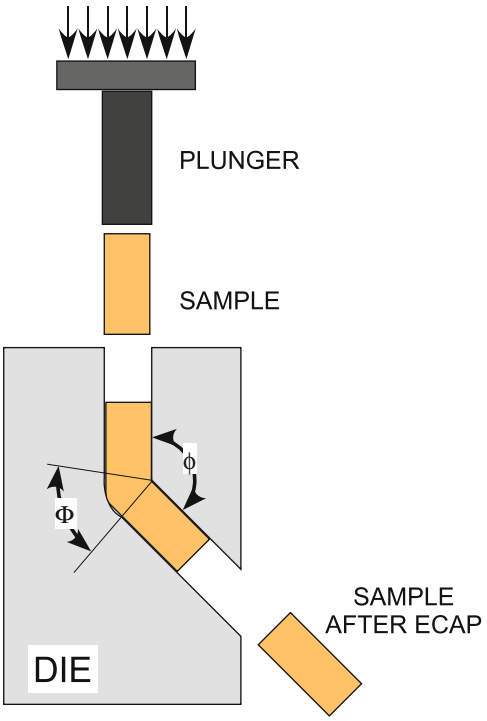

Fig. 1.4 Schematic of the die used in Equal Channel Angular Pressing (ECAP). The included angle ϕ in this case is about 120°, but can be as small as 90°. The angle Φ subtended by the external radius is also an important parameter. Various obtuse die angles and dimensions may be used. Very large forces are required to move the workpiece through such dies.

Since the angle change renders the process inherently anisotropic, it is common practice to run the specimen through the die multiple times (these are called multiple passes), rotating the specimen between consecutive passes. Multiple passes may also be used to increase the fraction of the sample that has been subjected to the large deformations (portions of the specimen ends are typically much less deformed). The various protocols used for these multiple passes and rotations are called processing routes (commonly referred to as A, B, C... routes). Each route has a different yield in terms of grain size and the likely development of texture (relative orientation of grains), and also in the fraction of the specimen that achieves significant grain refinement. The use of multiple passes typically yields ultra-fine-grain (ufg) size materials relatively easily, but nanocrystalline grain sizes are very difficult to obtain. These techniques have been used on a variety of metals successfully. In particular, metals with body-centered cubic (*bcc*), face-centered cubic (*fcc*) and hexagonal-close packed (*hcp*) crystal structures have been processed in this way.

An example of the microstructure of a material made by equal channel angular pressing is shown in Figure 1.5. The average grain size of this material is 200 nm. A selected area diffraction (SAD) pattern is also shown, and indicates the presence

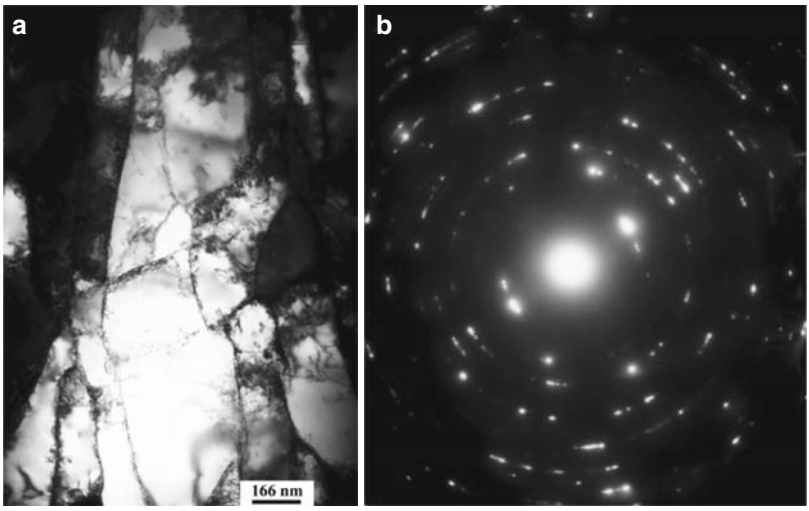

Fig. 1.5 (a) Microstructure of tantalum produced by Equal Channel Angular Extrusion (ECAE), four passes at room temperature through a 90° die. (b) Selected Area Diffraction (SAD) pattern for this sample, showing the presence of many low angle grain boundaries. The fraction of grain boundaries that are low-angle rather than high-angle can be an important feature of the microstructure.

of low-angle grain boundaries (typical of this SPD approach). The high dislocation density in many of the grains is a result of the large plastic work that must be introduced in order to generate this microstructural grain refinement. As in the consolidated case, materials produced by this SPD process contain large internal dislocation densities because the processes of grain refinement result in significant numbers of retained dislocations. There is often a significant texture produced by this process, although the degree of texture does depend on the specific route used and varies strongly from one material to another. Elongated grains are another characteristic feature of such processes, and as a result these materials may have anisotropy in the yield strength (that is, the yield strength – defined in Chapter 2 – may be different in different directions). The nature of the grain boundaries produced by equal channel angular pressing is a matter of some controversy. It appears that the structure of the grain boundary may be strongly dependent on the temperatures at which the processing is conducted for a given material. In a related issue, the degree to which rotational recrystallization plays a part in the development of the fine grains also remains uncertain.

1.4.3.5 High-Pressure Torsion

Another kind of SPD process is shown in Figure 1.6, and is known as the high-pressure torsion or HPT process (Liao et al., 2006). Relatively small samples are subjected to combined high-pressure and severe torsional deformations using large

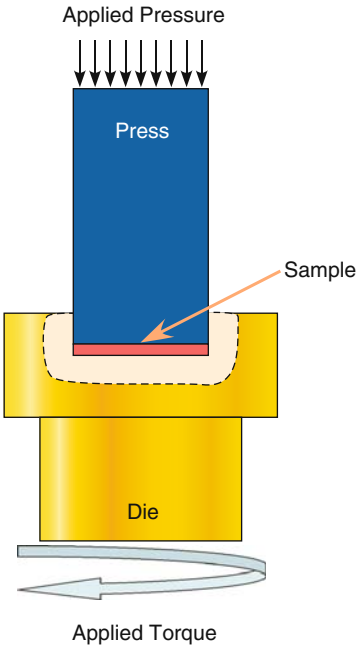

Fig. 1.6 Schematic of High Pressure Torsion (HPT) process. A thin specimen is compressed and then subjected to large twist within a constraining die. The typical sample size is about 1 cm in diameter and about 1 mm thick.

multi-axial presses. Pressures of several GPa are used, and the torsional strains can be very large (depending on the total angle of twist). Since thin specimens are being considered, the strains generated by the compression are relatively small. For any given increment in the angle of twist θ, the local increment in shear strain is given by

$$\delta\gamma = \frac{r\delta\theta}{h}, \tag{1.1}$$

where r is the radial distance from the center of the disc and h is the disc thickness. Very large strains can thus be generated by using small thickness samples. For example, a full rotation of 360° will lead to a shear strain of approximately 30 in a sample that is 10 mm in diameter and 1 mm thick. These very large strains can lead to much more refined microstructures than can be obtained through ECAP processes. The superimposed pressure is necessary to keep the sample from breaking apart, and issues of workability typically still require performing this HPT operation at elevated temperature. The major difficulty with this technique, however, is the small size of the specimen that is subjected to the very large strain. Further, the strain is quite inhomogeneous, with the center of the specimen seeing no strain at all. At this point, therefore, the technique is a good way to understand what the effects of severe plastic deformation will do to materials, but this is not a good approach for generating significant quantities of nanomaterials.

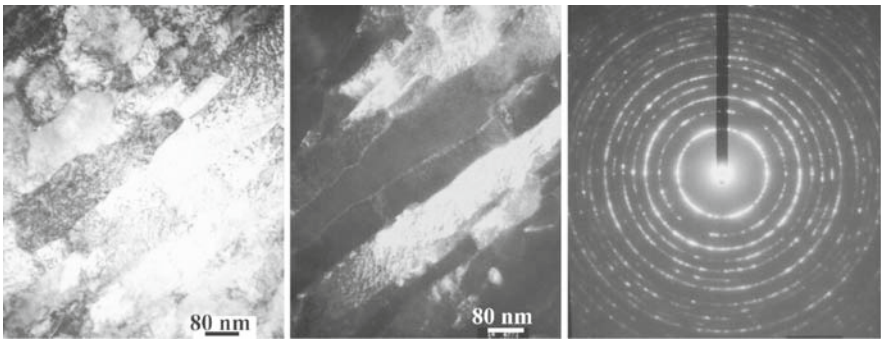

Fig. 1.7 Microstructure of tungsten produced by high-pressure torsion (HPT). (a) A bright field TEM micrograph. (b) A dark field TEM micrograph. (c) A selected area electron diffraction pattern from this field. The grains contain a high density of defects (because of the plastic work associated with the HPT process). The grains are also elongated, with widths on the order of 80 nm and lengths of about 400 nm. Grain orientation appears to be along the shearing direction. The selected area electron diffraction shows nearly continuous rings, with no obvious intensity concentration along the rings, indicating large angle type grain boundaries in the sample. Reprinted from Acta Materialia, Vol. 52, Issue 7, P. 11, Q. Wei, L. Kecskes, T. Jiao, K.T. Hartwig, K.T. Ramesh and E. Ma, Adiabatic shear banding in ultrafine-grained Fe processed by severe plastic deformation. April 2004, with permission from Elsevier.

An example of a microstructure generated by HPT is shown in Figure 1.7. The material shown is pure tungsten, which is a notoriously difficult material to deform plastically. The final grain size has a minimum dimension of about 80 nm, and some elongation of the grains is observed. An SAD pattern is also shown, demonstrating the nanocrystalline nature of the structure. Note again the large number of dislocations within the grains, a characteristic of severe plastic deformation processes. Elongation along the shearing direction is evident, and a range of grain sizes is present. The combination of finer grains but greater heterogeneity of the microstructure is characteristic of HPT processes as compared to ECAP processes. An excellent discussion of the controllable process parameters is provided by Zhilyaev (Zhilyaev et al., 2003). There appears to be a limit to the smallest achievable grain size via HPT, with some indications that the limitation is due to dynamic recrystallization.

1.4.3.6 Surface Mechanical Attrition Treatment

Large plastic deformations can also be obtained on the surface by impacting the surface repeatedly with hardened materials (as in shot peening). The typical approach involves seating the sample within a chamber that is loaded with a large number of hardened steel balls, and then shaking the entire chamber using a vibration generator (Tao et al., 2002). By proper tuning of the frequencies, the steel balls can be caused to impact the specimen at relatively high velocities and generate fairly high strains

in a surface layer on the sample. Continued vibration can lead to microstructural refinement of the surface layer. This process is very similar to the mechanical attrition process used in ball milling to generate nanoparticles; since it is constrained to a surface, the process is called surface mechanical attrition treatment or SMAT. The distinction is the presence of a surface layer and related strain gradients and microstructural gradients. Control of the atmosphere in the chamber, the frequency of vibration, and temperature allows one to control the microstructures that are generated.

1.4.3.7 Rolling and Accumulative Roll Bonding

Very large plastic deformations can also be generated by repeated rolling. Indeed, the processes of grain refinement during severe plastic deformation were first examined in repeated rolling processes, because of the applications in the metalworking industry. While repeated rolling does requires substantial workability, the development of protocols involving rolling followed by annealing and then subsequent secondary rolling allows for the development of very fine microstructures. Rolling can also be performed at cryogenic temperatures, which has been shown to allow the development of finer grains. A version of rolling called Accumulative Roll Bonding (ARB) involves rolling a material to a thin-sheet, then cutting the sheet in two, stacking the sheets and rolling again to further reduce the thickness, and then repeating this process (Saito et al., 1999). Accumulative roll bonding has been used to develop bulk ultra-fine-grained and nanostructured metals, both from alloys and pure metals, and such an ARB process can be adapted for continuous production of substantial quantities of material (this is a key difficulty with a number of the other SPD techniques).

1.4.3.8 Crystallization from the Amorphous State

Another approach to making bulk nanomaterials involves the crystallization of the material from an amorphous state or from the molten state. Control of the nucleation and growth process to emphasize nucleation can lead to very fine crystal sizes (Hono et al., 1995). Such control is, however, quite difficult to maintain, and so very few bulk nanomaterials are made in this way at this time.

1.5 Closing

Now that we have some sense of how to make nanomaterials, we develop the mechanics of materials in the next chapter. We can then use that understanding to focus on the mechanics of nanomaterials in subsequent chapters.

1.6 Suggestions for Further Reading

1. L. Foster, Nanotechnology: Science, Innovation, and Opportunity. Prentice Hall, Upper Saddle River, NY, 2005.
2. G. Cao, Nanostructures & Nanomaterials: Synthesis, Properties & Applications. Imperial College Press, London, 2004.
3. Y. Gogotsi, Nanomaterials Handbook. New York, CRC Press, 2006.
4. B. Bhushan, Springer Handbook of Nanotechnology. Springer, New York, 2007.
5. P.C. Hiemenz and R. Rajagopalan, Principles of Colloidal and Surface Chemistry. CRC Press, New York 3rd ed., 1997.
6. D.D. Brandon and W.D. Kaplan, Microstructural Characterization of Materials. Wiley, New York, 2nd ed. 2008.

1.7 Problems and Directions for Research

1. Identify a source of silver nanoparticles, and find out what particle size distribution is available. How does the company determine this distribution? What is the cost of the nanoparticles, and what are the sample masses (or volumes) that are available?
2. Identify the risks associated with handling silver nanoparticles. What literature is available on their toxicity, if any? How should they be stored? Is there a danger of fire if the particles are stored in air?
3. Repeat the problem above, but this time consider aluminum nanoparticles. As always with respect to safety and risk management, the key is to (a) know and document the risks, (b) know and document safe handling procedures and (c) know and document emergency response procedures in case of an accident or mishandling. Write a three page report that includes (a), (b) and (c) above (one page each) for aluminum nanoparticles.
4. Consider the ECAP process shown in Figure 1.4. The included angle is $\phi \geq 90^\circ$, and often the outside corner is not sharp but rounded, subtending an angle Φ with the sharp inner corner. Then the total shear strain developed by the ECAP process is given by $\gamma = \frac{N}{\sqrt{3}}[2\cot(\frac{\phi}{2}+\frac{\Phi}{2}) + \Phi\csc(\frac{\phi}{2}+\frac{\Phi}{2})]$, where N is the number of passes (the number of times the workpiece is reinserted). Using the literature, identify an ECAP route and the number of passes needed to achieve a shear strain of 4.
5. Consider the problem of the industrial production of bulk nanomaterials. In your opinion, which of the processes described in this chapter is best suited to scale-up? Why? What are the potential limitations of this process? What do you think would be the most expensive part of the facility required for scale-up of this process? You will need to define an expected output capacity.

References

Agnew, S. R., B. R. Elliott, C. J. Youngdahl, K. J. Hemker, and J. R. Weertman (2000). Microstructure and mechanical behavior of nanocrystalline metals. *Materials Science and Engineering a-Structural Materials Properties Microstructure and Processing 285*(1–2), 391–396.

Ahmadi, T. S., Z. L. Wang, T. C. Green, A. Henglein, and M. A. ElSayed (1996). Shape-controlled synthesis of colloidal platinum nanoparticles. *Science 272*(5270), 1924–1926.

Bhattacharyya, S., O. Auciello, J. Birrell, J. A. Carlisle, L. A. Curtiss, A. N. Goyette, D. M. Gruen, A. R. Krauss, J. Schlueter, A. Sumant, and P. Zapol (2001). Synthesis and characterization of highly-conducting nitrogen-doped ultrananocrystalline diamond films. *Applied Physics Letters 79*(10), 1441–1443.

Birringer, R., H. Gleiter, H. P. Klein, and P. Marquardt (1984). Nanocrystalline materials an approach to a novel solid structure with gas-like disorder. *Physics Letters A 102*(8), 365–369.

Brust, M., M. Walker, D. Bethell, D. J. Schiffrin, and R. Whyman (1994). Synthesis of thiol-derivatized gold nanoparticles in a 2-phase liquid-liquid system. *Journal of the Chemical Society-Chemical Communications 7*, 801–802.

Elsherik, A. M. and U. Erb (1995). Synthesis of bulk nanocrystalline nickel by pulsed electrodeposition. *Journal of Materials Science 30*(22), 5743–5749.

Hono, K., Y. Zhang, A. Inoue, and T. Sakurai (1995). Atom-probe studies of nanocrystalline microstructural evolution in some amorphous alloys. *Materials Transactions of JIM 36*(7), 909–917.

Hughes, D. and N. Hansen (1997). High angle boundaries formed by grain subdivision mechanisms. *Acta Mater 45*(9), 3871–3886.

Li, M., H. Schnablegger, and S. Mann (1999). Coupled synthesis and self-assembly of nanoparticles to give structures with controlled organization. *Nature 402*(6760), 393–395.

Liao, X. Z., A. R. Kil'mametov, R. Z. Valiev, H. S. Gao, X. D. Li, A. Mukherjee, J. F. Bingert, and Y. T. Zhu (2006). High-pressure torsion-induced grain growth in electrodeposited nanocrystalline ni. *Applied Physics Letters 88*, 021909.

Malow, T. R. and C. C. Koch (1998). Mechanical properties, ductility, and grain size of nanocrystalline iron produced by mechanical attrition. *Metallurgical and Materials Transactions a-Physical Metallurgy and Materials Science 29*(9), 2285–2295.

Meulenkamp, E. A. (1998). Synthesis and growth of zno nanoparticles. *Journal of Physical Chemistry B 102*(29), 5566–5572.

Mughrabi, H. (1983). Dislocation wall and cell structures and long-range internal stresses in deformed metal crystals. *Acta Metallurgica 31*(9), 1367–1379.

Musil, J. and J. Vlcek (1998). Magnetron sputtering of films with controlled texture and grain size. *Materials Chemistry and Physics 54*(1–3), 116–122.

Nicoara, G., D. Fratiloiu, M. Nogues, J. L. Dormann, and F. Vasiliu (1997). Ni-zn ferrite nanoparticles prepared by ball milling. In *Synthesis and Properties of Mechanically Alloyed and Nanocrystalline Materials, Pts 1 and 2 - Ismanam-96*, Volume 235- of *Materials Science Forum*, pp. 145–150. Transtec.

Ren, Z. F., Z. P. Huang, J. W. Xu, J. H. Wang, P. Bush, M. P. Siegal, and P. N. Provencio (1998). Synthesis of large arrays of well-aligned carbon nanotubes on glass. *Science 282*(5391), 1105–1107.

Saito, Y., H. Utsunomiya, N. Tsuji, and T. Sakai (1999). Novel ultra-high straining process for bulk materials - development of the accumulative roll-bonding (arb) process. *Acta Materialia 47*(2), 579–583.

Tao, N. R., Z. B. Wang, W. P. Tong, M. L. Sui, J. Lu, and K. Lu (2002). An investigation of surface nanocrystallization mechanism in fe induced by surface mechanical attrition treatment. *Acta Materialia 50*, 4603–4616.

Valiev, R. and T. Langdon (2006). Principles of equal-channel angular pressing as a processing tool for grain refinement. *Progress in Materials Science 51*, 881–981.

Valiev, R. Z., R. K. Islamgaliev, and I. V. Alexandrov (2000). Bulk nanostructured materials from severe plastic deformation. *Progress in Materials Science 45*, 103–189.

Zhilyaev, A. P., G. V. Nurislamova, B.-K. Kim, M. D. Baro, J. A. Szpunar, and T. G. Langdon (2003). Experimental parameters influencing grain refinement and microstructural evolution during high-pressure torsion. *Acta Materialia 51*, 753–765.

If you take care of the small things, the big things take care of themselves.

Emily Dickinson

7 Scale-Dominant Mechanisms in Nanomaterials

The unusual properties of nanomaterials all arise from mechanisms that are not intuitive to us at the human length scale. To gain an understanding of these properties – and to control them – we must discover the mechanisms that are operative at the length scales associated with the specific nanomaterial. From a science perspective, many of these unusual properties arise from the interactions of intrinsic length scales (associated with underlying deformation or functional mechanisms) with the extrinsic or external length scales associated with the nanomaterial or device. This chapter discusses a variety of such interactions, and describes the implications of some of them in terms of mechanical behavior. The emphasis is on deformation and failure mechanisms rather than on functional mechanisms, but many of the deformation mechanisms discussed here have direct implications for function.

A broad brush view of the major mechanisms associated with nanomaterials is presented in Table 7.1. Using the materials classification scheme of Chapter 1, this table lists the primary mechanisms associated with discrete nano (dn) materials, nano device (nd) materials, and bulk nanocrystalline (nc) or nanostructured (ns) materials. In each case, we consider the extrinsic and intrinsic length scales associated with the morphology, define the important interactions, and discuss some of the implications. For ease of discussion, we consider the discrete nanomaterials and nano device materials at the same time, because of the great commonality in the morphology.

7.1 Discrete Nanomaterials and Nanodevice Materials

7.1.1 Nanoparticles

A quick search of the internet will demonstrate that there is a large variety of materials that are colloquially considered to be nanoparticles. The term *nanoparticle* is

K.T. Ramesh, *Nanomaterials*, DOI 10.1007/978-0-387-09783-1_7,

Table 7.1 Scale-dominant mechanisms in nanomaterials, categorized in terms of materials classification, morphology, and length scale.

Type of nanomaterial	Morphology or application conditions	External length scales	Internal length scales	Mechanisms	Remarks
Discrete nano (dn) materials	Equiaxed nanoparticles	Particle diameter	Atomic spacing	Surface stress equilibration	Suggests core-shell nanostructures
	Nanotubes	Diameter, wall thickness, length	Atomic spacing, defect spacing	Buckling, telescoping, fracture	Very high stiffness and strength
	Nanofibers	Diameter, length	Atomic spacing, molecular weight	Fracture, surface interactions	Fiber-matrix interactions
Nanodevice (nd) materials	Nanoparticles	Diameter	Atomic spacing, functionalization density	Surface stresses due to functionalization	Interactions at optical wavelengths
	Nanowires and nanotubes	Diameter, length	Atomic spacing, defect spacing, functionalization density	Functionalization-induced deformations, twinning, flexure	Highly sensitive through flexure
	Nanoporous structures	Thickness	Pore size, pore spacing, functionalization density	Interactions with environment	Optical interactions, molecular sensitivity
	Thin films	Thickness	Atomic spacing, dislocation spacing, ledge spacing, functionalization density	Surface stresses, surface mobility, 2D mechanisms, passivation layers, substrate interactions, diffusion	Highly developed fabrication techniques
Bulk nanocrystalline nanomaterials	Micropillars	Diameter, height	Grain size, dislocation density	Dislocation mechanisms, twinning, grain boundary (gb) processes, grain rotation, shear failure, buckling, constraint effects	Specimen size effects, strain gradients
	Microtension specimens	Diameter, length	Grain size	Dislocation mechanisms, twinning, gb processes, grain rotation, constraint effects, necking, fracture	Specimen size effects, strain gradients
	Nanoindentation	Indent size	Grain size, dislocation spacing	Dislocation mechanisms, twinning, gb processes, grain rotation, release processes, pressure effects	Indentation size effects, strain gradients
	Components	Component size	Grain size	Dislocation mechanisms, twinning, gb processes, grain rotation, failure processes	Design of subscale structure, as in metallic foams

generally used to identify any particle that is less than 100 nm in the largest dimension. A variety of morphologies is thus possible within this loose definition:

- Spherical nanoparticles (nanospheres)
- Rod-like nanoparticles (nanorods)
- Plate-like nanoparticles (nanoplates)
- Some very complex shapes including dendrites

These morphologies can have very different properties, and indeed this accounts for the vast range of applications that are attributed to nanoparticles. Note that the surface area-to-volume ratio of nanorods and nanoplates can be very different from those of nanospheres. Since this ratio dominates many of the applications of nanoparticles, the morphology has a dramatic impact on the application.

Large fractions of the nanoparticles used in assorted technologies are also heterogeneous, consisting of complex structures made up of more than one material. Some nanoparticles appear to be nearly amorphous, with no clearly defined crystal structure, while others are clearly single crystals showing crystalline facets. The variety of mechanisms that are appropriate to the deformation of nanoparticles is as large as the variety of nanoparticles themselves, and we will not be able to discuss all of them in this book.

We will focus our discussion on nanoparticles that are nearly equiaxed, that is, with aspect ratio (ratio of smallest to largest dimension) close to one. The external length scale associated with a nanoparticle is then the particle diameter (by definition, less than 100 nm). The only internal length scale associated with the mechanical properties of the nanoparticle is the inter-atomic spacing. The magnitude of this spacing is typically on the order of 3 Åfor most elements, so that a nanometer contains perhaps 3 atomic spacings (Figure 7.1) separating 4 atoms, and a cubic nanometer would consist of perhaps 64 atoms. Particles consisting of fewer than 100 atoms are often called *nanoclusters*.

Consider a nanocluster of 64 atoms in a cubic lattice arrangement – if it were a cube of side 1 nm, most (about 80%) of those atoms would be on the surface of the nanocluster. Surface atoms are not surrounded by similar atoms on all sides and so have a different equilibrium spacing, and thus the cubic lattice must be distorted from the bulk equilibrium configuration. Such surface character can lead to unusual structures. Further, the surface atoms can interact strongly with other atoms or molecules in the environment, leading to the development of nanoparticles that are surface-active. Core-shell type nanoparticles can be developed relatively easily as a consequence, and these have great value in bioengineering.

Let us assume that the equilibrium interatomic spacing is a in the bulk crystal, while the particle dimension is D. If the particle is a cube of side D and the atoms are arranged in a cubic lattice, the total volume of the cube is D^3, while the volume corresponding to the atoms that are inside the cube (not exposed to the surface) is $(D-2a)^3$. The volume fraction f_{ext} of the atoms that are on the surface of the nanoparticle is therefore (note that the volume fraction is of the same order as the number fraction)

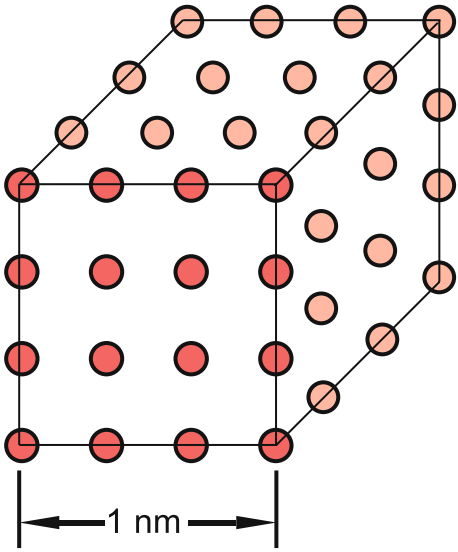

Fig. 7.1 Schematic of a cubic nanocluster consisting of 64 atoms, approximately 1 nm on a side. The majority of the atoms are on the surface of this nanocluster, and so will have a different equilibrium spacing than atoms in a bulk sample of the same material.

$$f_{ext} = 1 - \frac{(D-2a)^3}{D^3} = \frac{8a^3}{D^3} - \frac{6a^2}{D^2} + \frac{6a}{D}. \tag{7.1}$$

A quick solution of the resulting cubic equation shows that about half the atoms will be on the surface of a nanoparticle with dimension $D \approx 15a$. Since interatomic spacings are typically of the order of 3 Å, cuboidal nanoparticles are surface dominated (in terms of structure and mechanical response) if they are less than 5 nm in typical dimension. Larger nanoparticles (up to 20 nm, see Figure 7.2) have very large surface area-to-volume ratios in comparison to conventional micron-size particles (remember that this ratio goes as $\frac{1}{D}$), but the surface equilibration effect on internal structure becomes less of an issue.

The variation of the volume fraction of surface atoms with nanoparticle size is shown in Figure 7.2 for an assumed interatomic spacing of 0.3 nm. The rapid growth of the surface fraction as the particle sizes decrease below 20 nm is apparent, and the surface fraction dominates in the nano cluster domain.

Surface atoms see a different distribution of neighbors than interior atoms, and so have different energies than interior atoms. Note that it is not just the outermost layer of atoms that is affected – the influence of the surface will typically be felt by several layers of atoms (depending on the range of the interatomic potential). The precise number of layers that must be considered can only be derived from atomistic analysis considering the interatomic potentials. The influence of the surface fraction on the mechanical behavior depends on the difference between the energies of the atoms on the surface and the energies associated with the atoms in the interior of the

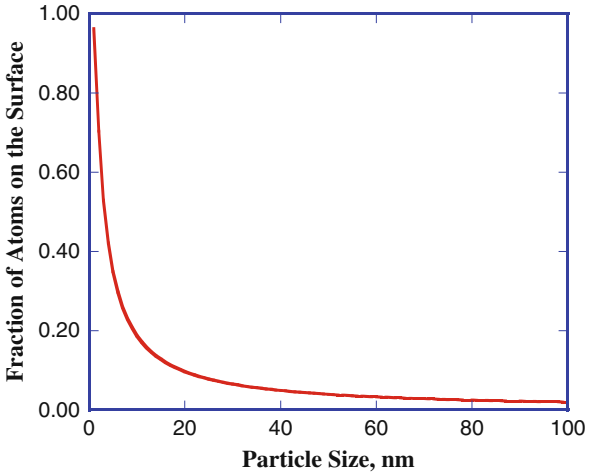

Fig. 7.2 Volume fraction of atoms on the surface of a cuboidal nanoparticle as a function of nanoparticle size, based on Equation (7.1) and an assumed interatomic spacing of 0.3 nm. Significant surface fractions are present below about 20 nm. Note that particle sizes below 0.6 nm are poorly defined.

particle. The discussion of the surface energy effects that follows is taken largely from the summary of the mechanics issues provided by Dingreville et al. (2005). If we define the difference between the energy of an atom at the surface and the energy of an atom at the interior as e_{si}, then we can define a surface free energy density (first defined by Gibbs, the grandmaster of thermodynamics) as the areal density Γ:

$$\Gamma dA = \sum e_{si}, \tag{7.2}$$

where the summation is over all atoms in the layers affected by the surface element dA, the capital A indicating that the surface element is in the undeformed or reference configuration (remember that the atoms rearrange themselves as a result of these surface interactions). The element da in the deformed configuration is related to the undeformed element dA through the surface strains:

$$da = dA(1 + \varepsilon^s_{11} + \varepsilon^s_{22}), \tag{7.3}$$

where the coordinate axes are chosen so that x_3 is normal to the surface (that is, the in-plane stresses are ε^s_{11}, ε^s_{22}, and ε^s_{12}). These surface strains are related to the surface free energy density through *surface stresses* $T^s_{\alpha\beta}$, using a concept similar to that presented in Equation (2.68) discussed in Section 2.4.1:

$$T^s_{\alpha\beta} = \frac{\partial \Gamma}{\partial \varepsilon^s_{\alpha\beta}}, \tag{7.4}$$

where the Greek subscripts α and β are used to imply that only surface quantities are being considered, *with the indices taking on values of 1 and 2 only*. This is effectively a definition of the surface stress, and we see that it can be derived from the surface energy density. How does the surface energy density Γ depend on the surface strain? As a first approximation, one can expand the surface energy in a Taylor series about the point $\varepsilon^s_{\alpha\beta} = 0$, and in principle the various terms in this series can be computed using atomistic calculations. For our purposes, it is simplest just to assume that for small strains the surface energy density is quadratic in the surface strain, with all higher order terms being negligible (the identical assumption is made in linear elasticity for the strain energy density). It then follows that the surface stress is given by (using Equation 7.4)

$$T^s_{\alpha\beta} = G_{\alpha\beta\gamma\delta}\varepsilon^s_{\gamma\delta}, \tag{7.5}$$

where again the Greek subscripts indicate that they range only over $1,2$ and the summation convention is implied. The coefficients $G_{\alpha\beta\gamma\delta}$ are the components of the *surface elasticity tensor*, which is a two-dimensional analog of the elastic modulus tensor discussed in Equation (2.65) of Section 2.4.1, but derived specifically for surfaces as a result of the fact that the surface energy Γ is different from the strain energy W in the interior of the solid. Note that like the elastic modulus tensor, we have

$$G_{\alpha\beta\gamma\delta} = G_{\beta\alpha\gamma\delta} = G_{\alpha\beta\delta\gamma} = G_{\gamma\delta\alpha\beta}, \tag{7.6}$$

for reasons identical to those discussed in Section 2.4.1. The values of the components of the surface elasticity tensor must be obtained either through atomistic calculations and then using Equation (7.2), or by direct measurement, although such measurements are extraordinarily difficult.

Equation (7.5) tells us that the effect of the free surface is to cause the top few layers of atoms to behave effectively as though they are made of a different material in terms of elastic behavior. One could view the particle as being a composite structure (Figure 7.3), with the inner core having the normal bulk properties and the outer

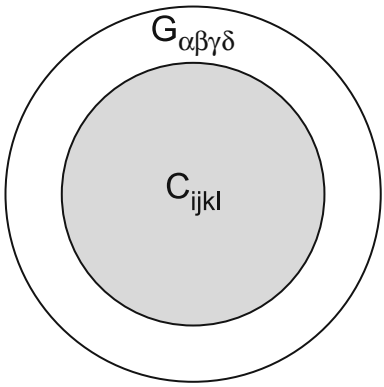

Fig. 7.3 Core-shell model of a nanoparticle viewed as a composite, with a surface layer that has different properties as a result of the surface energy and its effects on binding.

shell having different elastic properties, based on the surface energy. Whether the outer shell is stiffer or more flexible depends on the specific atomic species being considered (note that many nanoparticles are not single element particles, e.g., ZnO and CdS particles). From a mechanical viewpoint, the behavior of the surface layers will depend not just on the surface elasticity tensor but also on the particle shape (morphology), since a starfish-shaped particle can be expected to have a different surface response (at the level of Equation 7.2) than a spherical particle of the same material.

Composite mechanics approaches can be used to compute the effective elastic behavior of particles having such a core-shell structure. For example, Dingreville et al. (2005) show that the contribution of the surface energy to the effective modulus of a spherical nanoparticle is inversely proportional to the particle size. For large particles the effect can be ignored, but the effect can be significant for nanoparticles.

7.1.1.1 Functionalization

The applications of many nanoparticles are based on the fact that the surfaces of the nanoparticles can be modified through the addition of specific molecules in order to accomplish specific functions. This process is known as *functionalization*. For example, metallic nanoparticles might be coated with a layer of an organic compound, and then have specific biological molecules attached to the organic compound (Figure 7.4) so that this *functionalized* nanoparticle can interact with the biological environment (Bruchez et al., 1998).

The process of functionalization changes the surface stresses on the nanoparticle by changing the surface energies and, correspondingly, certain kinds of functionalization are easier for nanoparticles that have specific surface stresses. The surface

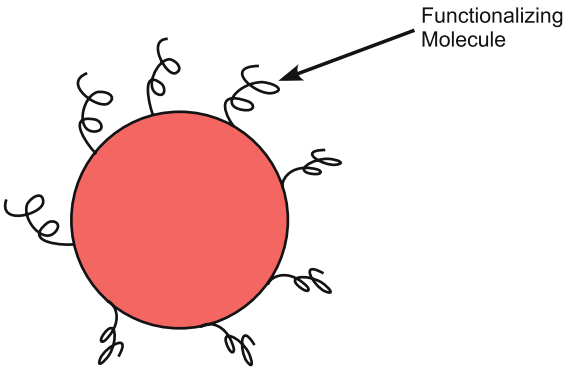

Fig. 7.4 A spherical nanoparticle carrying several organic molecules on its surface. The molecules are chosen to perform a specific function, such as recognizing a molecule in the environment, and so are called functionalizing molecules. The spacing of the functionalizing molecules defines the functionalization density. Since the molecules modify the surface stress state when they attach to the surface, the functionalization density modifies the surface stresses and can even modify the net conformation of the nanoparticle.

stress modification of the nanoparticle will depend on the density η_f of the functionalizing molecule that is applied to the surface (the density is defined as the number of functionalizing molecules per unit surface area). The reciprocal of the square root of this functionalization density provides another intrinsic length scale in the problem. There is an increasing array of biomedical applications of functionalized nanoparticles (Sanvicens and Marco, 2008), including potential treatments for some kinds of malignant tumors. Other kinds of functionalization can lead to the interaction of nanoparticles at optical wavelengths, leading to various sensor applications (a specific example in this area is the application of *quantum dots*; Alivisatos, 1996).

7.1.2 Nanotubes

There is a vast literature on carbon nanotubes, which are perhaps the best understood of the discrete nanomaterials. We do not attempt to reprise the entire literature on the mechanics of carbon (and other) nanotubes here, but some references are suggested at the end of this chapter. Here, we present just a brief discussion of the major issues and mechanisms.

By definition, nanotubes are tubes that have nanoscale diameters and some predefined wall thickness, with length-to-diameter ratios that are usually greater than 10. Carbon nanotubes consist of single or multiple walled structures that can be thought of as rolled up *graphene* sheets (see Figure 7.5). Each sheet is an atom-thick layer of carbon atoms arranged in a specific structure – depending on exactly how the sheets are rolled up, one obtains varieties of nanotube known as *armchair*, *chiral* or *zigzag* nanotubes (the adjectives indicate the apparent atomic arrangement). The hexagonal two dimensional lattice is mapped on to a cylinder of radius R with helicities characterized by so-called rolling vectors (n,m), and the different types of nanotubes are characterized by these (n,m) pairs.

The external length scales associated with a nanotube are the diameter, the wall thickness (different for single-wall and multi-wall nanotubes), and the length. The internal length scales associated with nanotubes are the interatomic spacing (as in nanoparticles) and the defect spacing (defects can control the mechanical properties of nanotubes). There are (Figure 7.6) three associated deformation mechanisms: column and shell buckling of the thin-walled tube, telescoping of the tube, and fracture of the tube. Telescoping is a deformation mode that is only possible in multi-walled nanotubes, but buckling and fracture can occur in all nanotubes.

Buckling is a structural instability in which a structure deforms suddenly with an abrupt drop in load-carrying capacity, and is thus a structural failure mechanism (as distinct from a material failure mechanism like fracture). There are many different kinds of buckling, the best known being the compressive buckling of slender columns (called Euler buckling, see the discussion of Equation 3.7). This is a structural instability in which the column ceases to remain straight, adopting a bent shape when the load exceeds a critical value called the Euler buckling load:

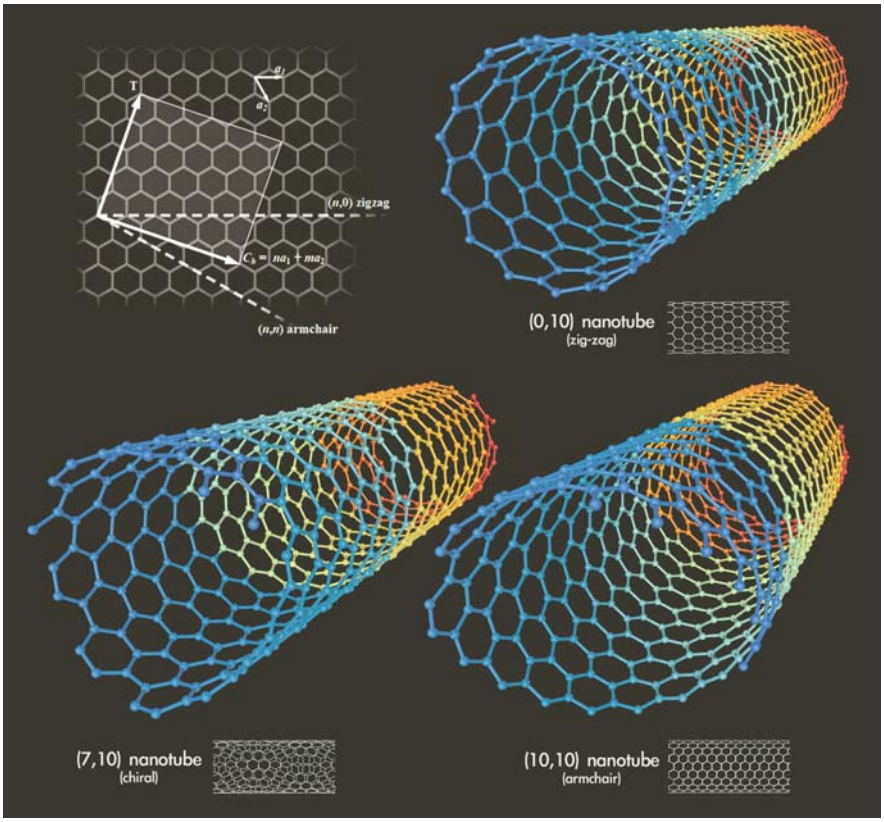

Fig. 7.5 Schematic of the structure of carbon nanotubes, showing the armchair, zigzag and chiral conformations. This beautiful illustration was created by Michael Stróck on February 1, 2006 and released under the GFDL onto Wikipedia.

$$P_{cr} = \frac{\pi^2 EI}{{L_e}^2} = \frac{\pi^2 EA}{\frac{{L_e}^2}{\rho_g}} = \frac{\pi^2 EA}{{S_R}^2}, \tag{7.7}$$

where L_e is the effective length of the column, and $I = A{\rho_g}^2$ is the moment of inertia, with A the cross-section area of the column and $\rho_g \triangleq \sqrt{\frac{I}{A}}$ is a geometric property of the cross-section called the radius of gyration. For a circular cross-section of radius r, $\rho_g = \frac{r}{2}$, while for a tube with inner radius r and wall thickness t, $\rho_g = \frac{\sqrt{r(r+t)}}{\sqrt{2}}$. The ratio of the effective length of the column to the radius of gyration is called the slenderness ratio $S_R = \frac{L_e}{\rho_g}$. Large slenderness ratios thus imply low critical buckling loads in compression.

Since the lengths of nanotubes are usually orders of magnitude larger than the diameters, such compressive buckling occurs very easily, and so nanotubes are rarely intended for use under compressive loading. The primary use of thin fibers like

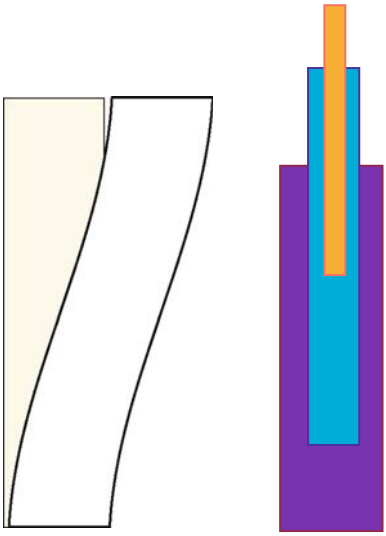

Fig. 7.6 Schematic of two possible modes of deformation and failure in nanotubes. (a) Buckling of a thin column. (b) Telescoping of a multi-walled nanotube. The fracture of nanotubes is a third mode, but is not shown.

nanotubes is always in tension. However, even when the intended application is tension, the nanotubes are typically also subjected to flexural forces (for example, as a result of off axis load), and in such cases the additional mode of asymmetric buckling of the tube wall becomes a possibility. An excellent discussion of the mechanics of buckling of carbon nanotubes viewed in a continuum context is presented by Pantano et al. (2004). Simulations of the buckling of single walled carbon nanotubes are presented from both molecular dynamics and continuum approaches by a number of authors, for example, Cao and Chen (2006).

A multiwalled carbon nanotube in tension may first fail through a telescoping process in which the inner walls are pulled out with respect to the outer walls (Cumings and Zettl, 2000, 2004). This mode arises because the shear strength of the interface between the walls is significantly lower than the strength of the multiwalled nanotube itself. The relative sliding of the walls appears to be nearly frictionless (Kis et al., 2006). The telescoping mode also suggests applications in sensing of small displacements and as encoders (Jiang et al., 2007).

If the nanotube is placed under tension, the primary failure mode is that of fracture (Yu et al., 2000b). The mode of fracture depends on the structure and composition of the nanotube, as well as on the number and location of defects within the nanotube (note that defects in a nanotube are primarily missing atoms or incorrectly located atoms). Unlike conventional crystalline metallic structures, nanotubes do not contain dislocations, and so dislocation plasticity mediated necking failures cannot occur. Multi-walled carbon nanotubes can use sliding between the layers in the walls to generate apparent plastic deformation before final fracture (this is related

to the telescoping mode) but single walled carbon nanotubes do not have this option. Multi-walled carbon nanotubes often fracture through failure first of the outer shell (this mode is sometimes called the "sword-in-sheath" mode) (Yu et al., 2000). When bundles of single walled nanotubes are tested in tension, a bundle appears to neck down to a single nanotube before fracture, but this corresponds to the progressive figure of multiple nanotubes within the bundle (Yu et al., 2000). Simulations indicate that single walled carbon nanotubes may fail ultimately through the reorganization of the atomic structure until individual bonds carry the load – an atomic version of necking.We discuss models for nanotube fracture in the next chapter.

7.1.3 Nanofibers

Nanofibers are by definition solid fibers in which the diameter is less than 100 nm, and typically the fiber lengths are many orders of magnitude greater than the fiber diameters. The primary external length scales are therefore the fiber diameter and the fiber length. Although there are a variety of nanofibers available, the vast majority of nanofibers of interest in nanotechnology are made from polymer precursors, typically by processes such as electrospinning. An excellent review of the latter topic is provided by Huang et al. (2003).

For polymer nanofibers, an internal length scale that appears is related to the molecular weight of the fiber, and can be viewed variously as the molecular length or as the *persistence length*. The persistence length is the length over which the orientation of one part of a long molecule is correlated with the orientation of another, so that it essentially measures the stiffness of the molecule, large persistence lengths implying stiff molecules (think of a really floppy molecule – the orientation of the end of the molecule has very little correlation with the orientation of the beginning of the molecule). For example, the persistence length of a rigid rod would be infinite, while the persistence length of DNA is around 50 nm. In conventional polymer fibers, with fiber diameters in the microns, the polymer persistence length is usually much smaller than the fiber diameter. The stiffness of the fiber is then determined not by the molecular stiffness as much as by the variety of configurations of the multiple molecules that make up the fiber. This is known as an entropic stiffness, the idea being that highly disordered states – with many possible configurations – are preferred over ordered states (fewer possible configurations) from an entropic viewpoint.

When the fiber diameter becomes comparable to the persistence length of the molecule, one should expect a dramatic change in the behavior of the fiber (because the molecular stiffness is itself now important, rather than simply the entropic stiffness). This suggests that nanofibers should have very different properties from conventional-sized fibers. Note that most polymer chains have relatively stiff carbon chain backbones. The process of making the nanofibers typically involves an effective drawing of the fiber, resulting in oriented molecules and again greater stiffness. Thus, in general, one should expect that the stiffness of the nanofiber would exceed

the stiffness of the conventional size fiber. Additional effects arise because of the increased surface area to volume ratio associated with nano fibers, for the same energetic reasons that were discussed in the case of nanoparticles.

There is very little experimental data on the mechanical properties of single polymer nanofibers, but there is a wealth of data on the mechanical properties of polymer nanofiber-reinforced composites (Huang et al., 2003). In such composites, the fiber matrix interactions become a dominant term in determining the mechanical properties. The flexibility and strength of these fibers also makes them attractive for device applications, where the large surface area can be used for functionalization. These fibers are often used as building blocks for larger structures, such as fiber mats (sometimes called *nanomats*) and in three-dimensional structures such as polymer scaffolds for tissue engineering (these provide matrices for cell implantation and the development of extra-cellular matrix, essential for tissue generation). The mechanical properties of the fiber mats and polymer scaffolds are themselves interesting, but the great applications of these structures are in the provision of large surface area for interaction with the biological and chemical environment.

7.1.4 Functionalized Nanotubes, Nanofibers, and Nanowires

Surface functionalization of one-dimensional nanostructures (nanotubes, nanofibers, and nanowires) has multiple applications, ranging from the modification of a fiber-matrix interaction for a composite to the development of sensors and actuators in the nanoscale domain. As with the nanoparticles, the functionalization of the surface results in a modification of the surface energies and therefore of the surface stresses, and the reciprocal of the square root of the functionalization density η_f (i.e., $\frac{1}{\sqrt{\eta_f}}$) provides an additional length scale. Such modifications can result in equilibrium shapes for the nanofibers that are far from straight (referred to as functionalization-induced deformation). The morphology of the nanowires and the nanotubes naturally lends itself to applications that take advantage of the easy flexural deformations. Indeed, such devices are highly sensitive to the environment through the combination of functionalization and the flexural mode (i.e., the bending stiffness is modified by the coupling to the environment, as when the functionalizing molecules interact with molecules in the environment). One specific approach that is often used in sensor applications is to examine shifts in the resonant frequency of the device (which depends on the flexural stiffness) as a result of interactions with the environment.

7.1.5 Nanoporous Structures

Nanoporous structures are typically thin film structures that are deliberately constructed to contain large numbers of nanosized pores. A common way to produce these materials is to construct a binary alloy made up two highly miscible metals, such as gold and silver, and then to dissolve out one element using a reactive agent.

The resulting porosity is extremely small, and subsequent thermal processing affords some control of size and distribution. It is also possible to make nanoporous structures by highly controlled etching procedures. The volume fraction of the pores can be very large, depending on the application. The primary external length scale in this case is the film thickness t_f, while the important internal length scales are the pore size l_p and the pore spacing λ_p. If the pore surface is functionalized, then the functionalization density also provides an intrinsic length scale through $\frac{1}{\sqrt{\eta_f}}$, which must by definition be less than l_p. The pore size and the pore spacing are related for a given pore volume fraction: smaller pores will be closer together, because there have to be a greater number of small pores to achieve a given pore volume fraction. The pore surface area to pore volume ratio increases as the pore size decreases, and so nanoporous structures are very efficient in terms of making surface area available for activation. If $l_p \approx t_f$, columnar structures are likely to be obtained. If $\lambda_p \approx t_f$, then the thin film typically contains one pore in its layer thickness. If the pore volume fraction is large enough, the pores are usually connected (essentially a *percolation* limit), and this is usually desirable for sensing applications. The resolution of the sensor (if functionalized) is related to η_f.

The large surface area generated by the pores results in strong interactions with the environment, and some interesting applications arise in catalysis. Such nanoporous structures are typically constructed in order to interact strongly with the environment, particularly in applications involving the sensing of gaseous environments (such as small concentrations of toxic gases or explosive residues). These devices can also be constructed to provide optical interactions, that is to provide optically perceptible changes on exposure to the target molecule (Chan et al., 2000).

7.1.6 Thin Films

The subject of thin films and the mechanics issues therein has been extensively investigated because of the applications in semiconductor technology, and we will not try to cover these issues here; the reader is referred to the supplementary reading material for detailed analyses. In terms of length scales of interest, however, the intrinsic length scales include the defect density, the dislocation spacing (if any dislocations are present), the surface ledge spacing (atomic-sized ledges are sometimes present on the surfaces), and grain size. The primary extrinsic length scale is of course the film thickness. The mechanics issues are very different for films with device and electronic applications as compared to films with mechanical applications (such as wear resistance).

7.1.7 Surfaces and Interfaces

Phenomena that occur at surfaces and interfaces can play a very large role in nanotechnology, and so also in nanomaterials. The mechanics associated with surface and interface interactions can be quite complex, ranging from issues such as friction

and contact angle (wetting) to residual stresses and delamination. Surface stresses can be used to control surface phenomena (for example in the self-organization of structures on surfaces). These are very important topics in nanotechnology, but will not be dealt with in this book.

7.2 Bulk Nanomaterials

A variety of internal mechanisms lead to scale-dependent or size-dependent behavior of bulk nanomaterials, and these are discussed here. This is an area of significant research activity as of this writing. In broad terms, the internal mechanisms are:

- Dislocation-mediated plasticity
- Deformation twinning
- Grain boundary sliding
- Grain boundary propagation (grain growth or shrinkage)
- Grain rotation

Each of these mechanisms will be discussed in this section. We begin with a discussion of dislocation mechanisms, relating primarily to issues of strength and plastic flow.

7.2.1 Dislocation Mechanisms

We have discussed dislocation plasticity in some depth in the sections on the plastic behavior of nanomaterials, but that section focused on the overall behavior of bulk nanocrystalline materials, and in particular on the effects of grain-size. A more general discussion of dislocation mechanisms is of interest in this chapter, because some of these mechanisms are only active under specific conditions. As always, it is the interaction of length scales that determines what the dominant mechanisms will be in any given problem (Greer, 2006).

There are a number of intrinsic length scales (Table 7.2) associated with dislocation mechanisms, and these are listed below:

- The dislocation core size R_c defines the smallest length scale that can be identified with a given dislocation.
- If the dislocation dissociates into two partial dislocations (a dissociation that will only occur if it is energetically favorable to do so), the spacing w_{sf} of the partials provides another length scale. The spacing of the partials is called the width of the stacking fault w_{sf}, because a stacking fault exists between the two partials. A stacking fault is an unexpected stacking, or error in the stacking, of the atomic planes. The energy associated with the stacking fault is called the stacking fault energy; if the stacking fault energy is high, the equilibrium spacing of the two

dissociated partials will be small. One could view the dissociated partials as representing an extended core for the dislocation, although the core is no longer cylindrical.

- The effective range R_e of the elastic stress fields around the dislocation core provides another length scale.
- If the dislocation density is ρ_D, then the average spacing between dislocations is given by $\lambda = \frac{1}{\sqrt{\rho_D}}$. Essentially, the other dislocations are considered to be either obstacles or sources of energy for re-patterning of the dislocation substructure.
- The average spacing L_S of dislocation sources (there are many possible dislocation sources, the classic example being the Frank-Read source). This spacing may relate to other features such as the dislocation density.
- The average spacing between obstacles (such as dispersoids) within a given crystal provides another length scale, L_O.
- The distance between grain boundaries (that is, the grain size d) provides another length scale. This length scale was the focus of discussion in the chapter on the mechanical behavior of nanocrystalline materials.

Table 7.2 Typical intrinsic length scales that arise from dislocation mechanisms.

Dislocation mechanism length scale	Symbol	Typical size
Dislocation core size	R_c	1 nm
Stacking fault width	w_{sf}	Several nm
Range of elastic stress field	R_e	?
Dislocation spacing	$\lambda = \frac{1}{\sqrt{\rho_D}}$	Highly variable, from 10 nm to 1 µm
Dislocation source spacing (inside grains)	L_S	?
Obstacle spacing (inside grains)	L_O	?
Distance between grain boundaries (grain size)	d	10 nm – 10 µm

Scale-dominant behaviors (i.e., behaviors that are the consequence of specific scaling) can be expected whenever an external length scale approaches one of these internal length scales. Such scale-dominant behaviors are to be viewed differently from the grain size dependent mechanical behaviors described in the previous chapter, in that they arise as a consequence of the competition between an internal and an external length scale, rather than as a consequence of competition between two internal length scales (which are the cause of most grain size strengthening mechanisms).

Consider, for instance, the mechanical behavior of a micropillar studied using the micro-compression technique described in Chapter 3. The two external length scales that define a micropillar are the diameter d_m and the height. Most experimentalists ensure that the height is a fixed multiple of the diameter (usually twice the diameter) in order to obtain accurate measurements of material behavior (Zhang et al., 2006), and so we can view the diameter as the only external length scale of interest. Clearly one would not expect the micropillar to have the same behavior as the bulk polycrystalline material if the grain size is comparable to the pillar diameter (i.e, $d_m \approx d$), since the averaging associated with many crystals is no longer possible.

If the micropillar diameter were to be smaller than the typical grain size, then the typical micropillar specimen would be a single crystal specimen. IF the single crystal contains an initial dislocation density, then the interaction that develops is certainly between the pillar size and the dislocation spacing, but there is also now the question of whether new dislocations can be generated inside the single crystal, which relates to the dislocation source spacing. If there are other obstacles inside the single crystal, such a dispersoids or precipitates, these scale interactions will also be important. In the specific case of a single crystal containing no other obstacles and no additional dislocation sources, the interaction between the specimen size and the dislocation spacing can evolve in a complex way, since a pre-existing dislocation density can be modified by the presence of free surfaces (which attract the dislocations because of the image forces), resulting in a reduction of the effective dislocation density. Such a dislocation starvation process (Greer and Nix, 2006) could result in the development of apparent enhanced strength. Similar issues arise with metal nanowires and some thin films (Nix et al., 2007).

7.2.2 Deformation Twinning

Deformation twins are small finite regions of a crystal that become reoriented during deformation (Figure 7.7), and deformation twinning provides another inelastic deformation mechanism, because collections of deformation twins are able to provide a macroscopic inelastic deformation. This is a deformation mechanism that is observed very often in some materials (for example, HCP metals like zirconium and hafnium) and only rarely in others (for example, aluminum). The mechanism is of interest to us because it is sometimes observed in nanomaterials even when it does not appear under equivalent conditions in coarse-grained versions of the material; it is thus a mechanism that is scale-dependent.

Deformation twinning processes have been studied for many years. One of the seminal papers in this area is that of Christian and Mahajan (Christian and Mahajan, 1995). Several characteristics of deformation twinning have been identified (although most of the work is in metals):

- First, the onset of deformation twinning appears to be relatively athermal, controlled more by the applied stress than by the current temperature or strain rate (in contrast, note the dislocation mechanisms are typically both temperature and strain rate-sensitive)
- Second, it appears that a critical stress is required to develop substantial twinning, although there is substantial argument over whether this is a threshold stress or simply a stress range
- Third, materials with high stacking fault energies (like aluminum) appear to have difficulty twinning

Nanocrystalline materials generally (but not always) twin more easily than their conventional grain-sized cousins. The reason for this remains somewhat unclear.

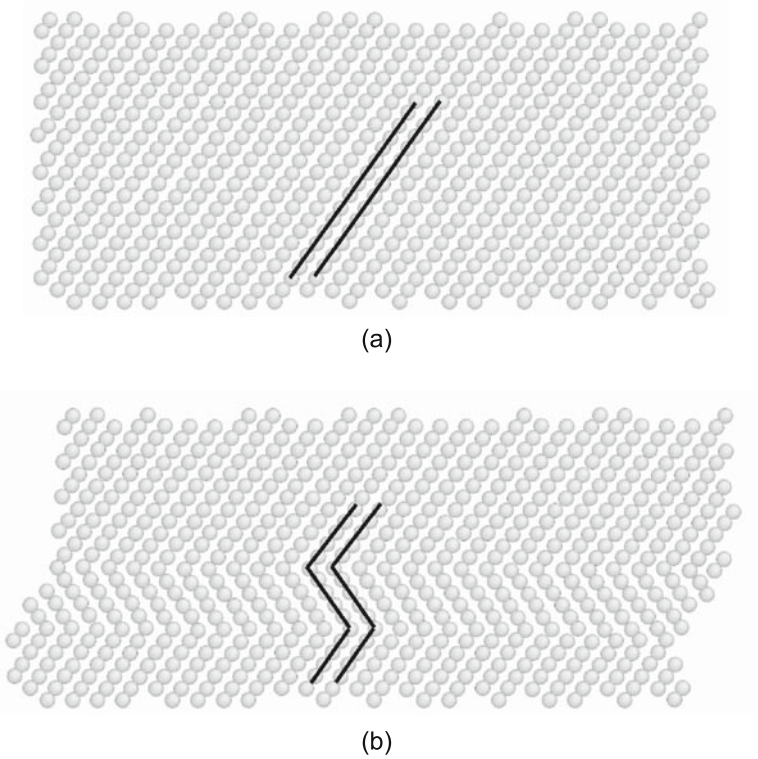

Fig. 7.7 The development of a twinned region in a material. The figures show the results of a molecular dynamics calculation of the simple shear of a single crystal of pure aluminum. (a) Atomic arrangement in undeformed crystal before shearing. The *straight lines* are drawn to guide the eye to the atomic arrangement. (b) After shearing, a region of the crystal has been reoriented (this region is called the twin). The twin boundaries can be viewed as mirror planes, and the *lines* show the new arrangement of the atoms.

Part of the difficulty is fundamental: there is no single accepted model that explains all of the observations of deformation twinning. A brief and high-level review of the basic concepts associated with deformation twinning is presented here.

Experimental observations demonstrate that deformation twins are nucleated, grow in length and width (Figure 7.8), and then interact with other twins. Models for deformation twinning must therefore account for nucleation, growth, and interaction. There is some understanding of the processes associated with the nucleation of deformation twins, and we shall discuss these processes shortly. However, there is little understanding of the dynamics associated with the growth of deformation twins, and there are few models that handle the processes associated with the interaction of twins. This lack of understanding of the fundamental mechanism places real limits on the development of models for the scale-dependence of deformation twinning in conventional and nanocrystalline materials:

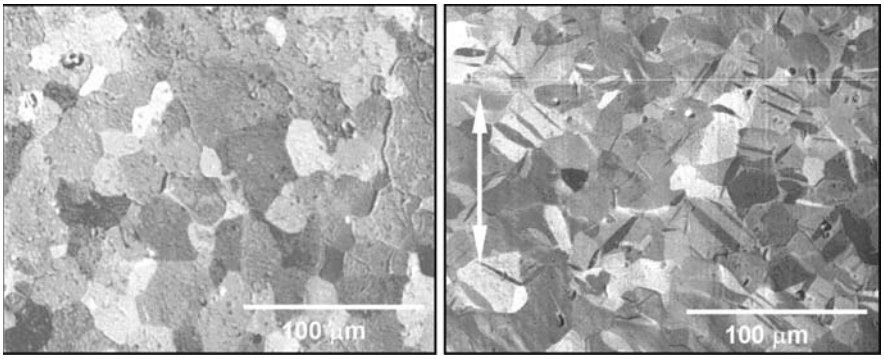

Fig. 7.8 Example of deformation twins in a metal (the hcp metal hafnium). (a) Initial microstructure before deformation. (b) Twinned microstructure after compressive deformation at low strain rates and at 298K. The twinned regions are the lenticular shapes within the original grain structure.

- The classical view of *twin nucleation* uses the idea that a twinned region in a crystal can be generated by the coordinated development of stacking faults within the crystal. A stacking fault is generated when a full dislocation dissociates into two partials, and one of these partial dislocations (called the leading partial) moves through the crystal ahead of the *trailing* partial. If a second stacking fault is generated on an adjacent layer of the crystal through the motion of partials on that layer, the crystal now contains a two layer defect. Conventionally, two stacking faults are not considered sufficient to be called a twin. If a third set of partials moves through the crystal on the third adjacent layer, the resulting three layer rearrangement is often called the twin nucleus. The question of twin nucleation thus amounts to the question of the generation of a twin nucleus consisting of three layers through the coordinated motion of partial dislocations. Twin nucleation has thus been addressed by examining the energetics of the generation of stacking faults and the forces associated with the motion of partial dislocations (e.g., Kibey et al., 2007).
- The *growth of twins* is a much thornier problem, because it involves several components: the energetics of growth, the dynamics of growth and the interaction with potential dislocation mechanisms. Twin growth is relatively fast, and many materials scientists speak of twin growth as essentially instantaneous. However, from an energetic viewpoint, the rate of twin growth must be controlled by some as-yet undefined driving force (the beginnings of such models have been developed for the twins that are observed in shape memory alloys (Rosakis and Tsai, 1995). Such growth models are important in being able to understand completely the common observation that twins occur more often in materials subjected to high-rate deformations.
- The *interaction of twins* with existing dislocation structures, the interaction of dislocations with twin boundaries, and the interactions of twins with other twins represent very complex mechanics and materials issues. Multiple twin populations are often observed in metals subjected to large strains at high-strain-rates. It

is apparent that twin nucleation is affected by the presence of pre-existing twins, and the shapes of twinned boundaries appear to be connected to the character of the local twin population. Current models are not capable of predicting even the likely fraction of the crystal that is twinned after a given deformation.

A general, if phenomenological, way of thinking about deformation twinning is to view twin development as a mechanism that competes with dislocation mobility. The idea here is that twinning will occur if a critical stress is reached, and that the material chooses either to deform through dislocation motion or through twinning, based on the available stress. The dislocation mobility is low for low temperatures or high strain rates, and so high stresses are required in order to develop plastic deformations. Deformation twins may develop instead of dislocation slip as a consequence of the high stresses. Thus, one would argue that at low temperatures, the mobility of dislocations is relatively low, and so a material may prefer to twin rather than deform through dislocation motion. Similarly, under high rates of loading, inertial or strain-rate history effects may be such as to make it difficult to move dislocations, so that twinning becomes the preferred mechanism. For the specific case of titanium, this was shown by Chichili et al. (1998) in Figure 7.9, which presents the measured twin number density as a function of the applied stress for a variety of conditions, including low and high strain rates and low and high temperatures.

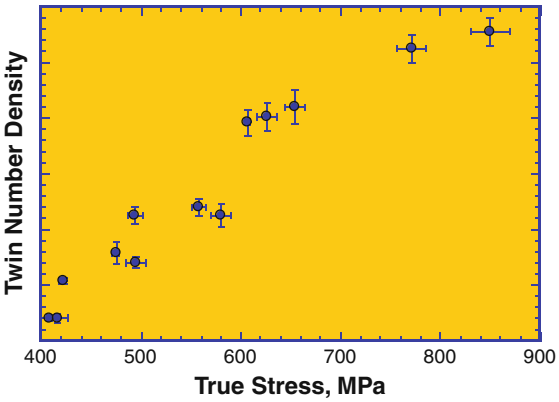

Fig. 7.9 Evolution of twin number density in titanium with applied stress, over a variety of strain rates and temperatures. The twin density is not correlated with strain rate or temperature (or strain), but only with applied stress (Chichili et al., 1998). Reprinted from Acta Materialia, Vol. 46, Issue 3, page 19, D.R. Chichili, K.T. Ramesh, K.J. Hemker, *The high-strain-rate response of alpha-titanium: experiments, deformation mechanisms and modeling*. Jan. 1998 with permission from Elsevier.

How does this relate to the question of twinning in nanomaterials? One could argue (as some do) that as the overall stress level that must be applied to deform nanomaterials increases, the probability of finding twins increases (i.e., because of the high applied stresses, it becomes possible to nucleate twins in a nanocrystalline version of a material that would not twin easily in conventional grain sizes). A more

substantive approach is to consider the stress levels required to nucleate partial dislocations as compared to full dislocations, e.g., (Chen et al., 2003a). The shear stress τ_f required to nucleate a full dislocation from a dislocation source of size d, assuming that the grain boundary is the source, is

$$\tau_f = \frac{2\alpha\mu b_f}{d}, \tag{7.8}$$

where $\alpha = 0.5$ for edge dislocations and $\alpha = 1.5$ for screw dislocations, μ is the shear modulus, and b_f is the Burgers vector corresponding to the full dislocation. In contrast, the shear stress τ_p required to generate the partial dislocation that results in twin nucleation must account for the additional work associated with the stacking fault:

$$\tau_p = \frac{2\alpha\mu b_p}{d} + \frac{\gamma}{b_p}, \tag{7.9}$$

where b_p is the Burgers vector associated with the partial dislocation and γ is the stacking fault energy. Identifying the grain boundaries as the dislocation sources allows one to associate these stresses with the grain size. For most materials under most conditions, $\tau_p > \tau_f$, full dislocations are preferentially generated, and twinning is unlikely. The stresses required to nucleate full and partial dislocations will be equal when

$$d_c = \frac{2\alpha\mu(b_f - b_p)b_p}{\gamma}. \tag{7.10}$$

At grain sizes below this critical grain size d_c, the nucleation of partial dislocations becomes easier than the nucleation of full dislocations and this partial dislocation generation implies that twinning may become a preferred deformation mode. Note that the Burgers vector for the full dislocation is always greater than the Burgers vector for the partial dislocation. The preferential generation of partial dislocations over full dislocations in nanocrystalline materials has also been observed in molecular dynamics simulations (Yamakov et al., 2002). More sophisticated models of this type have also been developed, which account for the different stresses that are required to generate leading partials, trailing partials and twinning partials (Liao et al., 2003). The potential increased incidence of twinning in nanocrystalline materials will have implications for the multiaxial constitutive functions that must be used to describe the mechanical properties of these materials.

An example of twinning in a nanocrystalline aluminum (mean grain size of 50 nm) is shown in Figure 7.10 (Cao et al., 2008). Aluminum has a high stacking fault energy, and does not appear to twin at conventional grain sizes, but develops deformation twins at nanocrystalline grain sizes, as first shown by (Chen et al., 2003a).

A second way in which deformation twinning has become of interest in nanocrystalline materials is based on the idea that the twin boundaries represent additional obstacles (akin to grain boundaries) or provide additional degrees of freedom in terms of deformation. Some highly twinned nanocrystalline or ultrafine grained materials have been observed to have both high strength and high ductility (Dao et al., 2006; Chen and Lu, 2007). The precise reasons for this behavior remain unclear as of this writing.

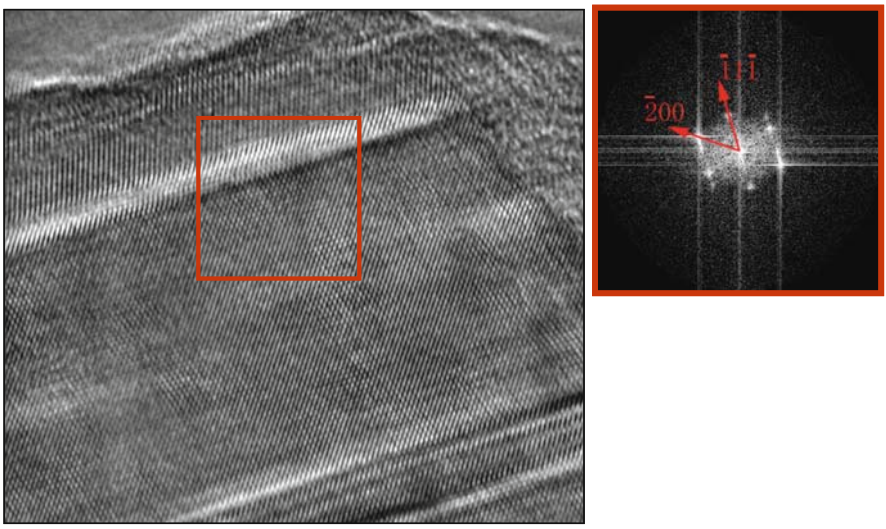

Fig. 7.10 High resolution electron micrograph of deformation twins developed in nanocrystalline aluminum subjected to large shearing deformations (Cao et al., 2008). The diffraction pattern on the right demonstrates the twinned character.

7.2.3 Grain Boundary Motion

The fact that the grain boundary volume fraction begins to dominate the behavior of bulk nanocrystalline materials leads one to examine the possible mechanisms that are directly associated with the grain boundary. To this point, we have discussed two different ways in which the grain boundary can affect the behavior of the material. First, the grain boundary may act as an obstacle to dislocation motion, or in general as an obstacle to the development of compatible deformations. Second, the grain boundary may act as a *source* of dislocations (or twins), and thus may actually aid the development of plastic deformations. However, the existence of so many grain boundaries also makes possible deformation mechanisms that directly invoke movement of (or at) the grain boundary. Idealizing the grain boundary as a plane separating two grains, one sees (Figure 7.11) that two motions are possible: (a) normal to the grain boundary and (b) in the plane of the grain boundary. In vector form, this can be expressed as

$$\boldsymbol{\delta} = \delta_n \mathbf{n} + \delta_t \mathbf{t} \tag{7.11}$$

where δ_n is the normal displacement of the boundary and δ_t is the tangential (in-plane) displacement of the boundary. The first component results in the growth or the shrinkage of the grain, while the second results in the relative sliding of two grains.

In general, thermodynamics does not favor the shrinkage of the grain, unless substantial amounts of energy are provided. In contrast, particularly in nanocrystalline

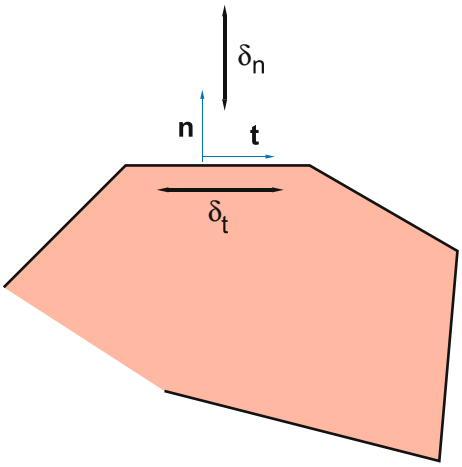

Fig. 7.11 The possible grain boundary motions: displacements δ_n in the direction normal to the GB (grain growth or shrinkage), and δ_t in a direction tangential to the plane of the boundary (grain boundary sliding). The unit normal vector is **n** and the unit tangent vector is **t**, as in Equation (7.11).

materials, thermodynamic processes favor grain growth. Thermally assisted grain growth is familiar to most mechanical engineers and materials scientists, since this is a classical method of grain coarsening and develops routinely during annealing processes. However, grain growth can also be a stress assisted process (Gianola et al., 2006), and this may be of importance to many deforming nanocrystalline solids.

Grain boundary sliding is a mechanism that is well known from studies of creep deformations of materials. This mechanism is not discussed in any detail here, but the approach itself is a classical one in materials science (e.g., Ashby and Verrall, 1973), involving diffusive processes.

7.2.4 Grain Rotation

As the grain size decreases, the grains in the bulk nanocrystalline materials become harder (in the sense that they do not deform easily). Is there a point at which a nanocrystalline material can be treated like a granular solid? The limiting condition would appear to be one of elastic grains deforming as a granular assembly. However, most bulk nanocrystalline materials cannot be viewed in this way at any length scale, because they generally maintain compatible deformations even at the grain boundaries (except perhaps at triple points or junctions) and because they usually retain the ability to develop some plastic deformations. Plastic deformations have been observed in the TEM for grain sizes as small as 5 nm. Still, the increasing strength suggests that some of the concepts that are relevant to granular materials may

also be important for nanocrystalline materials. We examine one of these concepts in this section.

There are two motions of grains (rather than grain boundaries) that may be of interest in nanocrystalline solids: grain translation and grain rotation. The rigid translation of grains is generally not a significant mechanism, although this may be important in the case of very heterogeneous grain size distributions. The rotation of grains, however, plays a significant part in accommodating deformations. For example, grain rotations have been observed in the development of shear bands in nanocrystalline metals (Wei et al., 2002). Joshi and Ramesh (2008b) have demonstrated that grain rotations lead directly to the development of localized shearing deformations in nanocrystalline solids, and suggest that this mechanism may result in the development of limited stable deformations and specific grain size regimes (Joshi and Ramesh, 2008c). The core concepts are discussed in this section.

There are few theoretical investigations of shear banding in bulk nanocrystalline materials as a function of grain size. The continuum approach cannot predict such size effects because of the absence of a length-scale in the governing equations. Strain gradient plasticity theories can be used, but these theories do not explicitly account for grain size (Carsley et al., 1997; Zhu et al., 1997). Joshi and Ramesh modeled the growth of shear bands in nanocrystalline and ultrafine-grained materials using an explicit consideration of grain rotation driven geometric softening. The model considers the development of shearing instabilities through a visco-plastic constitutive law for the material response coupled with micromechanics-based softening through grain rotation, motivated by the observations of Jia and co-workers (Jia et al., 2003; Wei et al., 2002). The grain size enters naturally through the grain rotation mechanism in this model.

The essence of the model is as follows. Assume that each grain in the material has anisotropic plastic behavior, with a hard orientation and a soft orientation, as shown in Figure 7.12a. The initial state of the material has all of the grains randomly oriented. Now, the average response of the polycrystalline material will clearly be different if the grains are all oriented in a specific direction. For example, a material with all of the grains oriented so that the soft orientation is in the direction of shearing will need a lower shear stress (than the randomly oriented polycrystalline material) to sustain further plastic deformation. Because the shear strength of the material decreases with grain orientation (this is called *geometric softening*), the grains will tend to rotate so that the soft plastic direction rotates into the direction of shearing. The model of Joshi and Ramesh demonstrates that a consequence of this specific geometric softening behavior is shear localization, that is, the development of the shear band. This is illustrated in Figure 7.12b, where the random orientation of the grains is shown as having changed into a specific orientation within a localized region called the shear band.

Consider the one-dimensional shear problem (Figure 7.13) of an infinitely long slab with finite thickness W subjected to a constant nominal shear strain rate $\dot{\gamma}_a$. In the absence of inertia (i.e., for slow loading), the balance of linear momentum reduces to an equilibrium equation, $\frac{\partial \tau}{\partial X} = 0$, where τ is the shear stress and X is the

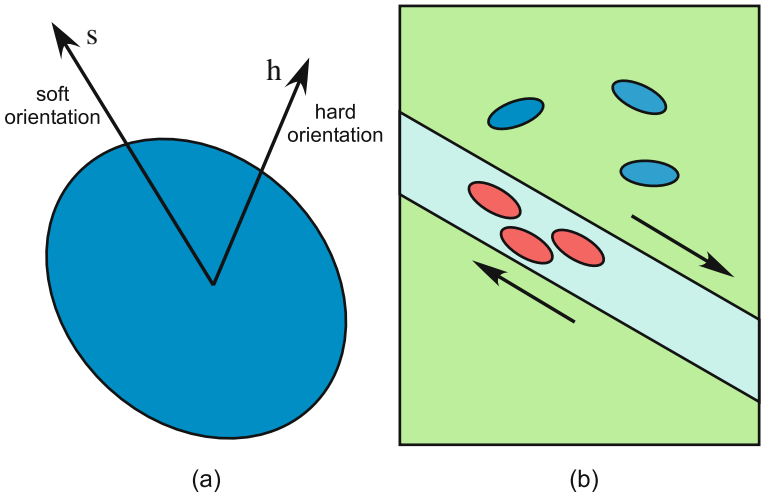

Fig. 7.12 (a) Schematic of a grain showing its soft and hard orientations (with respect to plastic deformation, not elastic stiffness). (b) The grains are initially randomly oriented in the material, but begin to orient themselves so that the soft direction is in the direction of shearing, and the process of grain rotation into the soft orientation results in the localization of the deformation into a shear band.

thickness direction. For simplicity, only isothermal problems are considered here (note that this eliminates the consideration of adiabatic shear bands). The material is assumed to be elastic/viscoplastic, so that the total strain rate can be decomposed into an elastic strain rate and a viscoplastic strain rate: $\dot{\gamma} = \dot{\gamma}_e + \dot{\gamma}_p$. From this we obtain

$$\dot{\tau} = \frac{\partial \tau}{\partial t} = \mu \dot{\gamma}_e = \mu(\dot{\gamma}_a - \dot{\gamma}_p), \tag{7.12}$$

where μ is the elastic shear modulus, $\dot{\gamma}_e$ is the average elastic strain rate, $\dot{\gamma}_p$ is the thickness-averaged plastic strain rate defined by $\frac{1}{W}\int \dot{\gamma}_p dX$, and the total applied strain rate is $\dot{\gamma}_a = \dot{\gamma}_e + \dot{\gamma}_p$.

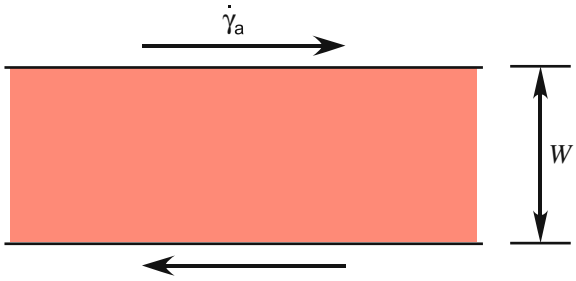

Fig. 7.13 Schematic of simple shearing of an infinite slab, showing the terms used in examining the shear localization process in simple shear (Joshi and Ramesh, 2008b).

A viscoplastic constitutive law is assumed for the material, assuming power-law strain hardening and power-law rate hardening, and allowing for the geometric softening that arises from grain rotation:

$$\frac{\tau}{\tau_0} = \left(1 + \frac{\dot{\gamma}_p}{\dot{\gamma}_0}\right)^m \left(1 + \frac{\gamma_p}{\gamma_p}\right)^n (1 - \bar{c}\phi), \tag{7.13}$$

where ϕ is an internal variable defined (in the next paragraph) as the number fraction of grains in a given region that have the soft orientation aligned to the shearing direction, and γ_p is the plastic strain. The terms $\dot{\gamma}_0$, τ_0, γ_0, n, and m in Equation (7.13) represent the characteristic strain rate, yield strength (of the polycrystalline material), yield strain (corresponding to τ_0), strain hardening index, and strain rate sensitivity, respectively. The factor $\bar{c}$ is defined as $\bar{c} = 1 - \frac{\tau_{s0}}{\tau_{h0}}$ where τ_{h0} and τ_{s0} are the yield strengths of the grain in the hard and soft orientations (corresponding to a single crystal).

By solving this equation for the strain rate, we obtain the evolution of plastic strain corresponding to this constitutive law:

$$\dot{\gamma}_p = \dot{\gamma}_0 \langle \left[\{ \frac{\tau}{\tau_0} \frac{1}{(1 - \bar{c}\phi)} \left(1 + \frac{\gamma_p}{\gamma_0}\right)^{-n} \} \right]^{\frac{1}{m}} - 1 \rangle, \tag{7.14}$$

where $\langle . \rangle$ is defined through $\langle f \rangle = \frac{(f + |f|)}{2}$.

7.2.4.1 Definition of the Internal Variable

Consider a representative volume element (hereafter referred to as an RVE or a *bin*) that contains a large number of grains N_b (b for bin). We define the internal variable as $\phi(t) = \frac{N_s}{N_b}$, where N_s is the number of grains in the bin that have the soft orientation aligned with the shearing direction, and the evolution of ϕ represents the evolution of rotation of the grains. Thus, as more and more grains rotate into the soft shearing orientation, ϕ increases and (through the $(1 - \bar{c}\phi)$ term) a softening mechanism develops. Joshi and Ramesh demonstrated that this softening mechanism leads to localization, with a shear band that is essentially the region where $\phi \approx 1$.

7.2.4.2 Evolution of the Internal Variable

The fraction ϕ of soft-oriented grains evolves through contributions from two specific mechanisms:

$$\dot{\phi} = \dot{\phi}_1 + \dot{\phi}_2. \tag{7.15}$$

The first component $\dot{\phi}_1$ in Equation (7.15) represents the contribution of overall plasticity (Figure 7.14) to grain rotation, while $\dot{\phi}_2$ represents the contribution due to interaction of a grain with nearest neighboring grains (Figure 7.15d). ϕ ceases to grow once it reaches unity (since no further re-orientation is possible), so that $\dot{\phi} = 0$ when $\phi = 1$.

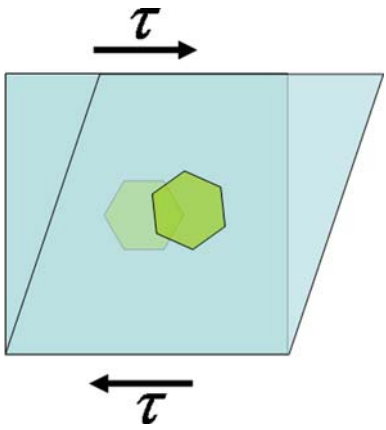

Fig. 7.14 Schematic of the rotation of ensemble of nano-grains occupying region $\mathfrak{R}$ embedded in a visco-plastic sea S subjected to shear. The *background image* shows the undeformed configuration.

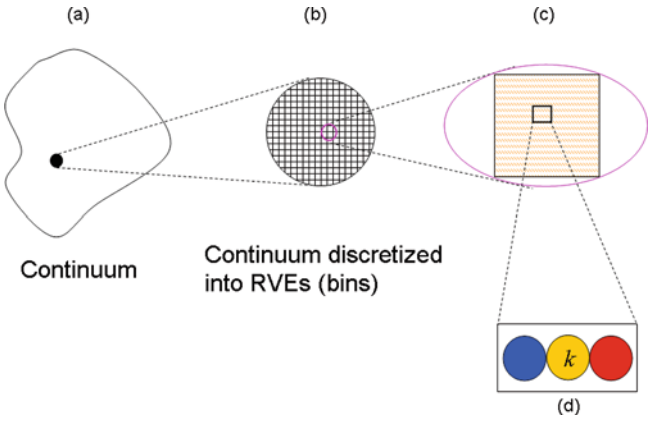

Fig. 7.15 A hierarchical approach to homogenization of grain rotation due to interface traction. (a) Material continuum. (b) Collection of bins in sample space. (c) Grains within a RVE. The *colored shading* represents the average grain orientation in that bin. (d) Interaction at the grain level. Grains with individual orientations are described by different colors.

7.2.4.3 Contribution of Overall Plastic Deformation

We focus on the contribution to rigid rotation of an ensemble of grains ($\mathfrak{R}$) due to overall plastic deformations in the viscoplastic sea (S) surrounding the ensemble (Figure 7.14). Strain compatibility at the interface of $\mathfrak{R}$ and S gives a rotation rate that is proportional to the rate of plastic deformation. Thus, the contribution of overall plastic deformation to the evolution of ϕ is given to first order by

$$\dot{\phi}_1 = \psi(\phi, \bar{d})\dot{\gamma}_p \tag{7.16}$$

where $\bar{d}$ is the mean grain size within the ensemble. The function ψ indicates the ease with which the ensemble $\Re$ can rotate rigidly in the sea, and is referred to as a *fabric factor* (because it represents, in some sense, a measure of the local *fabric* or microstructure). An ensemble residing in a region where surrounding grains are soft ($\phi > 0$) will rotate with relative ease as the soft surrounding medium deforms plastically. On the other hand, in a region where the grains are randomly oriented ($\phi \approx 0$), rotation (in the direction consonant with macroscopic shear) is difficult because the surrounding grains will not deform easily. For simplicity, let us set $\psi(\phi, \bar{d}) = \psi_0$, where ψ_0 is of order 1–10.

In practice, ensembles with very small $\bar{d}$ will tend to rotate to accommodate the global plastic deformations, while those with large $\bar{d}$ will tend to deform plastically through crystallographic slip. The mean grain size in the ensemble is determined from the grain size distribution, and in this way the grain size distribution may affect $\dot{\phi}_1$.

7.2.4.4 Contribution of Inter-Granular Interaction

Grain rotation may also be caused by the local interactions of a single grain with its neighboring grains of similar size. Grain rotation models based on interfacial contact resistance have been successfully implemented in simulating granular flow (Iwashita and Oda, 1998) including elastoplastic contact (Hu and Molinari, 2004). This latter elastoplastic contact mechanism can be included in this model for grain rotation in nanocrystalline materials through a hierarchical scheme. Using a three-grain model, the concept of interfacial interaction at the grain level is used to determine a driving force for rotation; subsequently, an evolution law for grain rotation is prescribed in terms of the driving force.

In granular materials, rolling resistance causes neighboring grains to create interfacial traction. Consider the interaction between three adjacent grains as shown in Figure 7.15 (for simplicity, we consider a 2D case).

Let the current rotation angles of the three grains (a, b and c) in Figure 7.15d be denoted as θ_a, θ_b and θ_c, respectively. Focusing on the central grain (b) and assuming that $\theta_a > \theta_b > \theta_c$, the interfacial tractions on grain b are then

$$F|_{ab} = k_t|_{ab}\delta_t|_{ab} \tag{7.17}$$

due to the interaction with grain a, and $F|_{bc}$ due to the interaction with grain c:

$$F|_{bc} = k_t|_{bc}\delta_t|_{bc}, \tag{7.18}$$

where k_t is the effective contact stiffness and the tangential displacements are δ_t (see Equation 7.11). These tangential displacements are of the form

$$\delta_t|_{ab} = \delta_t|_a - \delta_t|_b + R_a(\theta_a) - R_b(\theta_b), \tag{7.19}$$

with R_a and R_b denoting the radii of grains a and b. The grain boundary sliding mechanism is represented by the term $\delta_t|_a - \delta_t|_b$. Since this section is only considering grain rotation, we set the grain boundary sliding to zero, so that $\delta_t|_a - \delta_t|_b = 0$. Further, let us assume that all of the grains are the same size, so that $R_a = R_b = \frac{d}{2}$, where d is the grain diameter. Then Equation (7.19) gives us

$$\delta_t|_{ab} = \frac{d}{2}(\theta_a - \theta_b), \tag{7.20}$$

$$and \delta_t|_{bc} = \frac{d}{2}(\theta_b - \theta_c). \tag{7.21}$$

The net interface traction (per unit length) on grain b is

$$[\Delta F]_b = F_{ab} - F_{bc}, \tag{7.22}$$

and using Equations (7.20) it follows that

$$[\Delta F]_b = \frac{k_t d}{2}[\theta_a - 2\theta_b + \theta_c]. \tag{7.23}$$

The corresponding net torque on grain b is then given by

$$T_b = \frac{d}{2}[\Delta F]_b = \frac{k_t d^2}{4}[\theta_a - 2\theta_b + \theta_c]. \tag{7.24}$$

But what is the tangential contact stiffness k_t? This can be obtained from elastic-plastic contact micromechanics (Stronge, 2000). The contact stiffness of grains undergoing elasto-plastic deformation is given in terms of the radius r_c of the contact area by

$$k_t|_{ab} = \frac{8r_c}{C_{ab}}, \tag{7.25}$$

where C_{ab} is called the contact compliance for the two grains in the contact and is given by (Stronge, 2000)

$$C_{ab} = \frac{1-\nu_a}{\mu_a} + \frac{1-\nu_b}{\mu_b} = \frac{2(1-\nu)}{\mu}, \tag{7.26}$$

using the shear modulus (μ) and Poisson's ratio (ν), and assuming that these moduli are identical for the two grains.

In general, the contact area will evolve as grains rotate (Conrad and Narayan, 2000; Van Swygenhoven and Derlet, 2001), and will be higher for plastic contacts than for elastic contacts. Let us, however, assume a fully plastic contact for a polycrystalline material and set the radius of the contact equal to the grain radius, so

that $r_c = \frac{d}{2}$. Using Equations (7.26) in (7.25) and then using the result for $k_t|_{ab}$ in Equation (7.24), we obtain the driving force for grain rotation as the torque:

$$T_b == \frac{\mu d^3}{2(1-\nu)}[\theta_a - 2\theta_b + \theta_c]. \tag{7.27}$$

How will the grain respond to this driving force? The response will clearly depend on the surrounding grains and their grain boundaries as well. To simplify the problem, we postulate a kinetic relation between the evolution of grain rotation and the driving force, with the rate of rotation given by

$$\dot{\theta}_b = (m_r T)_b, \tag{7.28}$$

where m_r is a mobility coefficient, representing the resistance provided by the surrounding grains to the rotation of grain b. Equation (7.28) is similar to those adopted in describing grain rotation coalescence (Moldovan et al., 2001). In the latter work the driving force is due to anisotropic grain boundary energies and the plastic deformation is accommodated by grain boundary and lattice diffusion mechanisms, which are believed to be dominant at very small grain sizes ($d < 10$ nm) and at elevated temperatures. Similarly, in defining the mobility, we account for the viscoplastic resistance offered by the region surrounding the rotating grain.

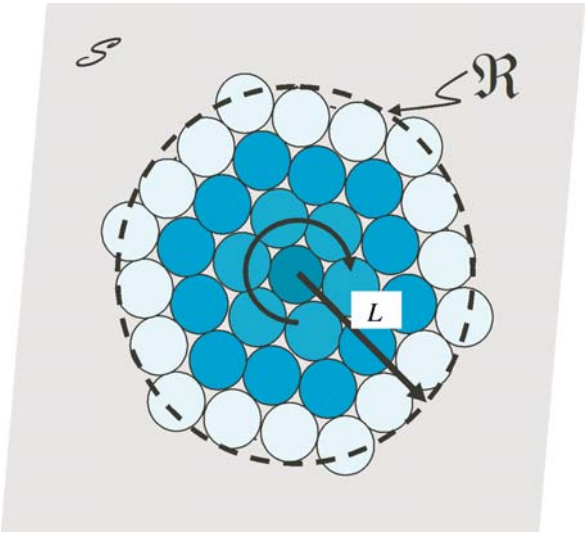

Fig. 7.16 Enlarged view of $\mathfrak{R}$ (Figure 7.14) showing intergranular interaction in the region. Rotation of the central grain is accomodated by rotation of the surrounding grains over a length L.

The key concept with respect to grain rotation is the following. Consider the rotation of a specific grain such as the central grain shown in Figure 7.16. If you were to be an observer sitting on another grain that is sufficiently far away from the rotating

grain, you will not even be aware that the central grain has rotated. However, grains neighboring the central grain will have to rotate to some degree to accommodate the rotation of the central grain. That is, the rotation of any single grain must be accommodated by the surrounding grains (and the grain boundaries), but there is a finite length (L) over which this accommodation occurs (Figure 7.16) and grains sufficiently far away from the rotating grain are unaffected by the rotation. This finite length (L) will depend on the interactions between the grains, and in particular on interactions at the grain boundaries (although the degree of plastic deformation of the grains will also be involved). The length scale for *rotational accommodation* will be smaller for elastoplastic grains (as in polycrystalline metals) than for purely elastic grains (a limiting example of which would be sand). This rotational accommodation mechanism must be present in all granular solids that contain some dissipative mechanisms (which may be localized to grain boundaries).

Using this rotational accommodation concept, we can (from a dimensional analysis viewpoint) define the mobility due to the viscoplastic resistance in terms of the accommodation length scale as

$$(m_r)_b = \frac{1}{L^3}\left(\frac{1}{\eta_{eff}}\right), \tag{7.29}$$

where η_{eff} is the effective viscosity of the accommodating region. This can be estimated in some cases using molecular dynamics simulations (Van Swygenhoven and Caro, 1997). From a mechanistic viewpoint, the effective viscosity itself can be derived (through addition of the corresponding strain rates) in terms of the intragranular and grain boundary mechanisms using the following argument. The effective strain rate $\dot{\gamma}_{eff}$ in the accommodating region is given by

$$\dot{\gamma}_{eff} = \dot{\gamma}_p + \dot{\gamma}_{gb}, \tag{7.30}$$

where $\dot{\gamma}_p$ is the strain rates due to plastic deformation mechanisms and $\dot{\gamma}_{gb}$ is the strain rate due to deformation at the grain boundaries. Assuming that the stress is uniform across this region, and defining the viscosities in the classical way, we have

$$\frac{\tau}{\eta_{eff}} = \frac{\tau}{\eta_p} + \frac{\tau}{\eta_{gb}}, \tag{7.31}$$

from which it follows that

$$\frac{1}{\eta_{eff}} = \frac{1}{\eta_p} + \frac{1}{\eta_{gb}}. \tag{7.32}$$

Thus the effective viscosity of the accommodating region has contributions from dislocation plasticity (η_p) and grain boundary mechanisms (η_{gb}). For example, the effective viscosity corresponding to grain boundary diffusion-type mechanisms can be computed using

$$\eta_{gb} = \frac{k_B T d^3}{64\delta_{gb}\Omega D_{gb}}, \tag{7.33}$$

where k_B is the Boltzmann constant, T is the absolute temperature, δ_{gb} is the grain boundary thickness, Ω is the atomic volume, and D_{gb} is the grain boundary diffusion coefficient (Murayama et al., 2002). The contribution to the effective viscosity (η_p) from dislocation plasticity is represented by the viscoplastic resistance provided by the grains themselves, and a lower bound for this is

$$\eta_p = \frac{\tau_{s0}}{\dot{\gamma}_0}. \tag{7.34}$$

What is the magnitude of L in Equation (7.29)? As the grain size increases, the likelihood of global plastic deformation dominates the likelihood of rotation, and eventually this grain rotation mechanism is no longer a significant contributor to the deformation and slip becomes the dominant mode of deformation. For most metals, where dislocation slip is relatively easy, grain rotation is unlikely to be an important contributor for grain sizes larger than about 1 µm, and may not be a significant contributor even in the ultrafine grain range. In ceramics, however, grain rotation may be significant even for much larger average grain sizes, because there is so little plasticity in ceramics (on the other hand, however, grain boundary mechanisms for inelastic deformation in ceramics are relatively few). In general, one can describe L in terms of the number j of other grains involved (in a given linear direction in the plane) in accommodating the rotation of a given grain, so that $L = jd$. This length scale is a natural length-scale for a bin. Since very large grains will deform by slip rather than rotate, we assume that L is a fixed length scale for a given material (for example, this might be 1 µm for metals). The number of grains involved in accommodating the rotation is $j = \frac{L}{d}$. In a nano-grained material, many grains ($j > 1$) are involved in the accommodation distance L. A quantitative measure of L remains to be established, but L can be viewed in a manner analogous to the microstructural length scales derived in strain gradient plasticity theories (Gao et al., 1999).

7.2.4.5 Homogenized Representation of Grain Rotation

An expression for the second contribution $(\dot{\phi}_2)$ to the evolution of grain rotation can be derived by homogenizing the evolution of θ over the RVE (Figure7.15c). The average grain orientation over the RVE is

$$\bar{\theta} = \frac{1}{N_b} \sum |\theta_k|. \tag{7.35}$$

The number of favorably oriented grains in a bin is counted by performing a weighted averaging with a penalty function $\zeta_k = \delta(|\theta_k| - \theta_s)$, where θ_s is the favorable orientation (aligned with the band orientation). Note this uses a delta function $\delta(|\theta_k| - \theta_s)$, which has value unity when the argument $(|\theta_k| - \theta_s)$ is zero, that is $|\theta_k| = \theta_s$, and is zero for all other θ_k. Further, note that as $\bar{\theta} \to \theta_s,\ \phi \to 1$. Thus for the RVE we have

$$\phi_2 = \frac{1}{N_b} \sum \zeta_k |\theta_k|. \tag{7.36}$$

The average rate of change of ϕ_2 is then (using the kinetic relation, Equation 7.28)

$$\dot{\phi}_2 = \frac{1}{N_b}\sum \zeta_k \dot{\theta}_k = \frac{1}{N_b}\sum \zeta_k (m_r T)_k. \tag{7.37}$$

Using Equation (7.27), we obtain

$$\dot{\phi}_2 = \frac{k_t d}{4 j \eta_e}\left[\frac{1}{j^2 d^2 N_b}\sum \zeta_k(\theta_a - 2\theta_b + \theta_c)\right]. \tag{7.38}$$

Examining Equation (7.38), we identify the terms in the square brackets as approximating the second derivative $\frac{\partial^2 \phi}{\partial X^2}$ in the continuum limit, so that we develop the rate equation

$$\dot{\phi}_2 = \frac{k_t d}{4 j \eta_e}\frac{\partial^2 \phi}{\partial X^2} = D_r \frac{\partial^2 \phi}{\partial X^2}, \tag{7.39}$$

where we have identified a new *rotational diffusion coefficient* D_r as

$$D_r = \frac{k_t d}{4 j \eta_e} = \frac{1}{j \eta_e}\left(\frac{\mu d^2}{2 - \nu}\right). \tag{7.40}$$

Equation (7.39) may be viewed as characterizing a rotational diffusion mechanism that tends to diffuse variations in ϕ through inter-granular interactions.

Putting together Equations (7.15), (7.16), and (7.40), the net evolution of the internal variable ϕ is

$$\dot{\phi} = \psi \dot{\gamma}_p + D_r \frac{\partial^2 \phi}{\partial X^2}. \tag{7.41}$$

This evolution equation can be integrated together with the momentum balance and constitutive laws to solve the problem of a nanocrystalline material in which grain rotation is a possible mechanism. We now see that the primary consequences of the grain rotation mechanism are the existence of a diffusive term and the corresponding length scale.

The governing equations for the problem of simple shear of a nanocrystalline material incorporating grain rotation are summarized below:

$$\frac{\partial \tau}{\partial X} = 0 \tag{7.42}$$

$$\frac{\partial \tau}{\partial t} = \mu\left(\dot{\gamma}_a - \bar{\dot{\gamma}}_p\right) \tag{7.43}$$

$$\dot{\gamma}_p = \dot{\gamma}_0 \langle \left[\frac{\tau}{\tau_0}\frac{1}{(1 - \bar{c}\phi)}\left(1 + \frac{\gamma_p}{\gamma_0}\right)^{-n}\right]^{\frac{1}{m}} - 1 \rangle \tag{7.44}$$

$$\dot{\phi} = \psi \dot{\gamma}_p + D_r \frac{\partial^2 \phi}{\partial X^2}. \tag{7.45}$$

Boundary conditions and initial conditions must be added to solve these equations. Joshi and Ramesh considered the simple shear of a slab of nanostructured

iron, with initial conditions that are zero everywhere except for the initially uniform shear strain rate. In order to account for typical material variability, an initial defect distribution ϕ_i was assumed in the form $\phi_i(X) = \phi_0 exp[-A(\frac{X}{W} - 0.5)^2]$, where ϕ_0 is the largest initial value of ϕ in the distribution and A is a dimensionless parameter which is like a wave-number. Their results on nanostructured iron are of interest because of the experimental observations of shear bands in this material (Jia et al., 2003).

The values for the various parameters used by Joshi and Ramesh are listed in Table 7.3 (corresponding to polycrystalline Fe). Given the heavy plastic work during severe plastic deformation processes, the parameter $\bar{c}$ was obtained at large strains (~ 1) from the results of Spitzig and Keh (1970) on iron single crystals.

Table 7.3 Basic parameters for grain rotation model in polycrystalline iron, as developed by Joshi and Ramesh.

Parameter	Value
Average grain size d, in nm	300
Shear modulus μ, in GPa	76
Poisson's ratio ν	0.3
Normalizing strain rate $\dot{\gamma}_0$, per second	5×10^{-4}
Normalizing stress τ_0, MPa	900
Perturbation "wave number"	5×10^4
Strain hardening index n	0.01
Rate hardening index m	0.005
Anisotropy factor $\bar{c}$	0.07
Plastic contribution coefficient ψ	10
Maximum initial value of ϕ, ϕ_0	0.005
Far-field initial value of ϕ, ϕ_∞	0
Rotational accommodation length scale L, μm	1.0

For a material with this initial distribution in ϕ, Figure 7.17 shows the evolution of ϕ as a function of nominal strain near the band. The internal variable (representing the degree of rotation of the grains into the soft orientation) increases rapidly at the center of the initially perturbed region once the strain reaches 0.02, and stops evolving ($\dot{\phi} = 0$) once ϕ reaches the maximum value ($\phi = 1$) in the center. Physically, this represents a stage where following the localization the grain reorientation process saturates, so that no further reorientation occurs in that region. At the onset of severe localization, the plastic shear strain rate is very high ($\approx 10^3 \dot{\gamma}_a$). With increasing nominal strain, $\dot{\gamma}_p$ drops in the band center (Figure 7.18) in this strain hardening case because ϕ is constant there but the plastic strain continues to grow. Following a fully developed band (defined by a finite thickness over which $\phi = 1$), $\dot{\gamma}_p$ remains high at the edges of the band where ϕ has not saturated. Subsequent band growth is driven by rotational diffusion and strain hardening. The plastic shear strain in the band center is fully resolved by the simulation (Figure 7.19).

In Figure 7.20, the overall stress-strain response for a defect-free material is presented (curve A) and compared with the response obtained from a sample with the perturbation (curve B, solid line). With the perturbation, the sample exhibits

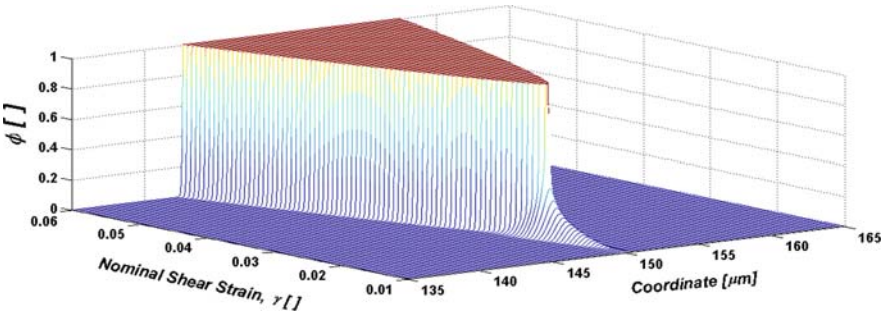

Fig. 7.17 Evolution of grain orientation fraction (ϕ) around the band center. Note the rapid early growth, the spatial localization, and the saturation of ϕ. Also note the spreading of the band, i.e., the increasing band thickness - this is also observed in experiments.

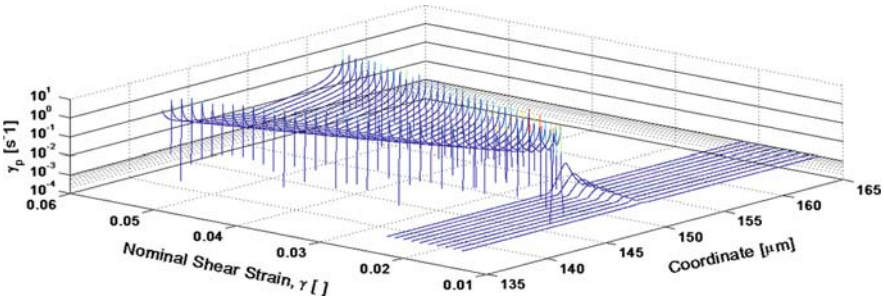

Fig. 7.18 Evolution of plastic shear strain rate ($\dot{\gamma}_p$) around the band center. The greatest activity in this variable is at the band boundaries, where the grains are reorienting into the soft orientation for shear.

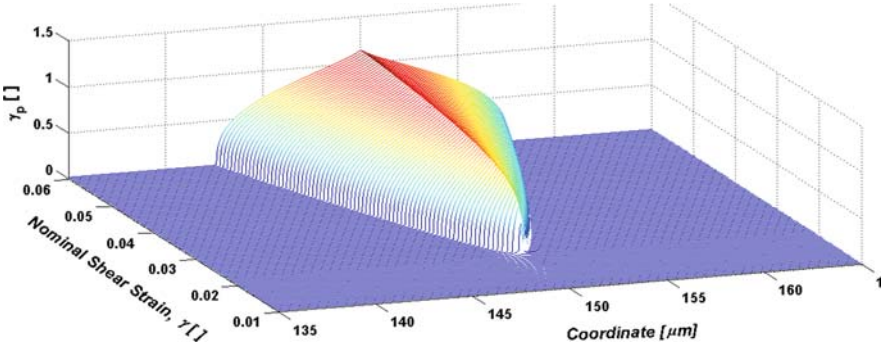

Fig. 7.19 Evolution of the plastic shear strain γ_p around the band center. After localization, γ_p evolves slowly indicating that the plastic flow inside the band develops at the rate of strain hardening at higher nominal strains.

a brief period of strain hardening following yield. The strain hardening is followed by a rapid drop in the stress corresponding to severe localization, with the magnitude of the drop determined by the material hardening and the anisotropy parameters. The nominal strain corresponding to the stress collapse is termed the critical strain γ_{cr}, and should be related to (but less than) experimental measures of the critical strain for localization. Following the stress drop, a softening response is observed. Such a macroscopic softening response of a strain hardening material indicates the dominance of geometric softening over material hardening (Yang and Bacroix, 1996). The softening regime exhibits serrated behavior in the presence of strain hardening (this can be seen at a higher magnification on the stress-strain curve) due to the competition between the hardening and softening variables.

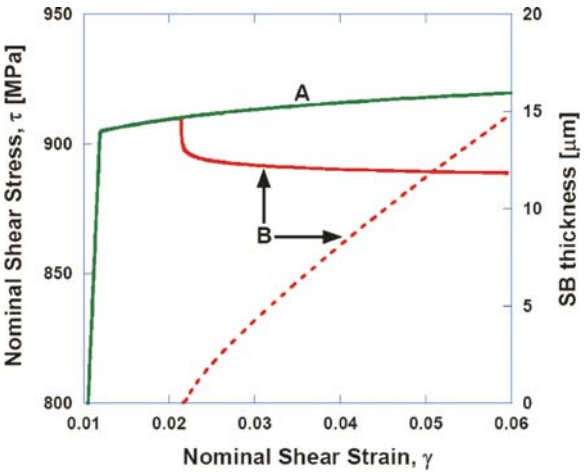

Fig. 7.20 Overall stress-strain response for a defect-free sample (curve A) and a sample with an initial defect in ϕ (curve B). Curve B' indicates the development of the shear band thickness corresponding to curve B.

We define a fully developed shear band as a region where ϕ reaches the maximum value and use this definition to also determine the thickness of the shear band. After localization, the material hardening together with rotational diffusion controls the broadening of the shear band. The development of the thickness of the shear band is also shown in Figure 7.20 as a function of overall strain.

7.2.4.6 Effect of Grain Size

The grain size explicitly appears in two quantities in the governing equations: the polycrystalline yield strength (τ_0) and the rotational diffusion coefficient D_r. Consider three grain sizes (100 nm, 300 nm, and 1 μm), with $n = 0.01$ and $m = 0.005$ held constant for all the grain sizes under consideration. Using the Hall-Petch

relation for Mises yield in iron, the shear strengths $\tau_0 = \frac{\sigma_y}{\sqrt{3}}$ are 1300 MPa, 900 MPa (300 nm), and 290 MPa (1 μm).

Figure 7.21 shows the band thickness evolution for different grain sizes. Whether a shear band will develop is strongly grain size dependent. If a shear band does develop, the band thickness is larger for larger grain sizes (at equivalent nominal strains), because the rotational diffusion term depends on the grain size.

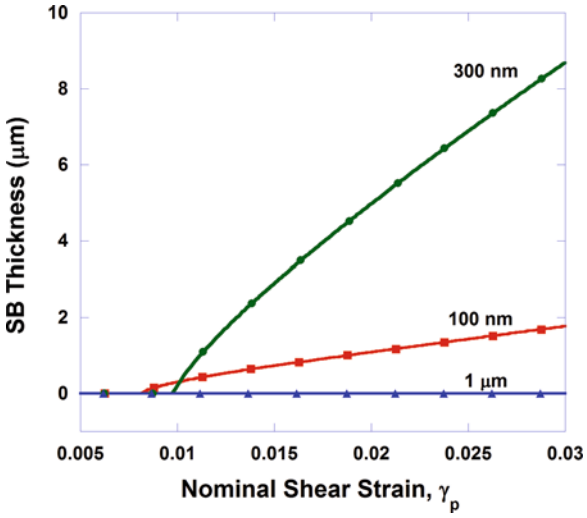

Fig. 7.21 Evolution of shear band thickness for different grain sizes, assuming grain rotation mechanism. The material hardening parameters are held constant for all the grain sizes. The applied strain rate is 10^{-3} s^{-1}.

7.2.4.7 Relative Contributions of Grain Boundary and Grain Mechanisms to η_e

With this definition of the effective viscosity η_e, a transition from dislocation dominated mobility to grain boundary dominated mobility will occur (comparing the two terms in Equation 7.32) at a transition grain size given by

$$d_{tr} = \left(\frac{64 \delta \Omega D_{gb} \tau_{s0}}{k_B T \dot{\gamma}_0} \right)^{\frac{1}{3}}. \tag{7.46}$$

This transition size depends on grain boundary diffusion and grain boundary thickness variables, and is about 9 nm in the specific case of iron. The grain boundary viscosity η_{gb} is likely to be dominant for smaller grain sizes (although it will certainly continue to play a role even at much larger grain sizes). Note that

below the transition grain size we will then have the rotational diffusion coefficient increase as the grain size decreases, because in that domain $\eta_e \sim \eta_{gb}$, and then $D_r \propto \frac{1}{d}$.

7.2.4.8 Comparison with Experiments

Joshi and Ramesh considered two quantitative comparisons between the model and specific experiments: (a) bcc-Fe of Jia et al. (2003), and (b) fcc-Al of Sun et al. (2006). Both experiments under consideration involved uniaxial loading whereas the model was developed for the case of simple shear and considers only a single shear band. However, the model was able to distinguish between the two material behaviors.

Experiments (Jia et al., 2003; Wei et al., 2002) on nanostructured and ultrafine grain iron show that shear bands occur immediately following yield. Joshi and Ramesh were able to reproduce this behavior in the large using physically reasonable parameters. However, in real bcc structures the hardening parameters may be modified by the grain size due to the variety of processing routes used for generating bulk nanostructured materials. Consolidated Fe (Jia et al., 2003) exhibits low but finite strain hardening ($n \approx 0.01 - 0.04$) in the nanostructured regime whereas at larger grain sizes n is high (≈ 0.26) (Malow et al., 1998). Thus the strain hardening increases with grain size in NS-Fe, and the model should account for such variations (similar changes occur in the rate sensitivity, which decreases with grain size).

Using the same perturbation parameters as in the bcc-Fe case, the model predictions were compared with the experimental observations of Sun et al. (2006) on equal channel angular extruded commercially pure aluminum (ECAE-CP-Al). Unlike in the case of the iron, the model does not predict shear banding for these three grain sizes in CP-Al. The quasi-static compression experiments (Sun et al., 2006) also showed no shear bands for 350 and 470 nm cases, although apparently anomalous shear bands were observed for the 590 nm case. Our model does not predict shear band development in such rate-sensitive materials as nanostructured and UFG-fcc metals. Indeed, shear bands have not been reported in NS or UFG pure fcc metals in general, although very "diffuse" bands have sometimes been observed in tension. The rate sensitivity effects are considered further by Joshi and Ramesh (2008a) when applying the grain rotation model to different crystal structures.

7.2.5 Stability Maps Based on Grain Rotation

Some additional understanding can be obtained by considering a scaled version of the governing equations (Equation 7.42) for the simple shear problem including

grain rotation. Let us set up the same governing equations in terms of normalized variables $\hat{X}$ for position, $\hat{\tau}$ for shear stress, and $\hat{t}$ for time, defining these as follows:

$$\hat{X} = \frac{X}{L} \tag{7.47}$$

$$\hat{\tau} = \frac{\tau m}{\tau_{s0}\bar{c}} \tag{7.48}$$

$$\hat{t} = \dot{\gamma}_0 t \tag{7.49}$$

where the scaling uses the parameters defined earlier. Using these scaled variables, the equilibrium condition is now

$$\frac{\partial \hat{\tau}}{\partial \hat{X}} = 0. \tag{7.50}$$

Similarly, the elastic relation from Equation (7.42) (the second equation in that set) becomes

$$\hat{\tau} = \frac{1}{\mathbf{M}}\left(\hat{\dot{\gamma}}_a - \hat{\dot{\gamma}}_p\right), \tag{7.51}$$

where the strength index $\mathbf{M}$ has been defined as

$$\mathbf{M} = \frac{\tau_{s0}\bar{c}}{\mu m}, \tag{7.52}$$

and will be utilized in constructing a stability map. The normalized evolution equation for the internal variable is

$$\hat{\phi} = \psi \hat{\dot{\gamma}}_p + \frac{D_r}{\dot{\gamma}_0 L^2}\frac{\partial^2 \hat{\phi}}{\partial \hat{X}^2}, \tag{7.53}$$

where $\hat{\dot{\gamma}}_p$ is the scaled visco-plastic shear strain rate.

The solution of this system of equations will tell us how the stress, strain, strain rate, and orientation number fraction will evolve for a given material subjected to simple shear. However, we can learn a great deal about the problem by studying the stability of the equations – that is, by finding out under what conditions a perturbation to one of the variables will grow (corresponding to instability) rather than decay (corresponding to stability). The basic approach is as follows: we assume a perturbation in one or more of the variables (e.g., the plastic strain), insert the perturbed solution into the system of equations, and ask whether the perturbation will grow. If it will grow, the system is unstable in that it cannot survive a perturbation; if it will not grow, the system is stable in that it suppresses perturbations and tends towards homogeneous solutions. In what follows, we analyze the stability of the governing equations using linear perturbation analysis (a limited kind of perturbation analysis, which effectively restricts our attention to early times, i.e., the onset of instability rather than the later stages of unstable growth). With $\hat{\tau}$ required to be homogeneous (which is the equilibrium condition), the stability of deformation is investigated by

perturbing the plastic strain γ_p and the internal variable ϕ from their homogeneous solutions, so that

$$\bar{\gamma_p} = {\gamma_p}^h + \delta\gamma_p(\tilde{t})\sin k\hat{X}, \tag{7.54}$$

and

$$\bar{\phi} = \phi^h + \delta\phi(\tilde{t})\sin k\hat{X}, \tag{7.55}$$

where, for example, ϕ^h is the homogeneous solution, $\delta\phi(\tilde{t})$ is the normalized temporal component of the perturbation to the solution (assumed small compared to ϕ^h), and k is the non-dimensional wave-number of the perturbation (we are essentially perturbing the amplitudes of these variables in space with a perturbation wavelength proportional to the reciprocal of k). Substituting the perturbed solutions in the normalized evolution equation (Equation 7.53) and retaining only the first order terms (linearized perturbation analysis) we find that the perturbations will grow only if

$$\frac{\partial\hat{\gamma}_p}{\partial\phi} > \frac{k^2 D_r}{\psi\dot{\gamma}_0 L^2}, \tag{7.56}$$

where the rotational diffusion coefficient D_r and the rotational accommodation length scale L are the quantities defined previously. Equation (7.56) represents the condition for instability. Letting $\phi^h = 0$, the constitutive law gives

$$\frac{\partial\hat{\gamma}_p}{\partial\phi} \approx \frac{\bar{c}}{m}\hat{\gamma}_p^h. \tag{7.57}$$

Thus the condition for instability is

$$\frac{\bar{c}}{m}\hat{\gamma}_p^h > \frac{k^2 D_r}{\psi\dot{\gamma}_0 L^2}, \tag{7.58}$$

from which it follows that the critical wavelength of a perturbation that will lead to a runaway instability is given by

$$\lambda_{critical} = \left[\left(\frac{\dot{\gamma}_0\hat{\gamma}_p^h\psi}{D_r}\frac{\bar{c}}{m}\right)^{\frac{1}{2}}\right]^{-1}. \tag{7.59}$$

This instability condition can be rewritten using the strength index defined earlier (Equation 7.52), giving

$$\lambda_{critical} = \left[\frac{\mathbf{M}}{(2-\nu)\psi\hat{\gamma}_p^h}\frac{d^2}{j}\frac{\eta_p}{\eta_{eff}}\right]^{\frac{1}{2}}. \tag{7.60}$$

Equation (7.60) should be interpreted as follows. It describes the critical wavelength of a perturbation of the system that will grow. That is, if the internal variable ϕ has a perturbation (a local variation) over a region with a size greater than $\lambda_{critical}$ (amounting to a wavelength greater than the critical wavelength), then that perturbation will grow, defining an instability that will become a shear band as shown in

the last section. Perturbations smaller than the critical wavelength will decay and will thus not be sufficient to initiate a shear band. The grain size dependence of $\lambda_{critical}$ appears through D_r in Equation (7.59). Note that if the material parameters are such that $\lambda_{critical} \approx d$, the material is *inherently unstable* in that this perturbation necessarily exists in the material, given the grain size. The condition $\lambda_{critical} < d$ is mathematically possible but is not physically meaningful unless grain size distributions are included.

For most materials the fabric factor ψ will range between 1 and 10. Setting $\psi = 10$ and $\hat{\gamma}_p^h = 1$, with $\dot{\gamma}_0 = 5 \times 10^{-4} s^{-1}$, we can examine the dependence of $\lambda_{critical}$ on grain size. Figure 7.22 shows the relationship between $\lambda_{critical}$ and grain size for three materials (Joshi and Ramesh, 2008c), bcc-Fe, fcc-Cu, and fcc-Al. For all these materials, there are in general three regimes in this log-log plot as the grain size is decreased. In the first regime ($d \geq 100\,\text{nm}$), the critical wavelength decreases with decreasing grain size, the maximum number of participating grains is determined by fixed L, and η_p is the rate limiting process. This rate limiting process continues to dominate the second regime ($100\,\text{nm} \geq d \geq 10\,\text{nm}$), which is governed by the limited number of participating grains, and $\lambda_{critical}$ decreases with a different slope. In the third regime ($d \leq 10\,\text{nm}$), the critical wavelength $\lambda_{critical}$ increases again as the grain size decreases. This is because the dominant rate limiting process changes from being bulk response to grain boundary driven. The region below the line $\lambda_{critical} = d$ in Figure 7.22 is the inherently unstable domain. As an example, for 300 nm grain size Fe, $\lambda_{critical}$ is approximately equal to the grain size. A similar calculation for 300 nm grain size Cu yields $\lambda_{critical} \approx 440\,\text{nm}$, which is somewhat higher than the grain size. Consequently, the Fe is inherently susceptible to instability over

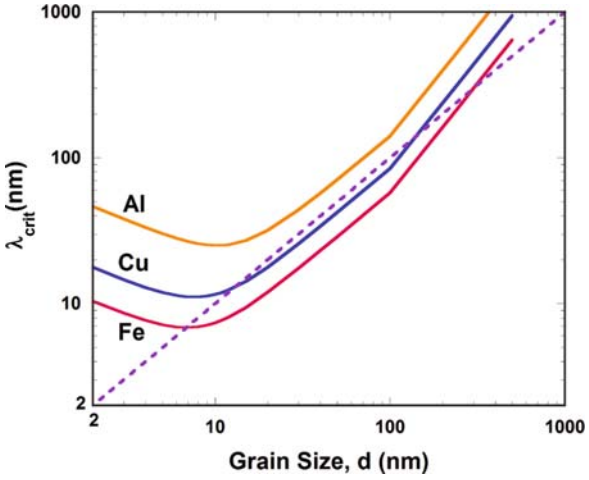

Fig. 7.22 The critical wavelength for instability as a function of grain size for three different metals (note that this is a log-log plot), with the critical wavelength computed using Equation (7.60). This figure has been obtained assuming that $j = 10$ below $d = 100\,\text{nm}$, while for $100\,\text{nm} < d \leq 1\,\mu\text{m}$, we have $L = 1\,\mu\text{m}$ and $j = \frac{L}{d}$. The *dashed straight line* represents the condition that $\lambda_{critical} = d$, which we call the inherent instability line.

a larger range of grain sizes than the Cu. For some materials the entire curve will be above the inherent instability line (e.g., the Al-curve in Figure 7.22). The grain size range over which a material is inherently unstable (if at all) is intimately tied to its elastic properties, plastic anisotropy, and the strain rate sensitivity. Equation (7.60) shows that materials with high crystallographic plastic anisotropy and low rate sensitivity are generally more susceptible to instability.

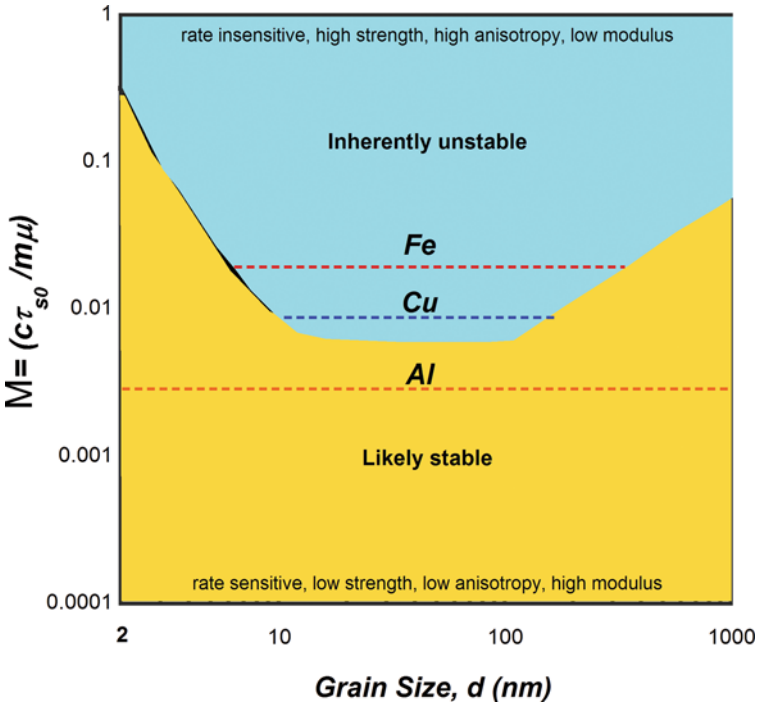

Fig. 7.23 Stability map, showing the domains of inherent instability in materials as a consequence of the rotational accommodation mechanism. The map is constructed in terms of the strength index and grain size, so that every material of a given grain size represents one point on the map, and a *horizontal line* represents all grain sizes of a given material. Reprinted figure with permission from S.P. Joshi and K.T. Ramesh, Physical Review Letters, Stability map for nanocrystalline and amorphous materials, 101(2), 025501. Copyright 2008 by the American Physical Society.

This stability analysis allows one to probe the likelihood of instability in the materials and microstructure space. Figure 7.23 presents a stability map where the ordinate is the previously defined strength index **M** that enables one to compare different materials while the abscissa is the grain size. The curve is the locus of points satisfying the inherent instability criterion ($\lambda_{critical} = d$, which was the straight line in Figure 7.22). If the point representing a given material and grain size lies in the saddle (the blue region), then the material is inherently susceptible to the rotational mechanism of shear instability. In general, materials with low strength indices show susceptibility over a smaller range of grain sizes compared to those with higher

strength indices. Thus, the iron is inherently susceptible to rotational instability over a larger grain size range than the copper, while aluminum does not exhibit any inherent instability. This prediction is qualitatively consistent with the available data on nc-Fe (Jia et al., 2003), nc-Cu (Cheng et al., 2005), and nc-Al (Sun et al., 2006). Note that a point in this figure (a combination of a given material and grain size) lying outside the inherent instability region (the orange region) does *not* unambiguously guarantee a stable response, as instability can still occur at larger perturbation wavelengths, but such a material would not be inherently unstable. Such maps provide useful guidelines to determine the probability of a material being unstable with respect to this softening mechanism for a range of defect wavelengths.

7.3 Multiaxial Stresses and Constraint Effects

It appears that nanomaterials have multiple mechanisms that are sensitive to multiaxial stresses and to constraints (some of which are manifested as pressure effects). Unfortunately these are difficult to characterize experimentally, and so they are discussed in the next chapter (focusing on some modeling approaches).

7.4 Closing

There are a variety of deformation mechanisms in nanomaterials that arise from length-scale interactions, with specific mechanisms developing in specific structures and for specific applications. These mechanisms sometimes result in remarkable properties, and a full understanding of the mechanisms may suggest applications that would not be conceived of otherwise. Some of these mechanisms are only discoverable from an experimental viewpoint, unless very large scale simulations are performed to capture the richness of possible phenomena.

7.5 Suggestions for Further Reading

1. Argon, A. (2008). Strengthening Mechanisms in Crystal Plasticity. Oxford University Press, Oxford.
2. Van Swygenhoven, H. and J. R. Weertman (2006). Deformation in nanocrystalline metals. Materials Today 9(5): 24–31.
3. Meyers, MA, A. Mishra, DJ. Benson, (2006). Mechanical properties of nanocrystalline materials. Progress in Materials Science 51: 427.
4. Kocks, U.F. A.S. Argon, M.F. Ashby, (1975). Thermodynamics and kinetics of slip. Progress in Materials Science 19: 1.

7.6 Problems and Directions for Research

1. Examine grain size effects in hard granular materials in terms of macroscopic inelastic deformation and failure processes. This provides a sense of the behaviors that are possible when grain boundary and contact mechanisms are primarily responsible for deformation.
2. The development of twins is often related to the ability to emit and move partial dislocations. What does this say about the maximum speed of twin tips?
3. Let us view a young deciduous tree as a buckling problem (a long thin column with a weight – corresponding to the foliage – concentrated at the top). Assume the tree trunk is circular, with a diameter of 3 cm, and assume the tree is about 3 m tall. Given that the Young's modulus of the wood is about 10 GPa, compute the maximum allowable weight of the foliage before buckling will occur. Can you climb to the top of this tree (in the winter) without inducing buckling?
4. What is the critical compressive buckling load for a "tree" made of a single-walled carbon nanotube? Obtain the cross-section geometry from the literature, but assume a length of 2 μm. The Young's modulus of a thin-walled carbon nanotube is about 1 TPa.

References

Alivisatos, A. P. (1996). Semiconductor clusters, nanocrystals, and quantum dots. *Science 271*(5251), 933–937.

Ashby, M. F. and R. A. Verrall (1973). Diffusion-accommodated flow and superplasticity. *Acta Metallurgica 21*, 149–163.

Bruchez, M., M. Moronne, P. Gin, S. Weiss, and A. P. Alivisatos (1998). Semiconductor nanocrystals as fluorescent biological labels. *Science 281*(5385), 2013–2016.

Cao, B., K. T. Ramesh, Li. B and E. Ma (2009). Twinning in nanocrystalline aluminum under high-rate shearing conditions. *Submitted for publication*.

Cao, G. X. and X. Chen (2006). Buckling of single-walled carbon nanotubes upon bending: Molecular dynamics simulations and finite element method. *Physical Review B 73*(15). 155435.

Carsley, J. E., W. W. Milligan, X. H. Zhu, and E. C. Aifantis (1997). On the failure of pressure-sensitive plastic materials .2. comparisons with experiments on ultra fine grained fe-10. *Scripta Materialia 36*(6), 727–732.

Chan, S., P. M. Fauchet, Y. Li, L. J. Rothberg, and B. L. Miller (2000). Porous silicon microcavities for biosensing applications. *Physica Status Solidi a-Applied Research 182*(1), 541–546.

Chen, M. W., E. Ma, K. J. Hemker, H. W. Sheng, Y. M. Wang, and X. M. Cheng (2003a). Deformation twinning in nanocrystalline aluminum. *Science 300*(5623), 1275–1277.

Chen, X. H. and L. Lu (2007). Work hardening of ultrafine-grained copper with nanoscale twins. *Scripta Materialia 57*(2), 133–136. Chen, X. H. Lu, L.

Cheng, S., E. Ma, Y. M. Wang, L. J. Kecskes, K. M. Youssef, C. C. Koch, U. P. Trociewitz, and K. Han (2005). Tensile properties of in situ consolidated nanocrystalline cu. *Acta Materialia 53*(5), 1521–1533.

Chichili, D., K. Ramesh, and K. Hemker (1998). The high-strain-rate response of alpha-titanium: Experiments, deformation mechanisms and modeling. *Acta Materialia 46*, 1025–43.

Christian, J. and S. Mahajan (1995). Deformation twinning. *Progress in Materials Science 39*, 1–157.

Conrad, H. and J. Narayan (2000). On the grain size softening in nanocrystalline materials. *Scripta Materialia 42*(11), 1025–1030.

Cumings, J. and A. Zettl (2000). Low-friction nanoscale linear bearing realized from multiwall carbon nanotubes. *Science 289*(5479), 602–604.

Cumings, J. and A. Zettl (2004). Localization and nonlinear resistance in telescopically extended nanotubes. *Physical Review Letters 93*(8). 086801.

Dao, M., L. Lu, Y. F. Shen, and S. Suresh (2006). Strength, strain-rate sensitivity and ductility of copper with nanoscale twins. *Acta Materialia 54*(20), 5421–5432.

Dingreville, R., J. Qu, and M. Cherkaoui (2005). Surface free energy and its effect on the elastic behavior of nano-sized particles, wires and films. *Journal of the Mechanics and Physics of Solids 53*(8), 1827–1854.

Gao, H., Y. Huang, W. D. Nix, and J. W. Hutchinson (1999). Mechanism-based strain gradient plasticity - i. theory. *Journal of the Mechanics and Physics of Solids 47*(6), 1239–1263.

Gianola, D. S., S. Van Petegem, M. Legros, S. Brandstetter, H. Van Swygenhoven, and K. J. Hemker (2006). Stress-assisted discontinuous grain growth and its effect on the deformation behavior of nanocrystalline aluminum thin films. *Acta Materialia 54*(8), 2253–2263.

Greer, J. R. and W. D. Nix (2006). Nanoscale gold pillars strengthened through dislocation starvation. *Physical Review B 73*(24), 245410.

Greer, J. R. (2006). Bridging the gap between computational and experimental length scales: A review on nanoscale plasticity. *Reviews on Advanced Materials Science 13*(1), 59–70.

Hu, N. and J. Molinari (2004). Shear bands in dense metallic granular materials. *Journal of the Mechanics and Physics of Solids 52*, 499–531.

Huang, Z. M., Y. Z. Zhang, M. Kotaki, and S. Ramakrishna (2003). A review on polymer nanofibers by electrospinning and their applications in nanocomposites. *Composites Science and Technology 63*(15), 2223–2253.

Iwashita, K. and M. Oda (1998). Rolling resistance at contacts in simulation of shear band development by dem. *Journal of Engineering Mechanics-ASCE 124*(3), 285–292.

Jia, D., K. T. Ramesh, and E. Ma (2003). Effects of nanocrystalline and ultrafine grain sizes on constitutive behavior and shear bands in iron. *Acta Materialia 51*(12), 3495–3509.

Jiang, H., M. F. Yu, J. Q. Lu, Y. Huang, H. T. Johnson, X. G. Zhang, and P. Ferreira (2007). Carbon nanotube electronic displacement encoder with sub-nanometer resolution. *Journal of Computational and Theoretical Nanoscience 4*(3), 574–577.

Joshi, S. and K. Ramesh (2008a). Grain size dependent shear instabilities in bcc and fcc materials. *Materials Science and Engineering A 493*, 65–70.

Joshi, S. P. and K. T. Ramesh (2008b). Rotational diffusion and grain size dependent shear instability in nanostructured materials. *Acta Materialia 56*(2), 282–291.

Joshi, S. P. and K. T. Ramesh (2008c). Stability map for nanocrystalline and amorphous materials. *Physical Review Letters 101*(2), 025501.

Kibey, S., J. B. Liu, D. D. Johnson, and H. Sehitoglu (2007). Predicting twinning stress in fcc metals: Linking twin-energy pathways to twin nucleation. *Acta Materialia 55*(20), 6843–6851.

Kis, A., K. Jensen, S. Aloni, W. Mickelson, and A. Zettl (2006). Interlayer forces and ultralow sliding friction in multiwalled carbon nanotubes. *Physical Review Letters 97*(2), 025501.

Liao, X. Z., F. Zhou, E. J. Lavernia, S. G. Srinivasan, M. I. Baskes, D. W. He, and Y. T. Zhu (2003). Deformation mechanism in nanocrystalline al: Partial dislocation slip. *Applied Physics Letters 83*(4), 632–634.

Malow, T., C. Koch, P. Miraglia, and K. Murty (1998). Compressive mechanical behavior of nanocrystalline fe investigated with an automated ball indentation technique. *Materials Science & Engineering A A252*, 36–43.

Moldovan, D., D. Wolf, and S. Phillipot (2001). Theory of diffusion-accomodated grain rotation in columnar polycrystalline microstructures. *Acta Materialia 49*, 3521–3532.

Murayama, M., J. Howe, H. Hidaka, and S. Takaki (2002). Atomic-level observation of disclination dipoles in mechanically milled nanocrystalline fe. *Science 295*, 2433–2435.

Nix, W. D., J. R. Greer, G. Feng, and E. T. Lilleodden (2007). Deformation at the nanometer and micrometer length scales: Effects of strain gradients and dislocation starvation. *Thin Solid Films 515*(6), 3152–3157.

Pantano, A., M. C. Boyce, and D. M. Parks (2004). Mechanics of axial compression of single and multi-wall carbon nanotubes. *Journal of Engineering Materials and Technology-Transactions of the Asme 126*(3), 279–284.

Rosakis, P. and H. Y. Tsai (1995). Dynamic twinning processes in crystals. *International Journal of Solids and Structures 32*(17–18), 2711–2723.

Sanvicens, N. and M. P. Marco (2008). Multifunctional nanoparticles - properties and prospects for their use in human medicine. *Trends in Biotechnology 26*(8), 425–433.

Spitzig, W. and A. Keh (1970). The effect of orientation and temperature on the plastic flow properties of iron single crystals. *Acta Metallurgica 18*(6), 611–622.

Stronge, W. (2000). *Impact Mechanics*. Cambridge: Cambridge University Press.

Sun, P., E. Cerreta, G. Gray, and J. Bingert (2006). The effect of grain size, strain rate, and temperature on the mechanical behavior of commerical purity aluminum. *Metallurgical and Materials Transactions -A 37A*, 2983–2994.

Van Swygenhoven, H. and A. Caro (1997). Plastic behavior of nanophase ni: A molecular dynamics computer simulation. *Applied Physics Letters 71*(12), 1652–1654.

Van Swygenhoven, H. and P. Derlet (2001). Grain boundary sliding in nanocrystalline fcc metals. *Physical Review-B 64*(224105), 1–9.

Wei, Q., D. Jia, K. Ramesh, and E. Ma (2002). Evolution and microstructure of shear bands in nanostructured fe. *Applied Physics Letters 81*(7), 1240–1242.

Yamakov, V., D. Wolf, S. R. Phillpot, A. K. Mukherjee, and H. Gleiter (2002). Dislocation processes in the deformation of nanocrystalline aluminium by molecular-dynamics simulation. *Nature Materials 1*(1), 45–48.

Yang, S. and B. Bacroix (1996). Shear banding in strain hardening polycrystals during rolling. *International Journal of Plasticity 12*(10), 1257–1285.

Yu, M. F., B. S. Files, S. Arepalli, and R. S. Ruoff (2000a). Tensile loading of ropes of single wall carbon nanotubes and their mechanical properties. *Physical Review Letters 84*(24), 5552–5555.

Yu, M. F., O. Lourie, M. J. Dyer, K. Moloni, T. F. Kelly, and R. S. Ruoff (2000b). Strength and breaking mechanism of multiwalled carbon nanotubes under tensile load. *Science 287*(5453), 637–640.

Zhang, H., B. E. Schuster, Q. Wei, and K. T. Ramesh (2006). The design of accurate micro-compression experiments. *Scripta Materialia 54*(2), 181–186.

Zhu, X. H., J. E. Carsley, W. W. Milligan, and E. C. Aifantis (1997). On the failure of pressure-sensitive plastic materials .1. models of yield & shear band behavior. *Scripta Materialia 36*(6), 721–726.

...In that Empire, the craft of Cartography attained such Perfection that the Map of a Single province covered the space of an entire City, and the Map of the Empire itself an entire Province. In the course of Time, these Extensive maps were found somehow wanting, and so the College of Cartographers evolved a Map of the Empire that was of the same Scale as the Empire and that coincided with it point for point.

Jorge Luis Borges, On Exactitude in Science

8 Modeling Nanomaterials

8.1 Modeling and Length Scales

The length scales that are of interest to the mechanics of materials were discussed in Chapter 1. The focus there was on the devices and structures that typified the various length scales, and the intent was to define the range appropriate for nanomaterials. In subsequent chapters, typical mechanics approaches to characterizing and describing nanomaterials were considered. As in any field of science, however, we cannot truly understand nanomaterials unless we can develop mathematical models for them. This chapter focuses on the modeling approaches that are appropriate for nanomaterials.

It is worthwhile to consider explicitly the modeling process, in order to understand the various approximations being made. This process is represented schematically in Figure 8.1. The process is as follows:

- One starts with a physical problem of interest – let us say this is the problem of nanoindentation of a diamond Berkovich tip into a single crystal of copper.
- Immediately, the necessity for some form of idealization presents itself: for example, we do not know what the friction is between the nanoindenter tip and the sample, so we will typically idealize the problem as a zero friction problem at the interface. This is a physical idealization made for modeling purposes. A set of such physical idealizations results in an idealized problem that we still think is of interest.
- Next, we replace the physical problem with a mathematical problem: we choose the set of equations, with boundary and initial conditions, that we think best represents the idealized physical problem. Thus we may choose to represent the problem through Newton's equations for the motion of the individual atoms, with the atomic interactions specified through an interatomic potential (e.g., the Lennard-Jones potential). This translation into a mathematical problem represents another set of assumptions: we assume the potential is reasonable for copper (the Lennard-Jones potential is not), and that we can ignore quantum-level effects.
- Now that we have a mathematical problem that in some sense represents our physical problem, we choose a numerical approach to solving the mathematical

K.T. Ramesh, *Nanomaterials*, DOI 10.1007/978-0-387-09783-1_8,

problem: by choosing, for instance, a specific code with all of the specific algorithms incorporated in the code. There are different levels of accuracy with which specific numerical schemes will solve the same set of mathematical equations, so again we have a set of now *numerical* approximations.

- We then implement the numerical scheme and consider the solutions.

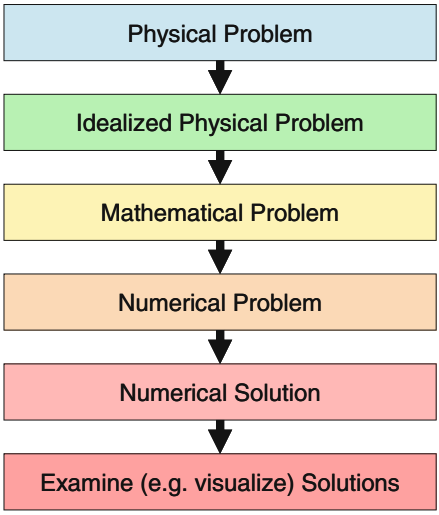

Fig. 8.1 Typical sequence of steps involved in modeling a mechanics of nanomaterials problem. Note the many layers of approximations involved, pointing out the danger of taking the results of simulations at face value.

It is important to remember when we look at the solutions that we have made (a) physical, (b) mathematical, and (c) numerical approximations, and we should always ask whether we have ended up solving the problem that we set out to solve. This is sometimes stated as the verification and validation problem for complex codes: in the words of Rebecca Brannon, are we solving the right equations, and are we solving the equations right? Eventually, the simulation results must be compared to experiments or to the results of entirely independent simulations.

Consider again the range of length scales presented in Chapter 1. Some of the modeling approaches that can be used to describe phenomena over this range of length scales are presented in Figure 8.2, together with the corresponding suite of materials (rather than mechanical) characterization techniques. As an example, we discuss the use of this figure to understand the plastic deformation of a material.

At very fine scales below those shown in Figure 8.2, the quantum mechanics problem must be solved, leading to calculations that are variously called ab initio or first principles computations (such calculations account for electronic structure). Slightly larger scale calculations (Figure 8.2) account for every atom (but not the electrons) by assuming an interatomic potential between the atoms and then solving the equations of motion for every atom. Such computations are called *molecular dynamics* calculations, and are generally limited by length scale and time scale (a mil-

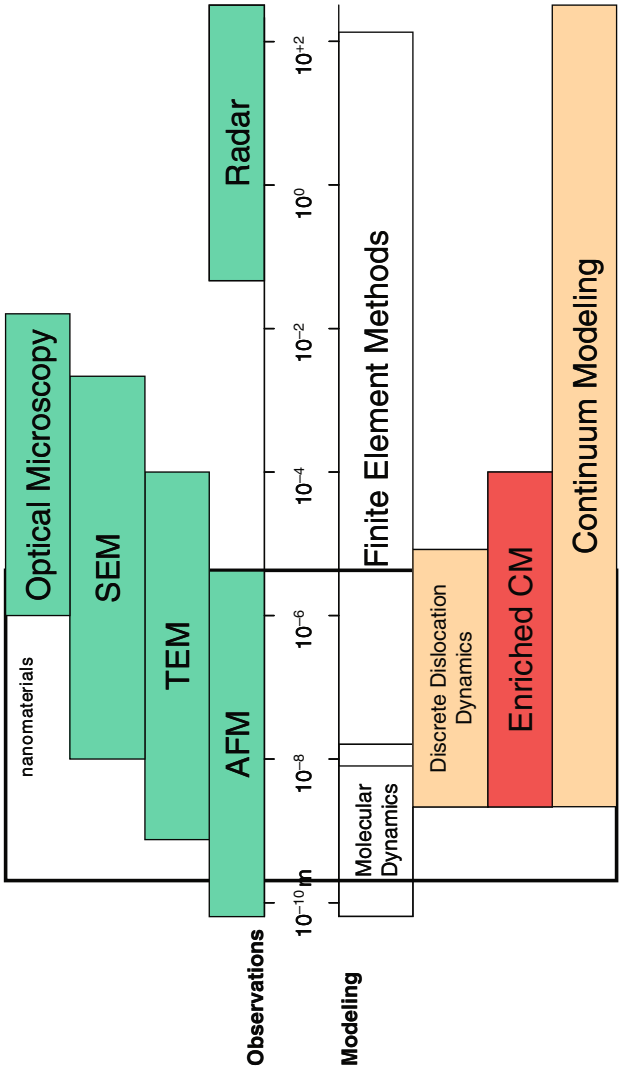

Fig. 8.2 The typical modeling approaches of interest to the mechanics of nanomaterials, and the approximate length scales over which each approach is reasonable. Note the significant overlap in length scales for several of the modeling approaches, leading to the possibility of consistency checks and true multiscale modeling. An example of the observations that can be made at each length scale is also presented, from a materials characterization perspective.

lion atom computation, with 100 atoms on the side of a cube, would be examining a physical cube that is about 40 nm on a side). Although computations of this size scale can address a number of important issues, they are incapable of accounting for a large number of dislocations.

Discrete dislocation dynamics simulations are larger scale computations that no longer have atomic resolution but that can track many thousands of dislocations.

Such computations are able to capture the development of some dislocation substructures, and to interrogate possible sources and sinks of dislocations. At larger scales still, *continuum modeling computations* such as crystal plasticity calculations do not attempt to resolve individual dislocations but do resolve individual crystals. Such calculations smear the dislocations into the continuous medium representing each crystal, and replace the dislocation evolution with hardening laws on given slip systems.

At even larger scales, the individual crystals are no longer resolved, and instead the computations examine the deformations of a homogeneous continuum that has some prescribed plastic behavior (such as those discussed in Chapter 2). This is the level of classical continuum mechanics, which contains no internal length scales. Some models incorporate ad hoc microstructural length scales into structured continuum calculations, and we refer to these as *enriched continuum* models (for example, the strain gradient models in vogue in 2008).

A computational approach derived from classical continuum mechanics that has been used with some success over a very wide range of length scales is the finite element method, particularly when coupled to computational techniques that are better able to resolve very fine scale physics. We will not discuss this numerical technique in any detail: there are many excellent books on the finite element method and its applications in mechanics.

An interesting observation from Figure 8.2 is the overlap between the scales at which each modeling approach is effective. These overlapping regions can be viewed in two ways. First, these are regions where information on the behavior of the material can be obtained using two different approaches, and such situations often greatly enhance our understanding. Second, these are regions in which the ability to resolve behavior at finer scales with one method while computing over larger scales with another method can lead to multiscale approaches that are able to capture phenomena that would otherwise be missed.

The range of typical interest in nanomaterials is shown in the big vertical box in Figure 8.2. Larger scales may be of interest for applications of nanomaterials, but the box describes the range where nanomaterials phenomena are determined, i.e., scale-dominant behaviors are typically observed. The microstructural characterization techniques associated with this range have been discussed in Chapter 3. All of the modeling approaches in the figure are useful for modeling nanomaterials, although it is clear that part of this size range is accessible only by molecular dynamics. The range of length scales where a number of modeling approaches overlap demonstrates that there is significant potential for understanding nanomaterials using multiscale approaches.

Another way to think about these length scales is to think about them in terms of the features of the material that are important at each length scale. This is illustrated in Figure 8.3, which shows the microscopic features typically associated with each length scale in metallic systems. At very small length scales, the behavior is dominated by atomic motions and so the atom is the critical feature. As the length scales increase, the arrangements of the atoms become important, and so we begin to see the effects of atomic clusters, point defects such as vacancies, and the unusual arrangement of atoms around dislocation cores.

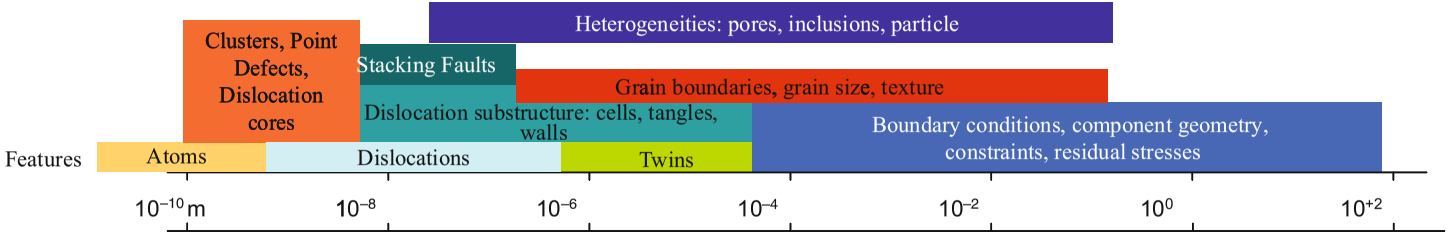

Fig. 8.3 The length scales associated with various microstructural features in metallic materials. For most crystalline materials, the behavior at larger length scales is the convolution of the collective behavior of features at smaller length scales.

At slightly greater length scales, dislocations themselves become the features that dominate the mechanical behavior, and dissociated dislocations lead to stacking faults. We then begin to see the influence of dislocation substructures, that is, the collective behavior of large numbers of dislocations: this includes the development of dislocation tangles, dislocation walls, cells and sub-grains.

At larger scales still, deformation twins begin to become important in some materials. Grain boundary effects, grain size effects, and texture effects can occur over a very wide range of length scales. At similar lengthscales, one begins to see the influence of heterogeneities in the material, such as inclusions, pores and precipitates. Most component features such as boundary conditions, geometry, constraints and residual stresses are at the larger scales in this figure. We have discussed most of these mechanisms and features in previous chapters.

From a modeling perspective, what becomes clear is that it is not possible to link directly actions and events at the atomic scale to mechanical behavior at the macro scale without accounting for the specific microstructural features that may develop at intermediate scales. The mechanical behavior at larger scales is modulated by the collective behavior of features and mechanisms at a number of smaller scales – it does not make sense to try to compute the behavior of a steel structure in terms of atomistic calculations unless one is certain that one can also capture all of the features of dislocation motion, dislocation tangling, and dislocation-grain boundary interactions. Microscale and mesoscale interactions are affected by atomistic behavior, but must be specifically accounted for as well in order to predict the material behavior.

Now that we have some insight into the physical processes active at each length scale, let us think again about the process of modeling discussed in Figure 8.1. Once we have chosen the physical problem that we would like to understand, we typically need to idealize that physical problem into something that we can actually solve. This process of idealization tends to be discipline-specific, in that the idealizations chosen by materials scientists tend to be different from the idealizations chosen by physicists or mechanical engineers. When we think more clearly about these idealizations, we realize that very often what we are doing is deciding which features of the deformation (Figure 8.3) our model is intended to capture. Thus, for example, we may choose to construct a model that accounts for dislocation density but does not account for individual dislocations or of the distributions of dislocation density associated with dislocation cell walls and dislocation tangles.

How do we decide which features we intend to include in the model? Often these are based on experimental observations that indicate that these particular microstructural features are (or are not) observed in the phenomenon or behavior that we wish to describe using the model. For example, suppose we are attempting to describe the deformations of an aluminum alloy. The modeler may know that dislocations are important in plastic deformations, and so she builds a model that accounts for dislocation density. Her model may not be capable of describing the clumping of dislocation density that characterizes dislocation cell walls, and she may believe this to be a reasonable idealization of the physics of deformation. However, TEM observations show that dislocation cells are important in describing the large plastic

deformations of aluminum, and the model will obviously not account for this feature of the deformation. The modeler cannot, in general, put into the model microstructural features that she does not know exist.

There is one modeling approach that should in principle account for all possible microstructural features, even those that the modeler does not consciously put into the model. In this approach, one accounts at a fundamental level for quantum mechanical interactions (some in the literature refer to this as a "first principles" approach), and then computes everything else explicitly from that basis. In principle, an explicit computation of this type that accounts for all of the possible interactions between the atoms should be able to reproduce all the possible behaviors at all possible length and timescales. In practice, of course, one is never likely to have the computing capacity to actually perform such a calculation and so this might be an exercise in futility.

However, the advantage of such an approach (even over limited scales) is that one might discover phenomena that one would otherwise never know about, because the fact is that performing experiments over a complete range of length scales and time scales is also prohibitively expensive, and so there are certainly phenomena that we have never observed simply because we have not known to look for them. A computation that handles the true complexity of nature at the fundamental level may thus truly discover the existence of phenomena, and we could then design an experiment to examine the veracity of such a discovery. This complexity-aware approach to modeling is extraordinarily expensive from a computational viewpoint, but has a certain intellectual appeal, and is likely to be of increasing importance as computational capabilities escalate.

The major modeling approaches used to study nanomaterials will be described in this chapter, with an emphasis on ultimately providing descriptions that can be viewed in a mechanics context. First, however, we discuss some of the scaling approximations and physical idealizations made by classical continuum mechanics.

8.2 Scaling and Physics Approximations

All models must make approximations in order to be useful. The question, of course, is how does one decide which approximations to make? In this section, we attempt to address this question with respect to nanomaterials. Since most of us approach the nanomaterials problem with a prior training in the macroscale sciences, it is important to remember that some phenomena at the nanoscale may have no macroscale counterparts, and we will not naturally think about them in terms of scaling down from the macroscale.

Continuum models (such as the mechanics models that we normally use at the macroscale) usually make four core approximations:

- It is assumed that classical mechanics (rather than quantum mechanics) represents the behavior. This will clearly be an issue when considering very small particles, such as quantum dots.

- Material behavior is assumed to hold pointwise in a continuous medium, where every material particle has an infinitesimal size. Thus the atomic or molecular structure is averaged out in this representation.
- Thermal effects are averaged out (we do not consider thermal vibrations of atoms or molecules explicitly).
- The chemistry is usually ignored, although it can be incorporated in some average sense.

The second and third items above both relate also to the concepts of differentiability and localization of equations (that is, when can we write the governing equations as field equations valid at every point?).

An interesting example of the influence of such approximations is that of the scaling of thermal effects. In solid mechanics, temperature shows up primarily in terms of thermal conduction as a diffusion term (or as a parameter that modifies material properties, e.g., through thermal softening). Thermal diffusion is represented mathematically in continuum mechanics through a second derivative (as in Equation 2.59). The idea of differentiability shows up here – is the second derivative well-defined (i.e., is the first derivative sufficiently continuous for us to be able to take a second derivative)? Physically, one can only even *define* the diffusion term if the temperature is smooth over a sufficiently large length scale: thermal energy is moved through the system by atomic or molecular collisions. As we consider smaller size scales, the mean free path of the molecule between collisions can become an issue – if the size scale of interest is comparable to the mean free path, the continuum definition of thermal diffusion is no longer sensible. Further, situations with strong gradients (such as interfaces and surfaces) begin to dominate behavior at small length scales. For these reasons, for example, the definition of thermal conduction along and across a carbon nanotube cannot be the continuum definition. Thus the assumptions implicit in continuum mechanics models must often be challenged on a case-by-case basis when dealing with nanomaterials.

The process of integrating information from multiple scales into a model to understand the behavior of a material (or more generally a system) is called multiscale modeling. Traditionally, all length scales (and timescales) below the current scale in a simulation are called subscales, and models are frequently said to represent various levels of subscale information in specific ways. We discuss some of these approaches next.

8.3 Scaling Up from Sub-Atomic Scales

There is a significant scientific effort focused towards the goal of being able to simulate the behavior of human-scale objects using atom-scale information. While there is an excellent argument to be made for invoking complexity only when one needs it, there is also the excellent argument that our intuition is so bad at the nanoscale that we do not know what complexity to invoke, and so we may learn a great deal by incorporating the complexity of atomic structure as the foundations of a modeling

approach. But how do we feasibly scale up from atomistics? There are many ways of approaching this issue, but for the purposes of this book we identify two specific approaches: the *enriched continuum* approach, and the *molecular mechanics* approach.

8.3.1 The Enriched Continuum Approach

This approach to the problem is often taken by those scientists coming to the problem from a continuum scale, and essentially views the equations of continuum mechanics as core equations. That is, it is assumed that the equations of continuum mechanics (such as the governing equations presented in Section 2.3) will be used for the solution of the problems of interest. This, of course, presupposes that the problems of interest are at $\geq$ nm scales, which is certainly the case for this book.

Given this assumption, atomic-level information primarily enters into the system of equations through the constitutive equation. This approach therefore views the constitutive equation as "informing" other continuum equations of the microscopic degrees of freedom in an averaged sense. Note that this has always been done at the microstructural level (that is our constitutive equations, such as in plasticity, have incorporated microstructural information such as the grain size). However, we recognize that the microscopic degrees of freedom that we choose to incorporate can also come from the quantum (sub-atomic) level.

This approach results in the incorporation of quantum-level information into continuum mechanics problems in a well-defined and consistent way. It has the advantage of being a great approach for the modeling of mechanics of materials, but it also has the disadvantage that we must do averaging, and depending on the way we take the average, we may end up averaging out many of the effects of interest to nanoscale phenomena. In terms of the topics of interest to this book, the informed continuum approach may be very effective for bulk nanomaterials but may miss important phenomena in discrete nanomaterials (an excellent example being quantum dots viewed as nanoparticles - it is the quantum effects that are key in this case).

An excellent and detailed description of these issues is provided by Phillips (2001).

8.3.2 The Molecular Mechanics Approach

This approach gets its name from the idea that the mechanics problem is considered at the molecular level. However, the fundamental concept here is that we must make relevant approximations at very small scales (specifically, sub-atomic scales such as electrons and nuclei) to develop the equations appropriate at the next scale up. We can then calculate interatomic or intermolecular interactions directly, and use these to define interatomic or intermolecular potentials. In a subsequent step, to

move to the continuum scale, we can use the interatomic potentials to compute the behavior of many-atom systems. The primary benefit of this approach is that it handles the *molecular structure* directly, and so leads to efficient *molecular dynamics* calculations.

Such an approach has the advantage that it is not tied to continuum dynamics (it does not assume the standard continuum equations), but has the disadvantage that the computations are much more complex, and therefore the physical limitations of the computing system may result in the simulations being scale limited. For example, as of this writing it is difficult to simulate a billion atom system, which amounts to a cube of side $\approx$300 nm.

For us, the primary interest is in interatomic bonds and bond strengths (which arise naturally from electron cloud interactions). It is immediately obvious that the problem quickly becomes intractable if we were to attempt to handle the interactions of every atom with every other atom in terms of electron cloud interactions. However, we can recast this problem in terms of short-range and long-range interactions, and handle each of these separately as approximations. That is, we do not need to consider short range interactions between every atom pair in the simulation, but only those between nearby atoms (within some specified zone of influence defined by the range of the short-range interaction). Even the long-range interactions will typically have some cut-off distance, beyond which they are negligible.

How are these short-range and long-range interactions obtained? Typically, one starts with Schrodinger's equation from quantum mechanics, which is something the reader has probably seen for a single particle interacting with a potential $V(\mathbf{r},t)$:

$$-\frac{\hbar^2}{2m}\nabla^2\psi(\mathbf{r},t)+V(\mathbf{r},t)\psi(\mathbf{r},t)=i\hbar\frac{\partial\psi(\mathbf{r},t)}{\partial t}, \tag{8.1}$$

where $\mathbf{r}$ is the position and m is the mass of the particle, $\hbar$ is Planck's constant, and $\psi(\mathbf{r},t)$ is the particle wave function. This latter quantity is most easily understood by noting that in one dimension $|\psi|^2dx$ is the probability that the particle is between x and $x+dx$. The quantity $|\psi|^2dx$ is called the probability density function for the particle. The right-hand-side of this equation reduces to $E\psi(\mathbf{r})$ in the time-independent case, where E is an energy (really an energy eigenvalue – one obtains different solutions ψ_α corresponding to energies E_α). We can write a similar equation to Equation (8.1) for an N-particle system, although it is somewhat more complex, and we would have to invoke the Pauli exclusion principle. The point, however, is that this can be done (writing the equation, that is – solving it can quickly become difficult).

In the case of interacting charged particles, for instance, the potential $V(\mathbf{r},t)$ would be

$$V(\mathbf{r},t)=\sum\frac{q_iq_j}{4\pi\varepsilon_0 d_{ij}}, \tag{8.2}$$

where q_i is the charge on the ith particle, and d_{ij} is the distance between the ith and jth particles.

For example, in the simple 1D case of a particle oscillating within a quadratic potential well, we have $V(\mathbf{r},t) = V(x,t) = \frac{1}{2}kx^2$, and the now time-independent Schrodinger equation reduces to

$$-\frac{\hbar^2}{2m}\frac{d^2\psi(x)}{dx^2} + \frac{1}{2}kx^2\psi(x) = E\psi(x), \tag{8.3}$$

which is the equation to a harmonic oscillator and is easily shown to have solutions

$$\psi_n(x) = \frac{1}{2^{n/2}n!^{\frac{1}{2}}}\left(\frac{m\omega}{\pi\hbar}\right)^{\frac{1}{4}} \exp\left(-\frac{m\omega}{2\hbar}x^2\right) H_n\left(\sqrt{\frac{m\omega}{\hbar}}x\right), \tag{8.4}$$

with the corresponding energies being quantized as $E_n = (n+\frac{1}{2})\hbar\omega$, n being an integer. In the latter two equations, the frequency ω is defined by $\omega = \sqrt{\frac{k}{m}}$, exactly as in the classical spring-mass system. The point of presenting this solution is to demonstrate that the Schrodinger equation behaves a little differently from the usual continuum spring-mass system, in that the energy states are discrete rather than continuous (only certain energies are allowed). Further, the probability of finding the particle (after all, this is what is defined by ψ_n) is non-zero at all x even for the discrete states. That is, you may find the particle anywhere, but it can only have certain discrete energy states. Some of the quantum character of the solution becomes evident.

The fact is that Schrodinger's equation is often written but rarely solved in books on things nano, particularly when it comes to books of this type that attempt to bring together multiple disciplines. This is because while Schrodinger's equation is easy to write, it quickly becomes difficult to solve for a many-body system, such as, for example, a cluster of 10 aluminum atoms with all of the nuclei and electrons. Thus various approximations become necessary.

One typical approximation is called the *Born-Oppenheimer* approximation, and uses the fact that the nuclei of atoms are much heavier than electrons, so that in most problems of interest the nuclei move slowly in comparison with the electrons. Thus, by separating the problem into the rapid motions of electrons and slower motions of nuclei, one can compute the electron ψ and energy E in a field of initially fixed nuclei. Then one updates the positions of the nuclei, and recomputes ψ and E.

In most cases, the problem reduces to finding the total energy E_T of a collection of particles as a function of the positions of the nuclei $\mathbf{R}_n$ and electrons $\mathbf{r}_e$:

$$E_T = E_T(\mathbf{R}_n, \mathbf{r}_e). \tag{8.5}$$

Note that the number of nuclei and number of electrons are usually very different in the problems relevant to materials. We can make some further approximations. If, for instance, we decide that we will approximate the total energy of the nuclei and electrons given by Equation (8.5) as

$$E_T(\mathbf{R}_n, \mathbf{r}_e) \approx E_{ion}(\mathbf{R}_n), \tag{8.6}$$

we are essentially replacing the total energy of the system with an energy that is calculated from the positions of the nuclei alone, and this is like computing an effective interaction between *ions*. If, on the other hand, we replace the large number of electrons instead with an electron density function $\rho(\mathbf{r})$, we obtain

$$E_T(\mathbf{R}_n, \mathbf{r}_e) \approx E_{approx}(\mathbf{R}_n, \rho(\mathbf{r})), \tag{8.7}$$

and approaches that solve problems using this approximation are called density functional theories.

A particularly interesting example of the approximation corresponding to Equation (8.6) is obtained when one sets the energy E_{ion} to be dependent only on the relative distances between particles d_{ij}, that is, ignoring directional influences, as

$$E_{ion} = \frac{1}{2}\sum V(d_{ij}), \tag{8.8}$$

where $V(d_{ij})$ is called a pair potential, and d_{ij} is the scalar distance between ion i and ion j. Many such pair potentials are used in the literature, with the canonical example being the *Lennard-Jones* potential:

$$V(d) = V_0\left[\left(\frac{\xi}{d}\right)^{12} - \left(\frac{\xi}{d}\right)^{6}\right], \tag{8.9}$$

with V_0 defining the depth of the potential well and ξ defining the length scale corresponding to the equilibrium separation of the atoms. This potential represents the interatomic interaction presented in Figure 4.9, which is reproduced here as Figure 8.4 for convenience.

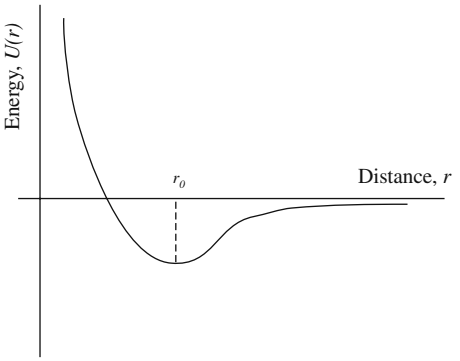

Fig. 8.4 Schematic of the Lennard-Jones interatomic pair potential $V(d)$.

In principle, this pair potential still involves interactions between every pair of atoms in the simulation. In practice, most simulations assume that the potential dies

off after the nearest neighbors, so that only a small number of interactions need to be included for each atom in the simulation.

A very large fraction of the calculations in the literature use such pair potentials. Increasingly sophisticated potentials are also used, incorporating some of the directional dependences of the bonds.

Another approximation of interest is the *embedded atom method* (EAM), which was developed for metals (Daw and Baskes, 1984) and essentially considers each metal atom to be embedded within an electron density field derived from the rest of the metal:

$$E_{total} = E_{interaction\ of\ nuclei} + E_{embedding\ of\ atom\ in\ electron\ gas} \tag{8.10}$$

$$= \frac{1}{2}\sum \phi(d_{ij}) + \sum F(\rho_n), \tag{8.11}$$

where the electron density is ρ. For example, in the special case of $F(\rho) = \sqrt{\rho}$, we obtain the *Finnis-Sinclair* potential.

EAM potentials are extensively used in simulations of the deformation of metals, and much of the literature on the atomistic modeling of nanocrystalline metals is based on such potentials. The parameters for such potentials are obtained in a variety of ways, and the usefulness of the simulation is typically determined by the quality of the potential that is used. Good EAM potentials are available for a small number of metals, including copper, nickel and aluminum. An example of such a potential is that developed by Mishin et al. (1999), and the resulting pair potential for aluminum is presented in Figure 8.5.

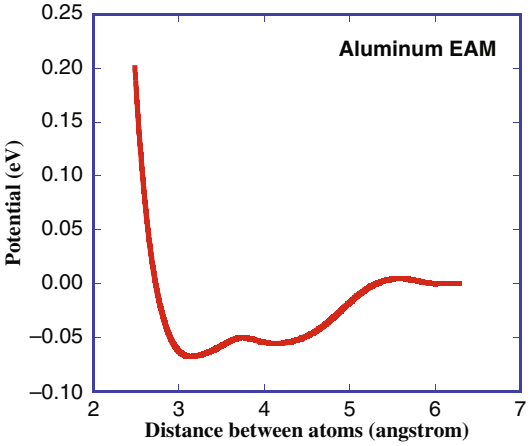

Fig. 8.5 The pair potential corresponding to the EAM potential for aluminum, using the parameters provided by Mishin et al. (1999).

In the next section, we consider computations involving multiple atoms that use such potentials in order to understand material behavior. Such computations that include the dynamics are called molecular dynamics.

8.4 Molecular Dynamics

In a molecular dynamics (MD) calculation, one seeks to determine the motions of all atoms in the simulation by solving Newton's equations of motion (rather than quantum mechanical equations), with the atoms interacting through assumed interatomic potentials (such as that in Equation 8.8). Aside from length scales, time scales also become an issue. Very small integration time steps are needed in order to obtain an accurate solution, and most MD calculations never go beyond a nanosecond in total time duration. In order to achieve the strain of interest in that time frame, MD computations typically run at equivalent strain rates on the order of $10^9 s^{-1}$. This section will not attempt to show the reader how to perform MD simulations, but rather to survey some of the issues involved as regards such simulations for nanomaterials. An excellent and relatively concise introduction to molecular dynamics simulations is provided by Rapaport (2004).

The basic computational process is as follows: one starts with the positions and velocities of a number of atoms (preferably a large number). The potential energy of the system is used to compute the force on each atom using an assumed interatomic potential. Since the masses of the atoms are known, these calculated forces allow us to compute the accelerations of each atom, and these accelerations can be used to update the velocities of the atoms, and the velocities are used to update the atomic positions. We then begin the process again. These can be very large simulations, depending on the number of atoms involved, given that every atom interacts at least with its nearest neighbors, and depending on the total times (total number of timesteps) that must be computed. There are very sophisticated codes now available in the public domain for solving problems using molecular dynamics. The best known of these is called LAMMPS, and is able to run effectively on a parallel processing platform (many computers working in parallel in terms of the numerical algorithms used for solving MD problems). Given the availability of such codes, molecular dynamics simulations are now in the reach of any scientist willing to make the effort.

As always with scientific computations, however, the key is to understand (a) precisely what is the scientific objective of the calculation (what are you looking for?), (b) precisely what is being computed (what equations are being solved numerically?) and (c) when can the computation provide reasonable results (what are the limits of the computational approach?). There is a significant danger in using canned computational packages, in that the user tends to assume that the results are always reasonable, while the developers may not have provided warnings or flags to indicate when the output is inaccurate or even meaningless.

There is a significant level of research activity, as of this writing, that uses molecular dynamics simulations to enhance our understanding of nanomaterials. Some of the work has been on the special case of carbon nanotubes, which involve carbon-carbon interactions. Since such interactions are covalent and quite directional, a classic pair potential involving only the atomic separation is not appropriate. Modifications of pair potentials that include some directional characteristics (sometimes called bond-angle character in the literature) include the Tersoff (Tersoff, 1988)

and Brenner (Brenner et al., 2002) potentials. In the case of bulk nanocrystalline materials, most of these simulations have been on metallic nanomaterials, using embedded atom method potentials. EAM potentials have been constructed and validated to various degrees for copper, nickel, and aluminum (e.g., Mishin et al., 1999). As is generally the case in nanomaterials, fcc metals are the best studied. Reviews of MD simulations in nanomaterials appear in the literature every two years or so, a recent example being Van Swygenhoven and Weertman (2006).

An example of a three-dimensional nanostructure developed for solution using molecular dynamics is presented in Figure 8.6. The figure shows several tens of grains of nanocrystalline nickel constructed using a Voronoi tessellation approach, and modeled using the LAMMPS software. The colors represent the coordination number associated with each atom, and the grain boundaries are identified by the distinctly different coordination numbers of the atoms compared with the atoms in the face-centered cubic crystals. This collection of atoms can now be subjected to mechanical loading (deformations) and the motions of the individual atoms can be tracked to understand deformation mechanisms.

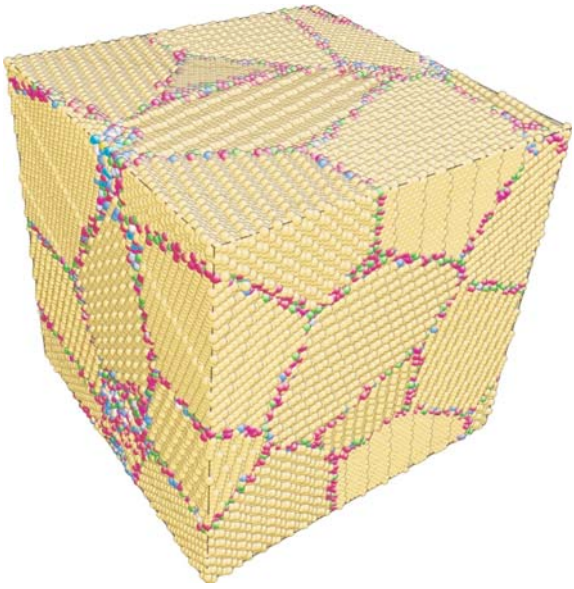

Fig. 8.6 Nanocrystalline material constructed using molecular dynamics. The material is nickel, and the atoms are interacting using an EAM potential due to Jacobsen. About 30 grains are shown. The color or shade of each atom represents its coordination number (number of nearest neighbors), with the atoms in the crystals having the standard face-centered-cubic coordination number. The change in coordination number at the grain boundaries is clearly visible. This collection of atoms can now be subjected to mechanical loading (deformations) and the motions of the individual atoms can be tracked to understand deformation mechanisms.

What have we learned, and what can we learn, from MD simulations of nanomaterials? In principle, of course, such simulations have tremendous potential for understanding the physics of these materials, because they give us access to time scales and length scales that are extremely difficult to investigate through experiments. We will discuss some of the advances in our understanding obtained through MD computations in the next paragraphs. The limitations of these calculations arise also from the scales at which they operate, and the continuing limitations of computing capacity. In general, larger simulations (in terms of number of atoms or length scale) are run for shorter total times because of the available computer cycles. Even the largest simulations that are currently feasible are unable to sample a cubic micron of volume for a total time of 1 ns. As a consequence, any physical mechanism that requires significant time to develop or significant space to organize itself cannot be captured using such simulations (although many MD aficionados continue to extrapolate from short times and small scales).

Some other distortions of the physics can also occur. To generate significant strains in very short times, extraordinarily high strain rates are applied (almost always higher than $10^7\,s^{-1}$), and thus the mechanisms that are observed in an MD simulation will not necessarily be observed in a physical experiment at strain rates many orders of magnitude smaller. Further, the dislocations that are developed in MD simulations often have extremely high accelerations, which can generate some pathological situations in terms of mechanics. Thermal equilibration of systems is a continuing challenge, since there is insufficient time for typical thermal diffusion mechanisms; some ingenious approaches have been developed to define a reasonable thermal state (Liu et al., 2004). The small sample sizes that are simulated and the sometimes two-dimensional nature of the simulations can restrict the number of available slip systems and deformation mechanisms. Most MD simulations also do not account for the initial defect structure that exists in real materials, and therefore miss many of the sources and sinks that are active in many nanomaterials (e.g., most of the simulated grains are completely clean and contain no initial defect structures, while most experimentally observed nanocrystals contain large numbers of initial defects such as stacking faults and pre-existing dislocations). Issues with regard to the types of grain boundaries considered must also be addressed. Finally, the nature of the (often periodic) boundary conditions that are applied can couple into the dynamics, causing difficulties with modeling some phenomena that are driven by wave dynamics.

Even with all of these limitations, however, MD simulations have been very useful for understanding nanomaterial behavior. For example, such simulations (e.g., Schiotz and Jacobsen, 2003) have indicated that there may in fact be a maximum in the strengthening that can be obtained by decreasing the grain size, so that below a certain critical grain size the strength begins to decrease again as the grain size decreases. This is called the inverse Hall-Petch effect and is somewhat controversial, in that it has been difficult to obtain incontrovertible experimental evidence that the effect exists (because of specimen preparation and testing difficulties). The MD results (such as those of Schiotz and Jacobsen, 2003) demonstrate that there are at least some physical reasons why such an effect might exist. Further, such simula-

tions have demonstrated that grain boundaries can be significant sources of dislocations (Farkas and Curtin, 2005) and that there are competing dislocation nucleation mechanisms that may become dominant as the grain size changes (Yamakov et al., 2001). The likely dominance of partial dislocations rather than full dislocations in nanocrystalline aluminum has been predicted by MD and subsequently observed through experiments (Chen et al., 2003a). Grain boundary sliding has been shown to be a plausible mechanism for effective plastic deformation in very small grain size metals (Derlet et al., 2003). The simulations also show that dislocations may not survive in the interior of small grains without externally applied stresses, that is, they may be emitted and then reabsorbed by grain boundaries (Yamakov et al., 2001). As a consequence, not seeing dislocations in the interior of nanograins within the TEM does not guarantee that dislocation-mediated plastic deformation did not occur. This is an insight that could not have been obtained definitively without the MD simulation.

It is apparent that such simulations continue to have great potential in this field. However, the limitations of strain rate, time scale and length scale must be carefully considered in attempting to relate MD simulations results to experimental measurements and to predictions of engineering behavior and possible applications. In the next section we discuss another modeling approach that examines larger scales in space and time.

8.5 Discrete Dislocation Dynamics

We have seen that the length scales that can be simulated with molecular dynamics are relatively small, $<1\,\mu m^3$. Even though such simulations are able to consider nanocrystalline materials (because the grain sizes are less than 100 nm), they are unable to consider time scales large enough to observe most of the conventional deformation mechanisms of interest to engineering. In addition, such small length scales do not permit the development of organized micron-scale structures, or the examination of materials containing grain size distributions.

A larger scale approach that shows some promise is that of discrete dislocation dynamics. This modeling approach does not seek to track the motions of individual atoms, but rather seeks to track the motions of individual dislocations as they move through a continuous medium. Each dislocation is supposed to interact with the medium in a specific way (typically derived from elasticity theory, but sometimes from atomistics), and the interactions of dislocations with each other can be explicitly handled using rules derived from well-developed dislocation theory (Hirth and Lothe, 1992). Very large numbers of dislocations can be tracked in this way, with specific rules for their motion through the medium and for their interactions with each other. The physics associated with the interactions of such dislocations is fairly well understood, but the equations of motion for dislocations at low velocities are still somewhat empirical. The most common equation of motion involves a dislocation drag type behavior, which is probably only accurate at relatively high dislocation velocities.

The advantage of such simulations is (aside from sheer length scale) that they can follow dislocation structures as they evolve, and can examine the development of deformation mechanisms that involve multiple dislocations (or dislocation densities). While discrete dislocation dynamics (often called DDD) simulations are now often used in the simulation of plastic deformations in single crystals and large polycrystals, they are only rarely used with respect to nanocrystalline materials at this time. Some examples of work of interest include that of Noronha and Farkas (2002, 2004) and that of Kumar and Curtin (2007). A significant effort to marry the length and time scales is needed to take advantage of this technique in the nanomaterial domain, but the return is likely to be well worth the effort.

8.6 Continuum Modeling

Much of this book has been focused on the continuum viewpoint with respect to nanomaterials, as in our discussions of elastic and plastic behavior. Some of the discussion has incorporated some microstructural features in an implicit sense, as when the grain size was used through the Hall-Petch term to change the yield strength (which is the continuum parameter).

8.6.1 Crystal Plasticity Models

Explicit continuum computations of the effect of microstructure are also possible, for example through the explicit computation of the behavior of a polycrystalline mass using crystal plasticity codes. Such calculations consider the simultaneous deformation of multiple crystals of various grain sizes, where each crystal is modeled as a continuum made up of a material that has anisotropic elastic properties and that develops plastic strain along specific slip systems. We can view such a model as being one level up in length scale from the discrete dislocation dynamics model, in that the crystal plasticity model does not account for individual dislocations but does account for the collective effects of dislocations through the assumption of a critical resolved shear stress for the onset of slip (the analog of the onset of motion of dislocations) and hardening rules for slip along primary and conjugate slip systems (the consequence of the interaction of dislocations). However, a continuum crystal plasticity model has no internal length scale, and therefore is unable to distinguish between a collection of large crystals and a collection of small crystals.

Some researchers have modified crystal plasticity models to incorporate a length scale by invoking the onset of yield differently for different sized crystals, typically by assuming a Hall-Petch style behavior. Such models do not add any new physical insight, since the length scale effect is assumed, but may be useful in looking at the behavior of textured polycrystalline systems. Other researchers have formally incorporated another phase at the grain boundary in a polycrystalline mass

(Wei et al., 2006), giving the new phase properties that correspond to an amorphous material, and computing the deformation of the crystals using a crystal plasticity model. While such a model certainly has academic interest, an amorphous phase is almost never found at grain boundaries in nanomaterials (see, e.g., Figure 8.7. The mechanics justification of the assumption of an amorphous phase at the grain boundary is typically that the atoms at the grain boundary are somewhat disordered, and therefore can be viewed as being part of an amorphous material. However, there is no evidence that the atoms at the grain boundary behave like an amorphous material in terms of plastic response. Indeed, molecular dynamics simulations suggest that the material at the grain boundary can be a source of dislocations, rather than behaving like an independent harder phase.

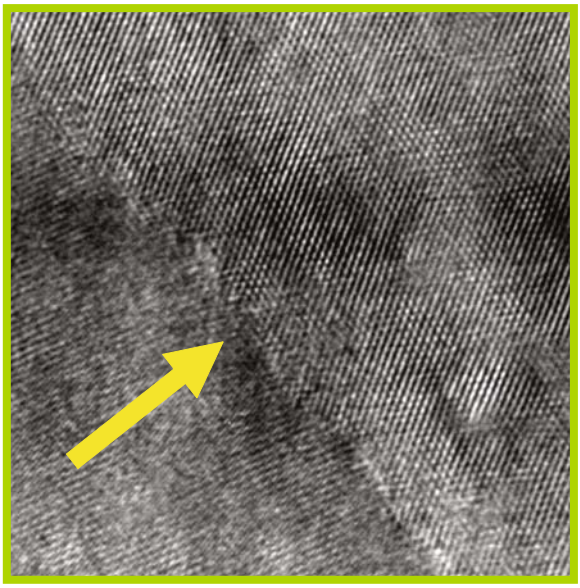

Fig. 8.7 High resolution micrograph showing the boundary between two tungsten grains in a nanocrystalline tungsten material produced by high-pressure torsion. There is no evidence of any other phase at the grain boundary, contrary to pervasive assumptions about the existence of an amorphous phase at the grain boundary in nanomaterials in crystal plasticity and composite simulations at the continuum level. Note the edge dislocations inside the grain on the right. Such internal dislocations are rarely accounted for in molecular dynamics simulations.

8.6.2 Polycrystalline Fracture Models

Finite element simulations of two-dimensional microstructures of polycrystalline ceramic materials are also performed, with a view to identifying the fracture processes in such materials, e.g., Kraft et al. (2008). An example of such a polycrystal

simulation is shown in Figure 8.8, which shows crystals of alumina modeled as elastic solids, with grain boundaries that can fail (with the failure process modeled through a cohesive function). The identical issues of length scale arise in such simulations (although dynamic simulations that incorporate wave propagation effectively include a length scale because of the finite wave speed). The current status of polycrystalline fracture computations is that three-dimensional fracture of the polycrystalline mass is extremely difficult to simulate, particularly with regard to the lack of mesh convergence when solving combined contact and fragmentation problems. The computational simulation of nanocrystalline ceramics remains a major challenge.

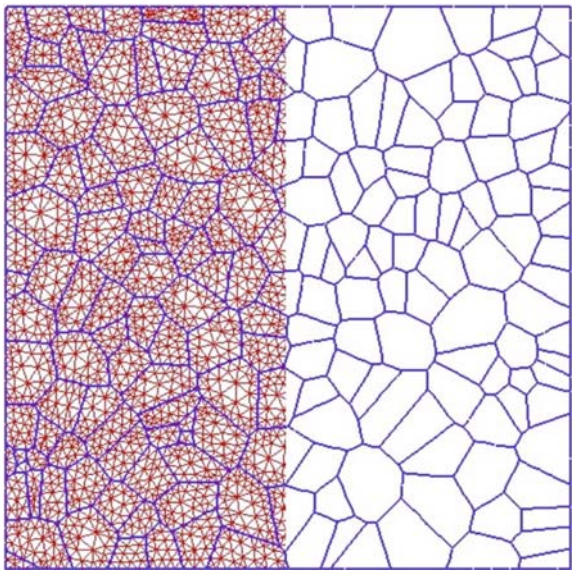

Fig. 8.8 Finite element model of a polycrystalline mass of alumina, with the crystals modeled as elastic solids (Kraft et al., 2008). The model seeks to examine the failure of the polycrystalline mass by examining cohesive failure along grain boundaries. Reprinted from Journal of the Mechanics and Physics of Solids, Vol. 56, Issue 8, page 24, R.H. Kraft, J.F. Molinari, K.T. Ramesh, D.H. Warner, *Computational micromechanics of dynamic compressive loading of a brittle polycrystalline material using a distribution of grain boundary properties*. Aug. 2008 with permission from Elsevier.

8.7 Theoretically Based Enriched Continuum Modeling

The discussions up to this point show the value of developing multiple scale approaches that can rigorously couple atomistic and continuum behaviors. Most of the methods by which this is done are computational, and indeed, this is one of the fastest-growing fields within scientific computing. We do not discuss such multi-

scale simulations in any great detail in this book. In this section we focus on some theoretically based approaches to enriching the continuum response with atomic level information, focusing primarily on the use of the Cauchy-Born rule.

As a specific example, we will consider the deformations of carbon nanotubes. Much more detailed discussions of such approaches can be found in the works of Huang et al. (e.g., Zhang et al., 2002, 2004) and Volokh (Volokh and Ramesh, 2006). This discussion follows the work of Volokh.

Carbon nanotubes typically have diameters on the order of ≤ 1 nm and lengths of 10–1000 nm. They are made entirely of carbon atoms, which are typically arranged in a hexagonal structure (Figure 8.9). The easiest way to think of a carbon nanotube is in terms of a two-dimensional sheet of carbon atoms arranged in the hexagonal structure and then wrapped around a cylinder of radius r. Let us consider a single-walled carbon nanotube, in which case only one sheet of atoms exists in the nanotube. While we understand how to model tubes of material from solid mechanics, how do we describe the mechanics of a tube such as that in Figure 8.9? The atomic structure must be accounted for in some fashion, and we show how that can be directly integrated into a continuum description next.

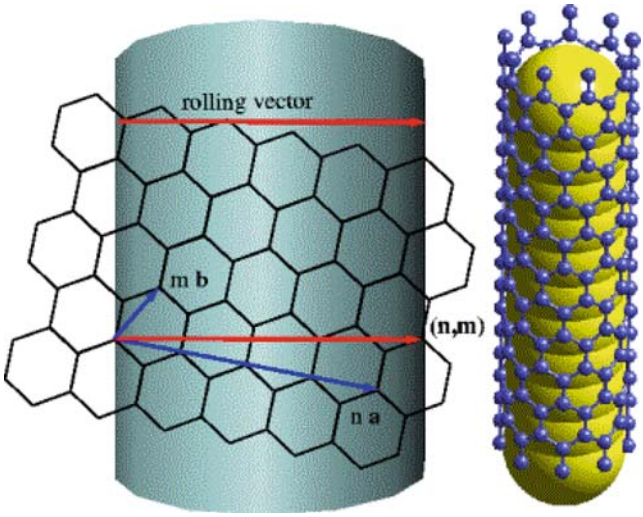

Fig. 8.9 Schematic of the structure of a carbon nanotube, viewed as a sheet of carbon atoms wrapped around a cylinder. The sheet can be arranged with various helix angles around the tube axis, which are most easily defined in terms of the number of steps in two directions along the hexagonal array required to repeat a position on the helix. Illustration by Volokh and Ramesh (2006). Reprinted from International Journal of Solids and Structures, Vol. 43, Issue 25–26, Page 19, K.Y. Volokh, K.T. Ramesh, *An approach to multi-body interactions in a continuum-atomistic context: Application to analysis of tension instability in carbon nanotubes*. Dec. 2006, with permission from Elsevier.

Since all of the atoms are carbon, the interactions between the atoms is the carbon-carbon interaction. Since carbon-carbon bonds are covalent and highly di-

rectional, a simple pair potential does not adequately describe the interaction. Tersoff (1988) and Brenner et al. (2002) developed models for carbon-carbon interactions that we will use here. Let us suppose that all of the carbon atoms in a nanotube, before deformation, are at positions $\mathbf{R}_i$. After deformation, we define the position of the ith carbon atom as $\mathbf{r}_i$, and assume that there are n atoms in the nanotube under consideration. Then Tersoff and Brenner identify the total energy of these atoms as

$$E_{total} = \frac{1}{2}\sum V(d_{ij}), \tag{8.12}$$

where d_{ij} is the distance between the ith and jth atoms, and is itself given by

$$d_{ij} = (\mathbf{r}_i - \mathbf{r}_j)\,.\,(\mathbf{r}_i - \mathbf{r}_j). \tag{8.13}$$

The pair potential $V(d_{ij})$ itself is given by

$$V(d_{ij}) = \frac{V_0}{S-1} f_c(d_{ij}) \left\{ \exp[-\sqrt{2S}\beta(d_{ij} - D_{ij})] - SB_{(ij)} \exp\, -\sqrt{\frac{2}{S}}\beta(d_{ij} - D_{ij}) \right\}, \tag{8.14}$$

where $D_{ij} = (\mathbf{R}_i - \mathbf{R}_j)\,.\,(\mathbf{R}_i - \mathbf{R}_j)$ is the initial separation between atoms, V_0 is a scaling measure, usually assumed to be 6 eV, and $S = 1.22$ where $\beta = 21\text{nm}^{-1}$. The equilibrium bond length is set to $D_{ij} = 0.145\,\text{nm}$. Equation (8.14) also contains a cut-off distance function $f_c(d_{ij})$, which ensures that the potential function only needs to be exercised over a finite distance, and yet rolls off to zero in a smooth fashion (thus retaining continuity). A typical cut-off function is

$$f_c = 1,\ d_{ij} < a_1 \tag{8.15}$$

$$= \frac{1}{2} + \frac{1}{2}\cos\frac{\pi(d_{ij} - a_1)}{a_2 - a_1},\ a_1 < d_{ij} < a_2 \tag{8.16}$$

$$= 0,\ d_{ij} < a_2, \tag{8.17}$$

with $a_1 = 0.17\,\text{nm}$ and $a_2 = 0.2\,\text{nm}$, thus including only the first-neighbor shell for each carbon atom. Equation (8.13) also contains a term written as $B_{(ij)}$, which is a common way of writing the symmetric part of B_{ij}:

$$B_{(ij)} = \frac{1}{2}(B_{ij} + B_{ji}). \tag{8.18}$$

The term B_{ij} itself represents the three-body coupling that is needed to define an angle (note two atoms define a line, while three atoms define an angle). Consider three atoms at locations $\mathbf{r}_i$, $\mathbf{r}_j$, and $\mathbf{r}_k$. We can define the vector joining the ith and jth atoms as $\mathbf{d}_{ij} = \mathbf{r}_i - \mathbf{r}_j$ and similarly we have $\mathbf{d}_{ik} = \mathbf{r}_i - \mathbf{r}_k$. Then the angle between the three atoms is given by ϕ_{ijk}, where

$$\cos\phi_{(ijk)} = \frac{\mathbf{d}_{ij}\,.\,\mathbf{d}_{ik}}{d_{ij}d_{ik}}. \tag{8.19}$$

Note the differences between the vectors and the scalars in the latter equation. Now that the angle between the three atoms is define, Tersoff-Brenner defines the three-body coupling term B_{ij} as

$$B_{(ij)} = \left[1 + \sum a_0 \left(1 + \frac{c_0}{d_0}^2 - \frac{c_0^2}{d_0^2 + 1 + \cos\phi_{ijk}^2}\right) f_c(d_{ij})\right]^{-\delta}, \tag{8.20}$$

where the various parameters are $a_0 = 0.00020813$, $c_0 = 330$, $d_0 = 3.5$, and $\delta = 0.5$. We can use this Tersoff-Brenner potential to calculate the interactions between the carbon atoms. Now that we have defined the atomistics, how can we connect the atomic positions to the continuum behavior? We do this by associating atomic positions to continuum deformations (Weiner, 1983). The initial ($\mathbf{D}_{ij} = \mathbf{R}_i - \mathbf{R}_j$) and current ($\mathbf{d}_{ij} = \mathbf{r}_i - \mathbf{r}_j$) relative positions of any two atoms are assumed to be connected to the deformation of the corresponding continuum by

$$\mathbf{d}_{ij} = \mathbf{F}\mathbf{D}_{ij}, \tag{8.21}$$

where $\mathbf{F}$ is the continuum deformation gradient tensor. This tensor is defined in continuum terms as the tensor that maps the vector $\mathbf{dX}$ between two nearby material particles in the reference configuration to the corresponding vector $\mathbf{dx}$ between the corresponding spatial positions of those particles in the current configuration:

$$\mathbf{dx} = \mathbf{F}\mathbf{dX}. \tag{8.22}$$

Here $\mathbf{x} = \chi(\mathbf{X}, t)$ is the spatial position in the current configuration of the material particle $\mathbf{X}$ in the reference configuration (see the section on kinematics in Chapter 2). In effect, we assume that the ith and jth atoms are in the vicinity of the point $\mathbf{X}$, as shown in Figure 8.10. Equation (8.21) provides a link between the atomistics and the continuum mechanics in terms of the deformations (the *Cauchy-Born* approximation), and was originally invoked for elasticity theory.

We have now connected the kinematics at the two scales, but we do not truly have a linking of scales unless we can link the corresponding energies. The key is to identify the strain energy in the continuum with the energies associated with the interatomic interactions (the bond energies) (Born and Huang, 1954). To do this, we define the potential energy density W of the continuum problem to be

$$W = W(\mathbf{E}) = \frac{1}{V_0} \sum V(d_{ij}), \tag{8.23}$$

where V_0 is the initial volume and $\mathbf{E}$ is the Green strain tensor defined by

$$\mathbf{E} = \frac{1}{2}[\mathbf{F}^T\mathbf{F} - \mathbf{I}], \tag{8.24}$$

with $\mathbf{I}$ the identity tensor. The Green strain tensor is simply the finite deformation analog of the infinitesimal strain tensor ε defined in Equation (2.28). Note that it

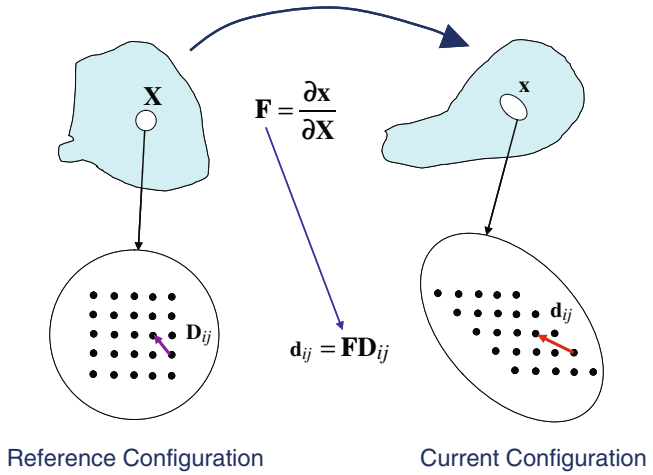

Fig. 8.10 Connection between continuum deformations and atomic positions as defined by Equation (8.21). We associate atomic positions in the two configurations with material and spatial vectors.

is not actually necessary to sum over all atoms to be able to compute the energy density function W. The sum can be replaced by an integral:

$$W(\mathbf{E}) = \frac{1}{V_0}\int V B_v dV, \tag{8.25}$$

where B_v is called the volumetric bond density function (Gao and Klein, 1998).

In terms of the atomic positions, we now have

$$\mathbf{d}_{ij} = \sqrt{\mathbf{D}_{ij} \cdot (\mathbf{I} + 2\mathbf{E})\mathbf{D}_{ij}}, \tag{8.26}$$

and the angles between the atoms are related to the Green strain tensor by

$$\cos\phi_{ijk} = \frac{\mathbf{D}_{ij} \cdot (\mathbf{I} + 2\mathbf{E})\mathbf{D}_{ij}}{d_{ij} d_{ik}}. \tag{8.27}$$

The stress tensor can then be computed as the derivative of the potential energy density through

$$\mathbf{S} = \frac{\partial W}{\partial \mathbf{E}}. \tag{8.28}$$

Note that this stress tensor is defined in the reference configuration (in mechanics terms it is called the second Piola-Kirchhoff stress tensor), but this is a refined point that is not critical to understand for the reader who does not wish to delve into the depths of the mechanics of finite deformations. The point is that the stress can be computed from the energy density, which can be computed from the interatomic potential.

The material property corresponding to the stiffness is obtained through the stiffness tensor $\mathbf{M}$:

$$\mathbf{M} = \frac{\partial \mathbf{S}}{\partial \mathbf{E}} = \frac{\partial^2 W}{\partial \mathbf{E}^2}. \tag{8.29}$$

This is the analog of the modulus of elasticity tensor (and is identical to that tensor in the linear elasticity limit). Thus we can compute the stiffness of the material at the continuum scale from the atomic positions and the interatomic potential. There are several refinements of this approach that are needed for the specific case of carbon nanotubes, because the atomic arrangements there are not those of a simple lattice. The reader is referred to the work of Huang et al. (Zhang et al., 2004) for examples of these details.

The elastic modulus of carbon nanotubes computed in this way (Zhang et al., 2002) is in fairly good agreement with that computed using MD simulations, and lies within the range of moduli measured using experimental methods. The Young's modulus predicted by Zhang et al. (2002) is $E = 705$ GPa, while Volokh and Ramesh predict $E = 1385$ GPa. These numbers fall within the range of numerous experimental (Figure 8.11) and modeling predictions (Figure 8.12) reviewed by Zhang et al. (2004). However, the assessment of the Young's modulus and stresses in the CNT is not trivial because the thickness of the CNT wall is difficult to define. The estimates of the Young's modulus given above were obtained with the assumption that the wall thickness is 0.335 nm (Zhang et al., 2002).

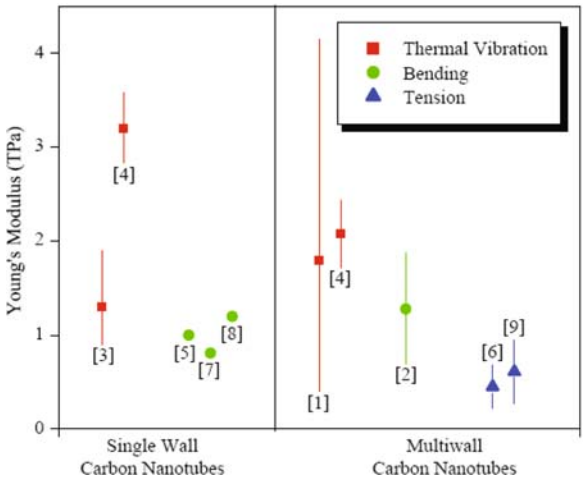

Fig. 8.11 Range of experimental measurements of the elastic modulus of carbon nanotubes, as summarized by Zhang et al. (2004). Note the theoretical predictions discussed here were 705 GPa (Zhang et al., 2002) and 1385 GPa (Volokh and Ramesh, 2006). Reprinted from Journal of the Mechanics and Physics of Solids, P. Zhang, H. Jiang, Y. Huang, P.H. Geubelle, K.C. Hwang, *An atomistic-based continuum theory for carbon nanotubes: analysis of fracture nucleation*. May 2004, with permission from Elsevier.

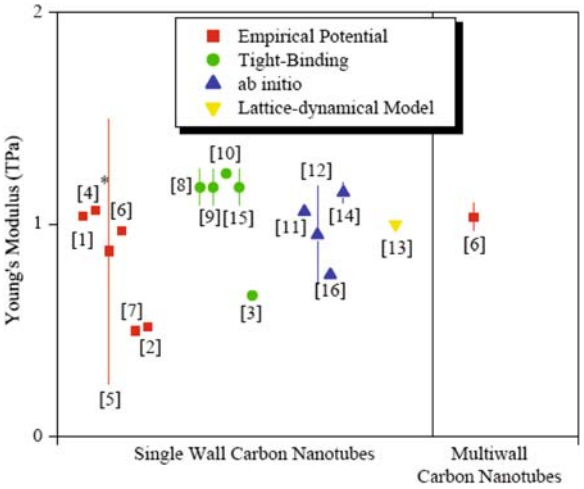

Fig. 8.12 Range of modeling estimates of the elastic modulus of carbon nanotubes, as summarized by Zhang et al. (2004), including a wide variety of first principles and MD simulations. Note the theoretical predictions discussed here were 705 GPa (Zhang et al., 2002) and 1385 GPa (Volokh and Ramesh, 2006). Reprinted from Journal of the Mechanics and Physics of Solids, P. Zhang, H. Jiang, Y. Huang, P.H. Geubelle, K.C. Hwang, *An atomistic-based continuum theory for carbon nanotubes: analysis of fracture nucleation*. May 2004, with permission from Elsevier.

It is also possible to use this mixed atomistic and continuum approach to estimate the likely failure strength of a carbon nanotube, using bifurcation analyses (Zhang et al., 2004; Volokh and Ramesh, 2006. As an example of the utility of such approaches, consider the results of Volokh and Ramesh (2006). These authors incorporate a physically distinct approach to handling the multi-body interactions needed to model carbon nanotube and similar systems, accounting for bond stretching and bond bending separately, but the scaling approach remains essentially that discussed above. They predict the onset of tensile instability in carbon nanotubes to occur at 21–25% Green strain (the theory predicts the onset of instability, rather than the final failure strain, which is the more easily measured quantity in experiments). Using observations within a TEM, Troiani et al. (2003) reported that they observed 50% elongation of the single-walled nanotubes before failure.

Some comparison with the experiments performed by Yu et al., (2000b) on multiwalled CNTs is also possible. These authors measured the critical strain to be between 10% and 14% experimentally on these multiwalled CNTs. The theoretical analysis of Volokh and Ramesh estimated the critical strains to be 21% for single-wall zigzag CNT and 25% for single-wall armchair CNT (these are two possible types of carbon nanotubes). Assuming that the addition of the wall layers leads to the stiffening of the CNT, the results of the theoretical analysis seem reasonable, because the critical strains would be expected to decrease and the critical stresses are expected to increase with CNT stiffening.

There is one additional caveat when comparing the results of such theoretical predictions with experimental measurements. Idealized and perfect nanostructures are assumed in the analyses, while real imperfect nanostructures are tested in practice. It is extremely difficult to develop defect-free nanotubes, and this is a particular problem when the tensile instability will be modulated by the defects (defects should trigger earlier onset of instabilities). The single SWCNT tests of Troiani et al. (2003) appear to be close to defect-free structures, and they appear to show the largest failure strains (note that these are failure strains, not the onset of the instability, which is what is predicted by this theoretical analysis). Other experiments have generally shown a wide range of failure strains (Yu, 2004), typically significantly smaller, but these are typically in less-clean structures. The presence of atomic defects can disturb the results of the measurements. Inclusion of the atomic imperfections in the theoretical models is of interest, but this is difficult to do.

Finally, note that theoretical predictions made using bifurcation analysis can also predict the bifurcation mode (like the buckling mode). Symmetric bifurcations are typical of rod necking (necking along the axis) while asymmetric bifurcations are typical of shell buckling (buckling of the wall of the nanotube). Volokh and Ramesh predict, for example, that ideally perfect armchair nanotubes are shell-like in terms of failure mode, while zigzag nanotubes are rod-like in failure mode. Such predictions have not yet been examined in experiments.

8.8 Strain Gradient Plasticity

Another approach to enriching continuum theories to account for subscale phenomena is to include explicitly a length scale in the continuum model. The most common way in which this is done is through *strain gradient* theories. Such theories have typically been developed to model size effects in mechanics, rather than specifically for nanomaterials, but the issues are related.

Many experiments, mainly from microindentation and nanoindentation, e.g., Nix and Gao (1998), have shown that materials display strong size effects when the characteristic length scale associated with non-uniform plastic deformation is in the range of a micron or less, and these effects are believed to result from intrinsic length scales in the materials studied. Classical plasticity theories do not have an intrinsic material length scale and thus fail to capture this strong size dependency of material behaviors. Several strain gradient plasticity theories have been proposed to address this problem. As an example, a strain gradient plasticity theory based on dislocation theory was introduced by Gao et al. (1999) and Huang et al. (2000), and is briefly discussed here.

An intrinsic length scale can be defined in materials through the concept of geometrically necessary dislocations (Ashby, 1970). The idea is that some of the dislocations in a material exist in the structure only to accommodate certain misfits, i.e., they are geometrically necessary in order to maintain compatibility (consider, for example, the misfit strains produced by a hard particle in a soft matrix when the

assembly is deformed plastically). These misfits amount to gradients in the plastic strain, and hence the term strain gradient. The total dislocation density in a material is then the sum of two components, called the statistically stored dislocations and the geometrically necessary dislocations:

$$\rho = \rho_S + \rho_G. \tag{8.30}$$

In this light, the Taylor relation between the shear strength τ and the total dislocation density in a material becomes

$$\tau = \alpha \mu b \sqrt{\rho_S + \rho_G}, \tag{8.31}$$

where $\alpha \approx 0.3$. From the Taylor relation, Gao et al. (1999) then derive a constitutive function that contains an internal length scale:

$$\sigma = \sigma_y \sqrt{f^2(\varepsilon) + l_g \eta}, \tag{8.32}$$

where σ_y is the yield stress, η is the effective plastic strain gradient, l_g is an intrinsic material length, and $\sigma = \bar{M}\tau$ is the effective stress, with $\bar{M}$ the Taylor factor or the ratio of tensile flow stress to shear flow stress (for polycrystalline FCC materials $\bar{M} \approx 3$ (Bishop and Hill, 1951a,b). The function $f(\varepsilon)$ is a plastic strain-hardening function. In the absence of a strain gradient ($\eta = 0$ so that $\rho_G = 0$), the density of statistically stored dislocations ρ_S can be expressed in terms of the strain hardening function:

$$\rho_S = \frac{\sigma_y (f(\varepsilon) - 1)^2}{\bar{M} \alpha \mu b^2}. \tag{8.33}$$

Geometrically necessary dislocations appear in the strain gradient field for compatible deformation. The relation between the density of geometrically necessary dislocations ρ_G and the effective plastic strain gradient η is

$$\rho_G = \frac{\lambda \eta}{b}, \tag{8.34}$$

where λ is Nye's factor (in polycrystalline FCC materials, $\lambda = 1.85$ for torsion, and $\lambda = 1.93$ for bending). Using Equation (8.34) in Equation (8.31), one obtains the intrinsic material length as

$$l_g = \frac{\bar{M} \alpha \mu^2}{\sigma_y^2} \lambda b. \tag{8.35}$$

For example, for polycrystalline FCC metals in bending this material length scale would be $l_g = 18\alpha^2 b \frac{\mu^2}{\sigma_y^2} \lambda b$. For non-uniform plastic deformations, the effects of plastic strain gradient are important when the characteristic length associated with the deformation becomes comparable to the intrinsic material length l_g. For most structural engineering materials, the intrinsic material length is on the order of mi-

crons, but for very pure annealed metals, it could be an order of magnitude larger. Using this as a basis, Gao et al. (1999) and Huang et al. (2000) proposed a multiscale approach to construct the constitutive laws, the equilibrium equations and the boundary conditions for strain gradient plasticity.

The presence of this length scale in strain gradient theories allows one to describe size effects in macroscopic behavior, such as the indentation size effect (smaller indentations appear to make the material seem harder) and particle-size effects in composites. An example of the application of strain gradient plasticity theory to nanocrystalline materials is presented by Gurtin and Anand (2008).

8.9 Multiscale Modeling

A number of multiscale modeling approaches have been developed that seek explicitly to couple atomistic and continuum models. Broadly speaking, these multiscale methods are classified in two ways: as hierarchical approaches or as concurrent approaches. In hierarchical approaches, measures from simulations at one scale are passed on to simulations at other scales, and most of the models that we have discussed so far are of this type (these are also called approaches to *coarse-graining* or *fine-graining*). In concurrent approaches, multiple length scales are simultaneously simulated, with different spatial resolutions in different regions of the body, and with some well-defined approach to hand off the scale-appropriate variables to each scale in each region. Entire books are devoted to these techniques, e.g., Liu et al. (2006) and we cannot usefully discuss them here. One particular approach, however, is mentioned because it has grown rapidly in usage in recent years and is relatively easily used with traditional finite element methods. This technique is called the Quasi-Continuum (QC) method and was developed in a series of papers by Tadmor et al. (1996) and Shenoy et al. (1999). The method links the atomistic and continuum scales through the finite element method, and therefore is able to utilize much of the expertise associated with computational mechanics. A review of the method is presented by Miller and Tadmor (2002) and there is an associated website www.qcmethod.com that acts as a clearing house for related research.

Examples of the use of this method for nanocrystalline materials are provided by Sansoz and Molinari (2005) and Warner et al. (2006). In a multiscale simulation of the deformation of nanocrystalline copper, Warner et al. (2006) use the quasicontinuum method to determine the properties of a suite of grain boundaries of various types (Figure 8.13). These results are used to develop constitutive equations for grain boundaries, and then these grain boundary properties are incorporated into a simulation of a collection of polycrystals (Figure 8.14) with a range of grain boundaries. These are therefore hierarchical multiscale simulations.

Based on these computations, Warner et al. (2006) predict the strength of nanocrystalline copper as a function of grain size, and compare their results (Figure 8.15)

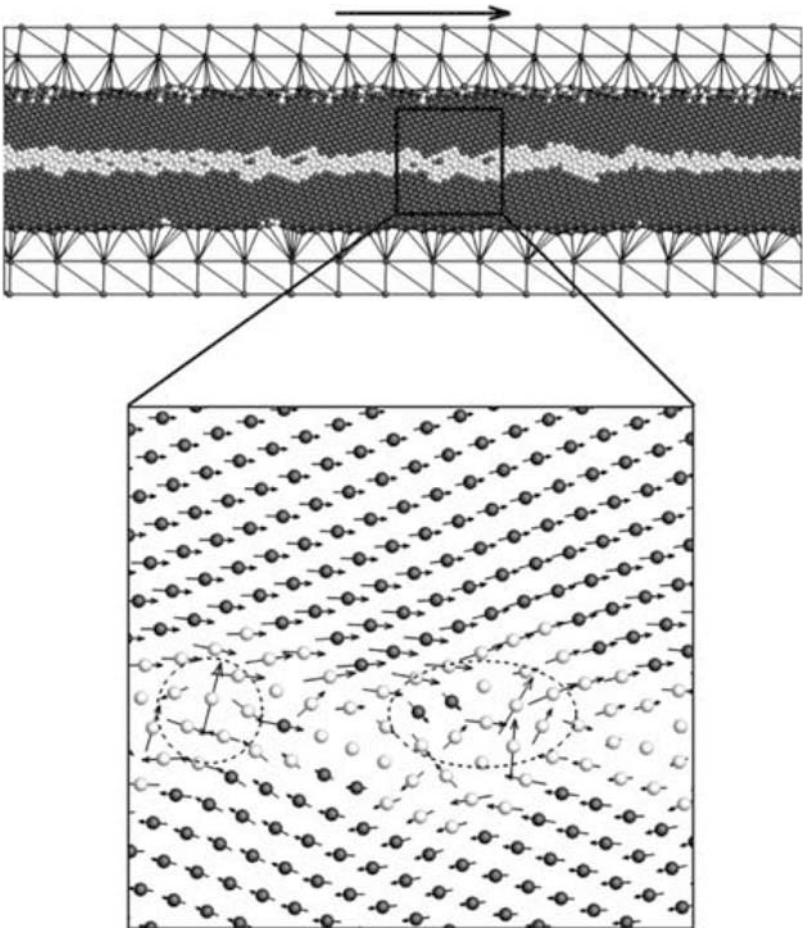

Fig. 8.13 Simulation of a copper grain boundary by Warner et al. (2006) using the quasicontinuum method. The *arrows* correspond to the displacement of each atom between two loading steps. Reprinted from International Journal of Plasticity, Vol. 22, Issue 4, Page 21, D.H. Warner, F. Sansoz, J.F. Molinari, *Atomistic based continuum investigation of plastic deformation in nanocrystalline copper*. April 2006, with permission from Elsevier.

with the results of MD simulations and the available experimental data. This comparison is fairly typical for nanocrystalline materials.

Note the molecular dynamics simulations predict much higher stresses than are observed in experiments. The finite element simulations also predict higher stresses than the experiments, but these are closer in magnitude to the observed behavior. The higher stresses that are derived in both kinds of simulations are partly because of the number of mechanisms that exist in the real world but that are not accounted for in the simulations due to issues regarding length scale and time scale (for example, diffusion and grain boundary migration). In addition, the simulations inevitably

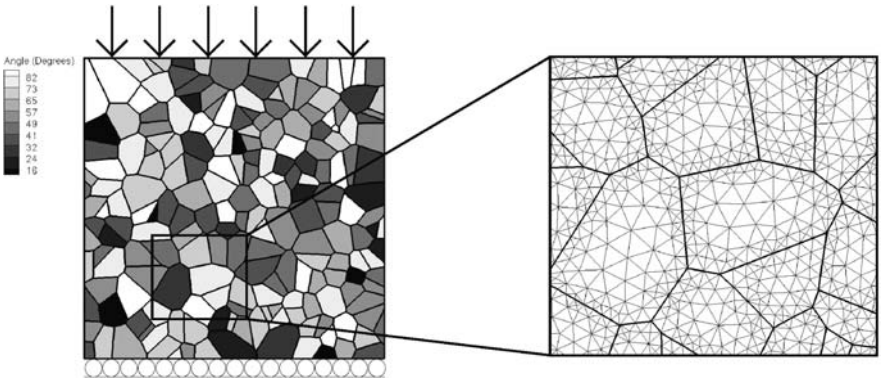

Fig. 8.14 Computational approach for simulations of nanocrystalline copper by Warner et al. (2006). The *grayscale* represents different orientations of the crystals. Reprinted from International Journal of Plasticity, Vol. 22, Issue 4, Page 21, D.H. Warner, F. Sansoz, J.F. Molinari, *Atomistic based continuum investigation of plastic deformation in nanocrystalline copper*. April 2006, with permission from Elsevier.

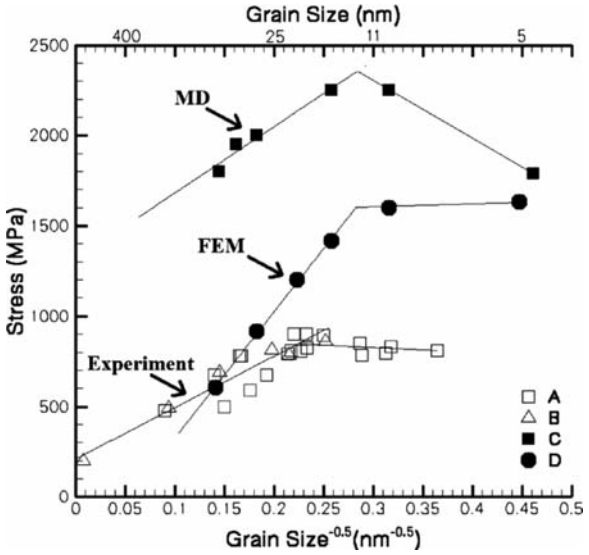

Fig. 8.15 Comparison of the predictions of the multiscale simulations of Warner et al. (2006) (identified with the *FEM symbol*) with molecular dynamics (MD) simulation results and experimental data on nanocrystalline copper. Note that the experimental results are derived from hardness measurements, while the FEM simulation results correspond to a 0.2% proof strength. Both MD and FEM simulations predict much higher strengths than are observed in the experiments. Reprinted from International Journal of Plasticity, Vol. 22, Issue 4, Page 21, D.H. Warner, F. Sansoz, J.F. Molinari, *Atomistic based continuum investigation of plastic deformation in nanocrystalline copper*. April 2006, with permission from Elsevier.

have limitations that arise from the assumptions made to render the problem computationally tractable. For example, the Warner et al. finite element simulations are 2D plane strain, and these authors point out that the fraction of grain boundary material is substantially lower in 2D simulations. Although the magnitudes of the stresses are very different, all of the simulations and the experiments indicate that the grain-size driven strengthening eventually saturates or even turns into a softening. These modeling results are consistent with the general observation of deviations from Hall-Petch behavior at small grain sizes that was discussed earlier.

8.10 Constitutive Functions for Bulk Nanomaterials

Now finally returning to the full continuum scale, we recognize that the solutions of problems in the mechanics of nanomaterials require the specification of full constitutive equations for these materials. These constitutive equations must be defined with parameters that can be determined either through experiments or through subscale or multiscale simulations (a sophisticated constitutive function that cannot have its parameters determined in some way will never be used). In some cases, the traditional definition of a constitutive equation may no longer be appropriate, and the nanomaterial may be better treated as a structure than as a material (for example, the behavior of a carbon nanotube used as an AFM tip). In other cases, the constitutive equation may need to be enriched by the addition of an internal length scale, or through the incorporation of an internal variable that has an independent evolution equation determined by subscale physics (e.g., the influence of grain rotation on the behavior of bulk nanocrystalline solids). In still other cases, almost entirely limited to bulk nanocrystalline materials, the traditional mechanics constitutive equations of elasticity, plasticity and fracture are all that are needed (with perhaps the additional considerations of viscoelasticity, creep or superplasticity).

8.10.1 Elasticity

The elasticity of bulk nanocrystalline materials is very similar to that of their coarse-grained cousins, with two caveats. First, the nanocrystalline material may have different anisotropy, as discussed in Chapter 4 on density and the elastic properties, because of the grain structure and perhaps orientation. Second, the nanocrystalline solid will typically have lower moduli, again as discussed in that chapter. From an experimental viewpoint, the stiffnesses of nanomaterials are dominated by the specifics of the processing route used to create the material, since defect populations, grain sizes, grain orientations, and grain size distributions are all controlled by the processing.

8.10.2 Yield Surfaces

Specifying the plastic response of nanomaterials requires first a specification of the yield behavior. In earlier chapters we have discussed the effects of grain size on the yield strength. However, most nanocrystalline materials do not behave the same in tension and compression, and therefore the traditional Mises yield surface cannot be used to specify the onset of yield.

Consider, for example, the case of nanocrystalline nickel. Nanocrystalline Ni pillars were studied through the microcompression of 20 μm diameter posts by Schuster et al. (2006). Since there are about a million grains across the cross section and about a billion grains in each post, this technique provides the effective response of the bulk material. An MTS Nanoindenter XP with the Continuous Stiffness Measurement extension was used with a truncated Berkovich indenter to apply the compressive load at a strain rate of $10^{-3}s^{-1}$. Following the method proposed by Zhang et al. (2006) , the pillar compliance was corrected for the effect of the elastic base and the corresponding stress and strain measures were corrected. The nano-Ni specimens showed very consistent compressive behavior. The compressive yield strength at 0.2% offset was an average of 1210 ± 20 MPa (σ_C).

The identical batch of material was also examined by Wang et al. (2004). They report a flow strength (at 3.5% strain) of 1260 MPa in tension (σ_T). The microcompression results show a compressive flow strength (σ_C) at 3.5% strain of 1460 MPa, 16% higher than Wang's tensile values. Therefore, the Mises yield surface is not appropriate for this material, because that yield surface assumes identical behavior in tension and compression. In this case, the compression-tension asymmetry is $\frac{\sigma_C}{\sigma_T} = 1.16$ (note that we compare the flow strengths at a given strain rather than yield due to general uncertainties in measuring initial yield). As an example of the differences between testing techniques for estimating strength, one obtains $\frac{\sigma_{Ch}}{\sigma_T} = 1.5$ if the compressive strength (σ_{Ch}) is estimated using the approximation that $H \approx 3\sigma_{Ch}$ and using Wang's measured microhardness.

Why is there a tension-compression asymmetry in nanomaterials? Cheng et al. (2003) addressed compression-tension asymmetry using a strength model based on dislocation emission from grain boundary sources for various regimes of grain size, and relating the uniaxial strength of materials to the self energy of a dislocation under pressure. Lund and Schuh (2005) addressed compression-tension asymmetry across a broad range of grain sizes using MD simulations and analysis. Jiang and Weng (2003) present analytical solutions for Cu using a weighted average of a crystalline phase (with grain size dependent mechanical properties) and an amorphous grain boundary (with size independent properties). In these analyses, the volume fraction of the grain boundaries increases with decreasing grain size and thereby affects the overall response. For example, the analysis applied to Cu shows increasing compression-tension asymmetry with decreasing grain size. The results on nanocrystalline nickel obtained from microcompression and comparison with the data of Wang et al. closely match the predictions of Jiang and Weng of the

compression-tension asymmetry (≈ 1.2) for Cu at a similar grain size. However, high-resolution electron microscopy of the nickel does not show the presence of an amorphous phase at the grain boundary.

Given this compression-tension asymmetry, what would be a reasonable yield surface? One simple yield surface that can incorporate separate tensile and compressive behaviors is the Mises-Schleicher yield surface, defined by

$$f(\sigma) = \bar{\sigma}^2 + (\sigma_C - \sigma_T)\sigma_{kk} - \sigma_C\sigma_T = 0, \tag{8.36}$$

where $\bar{\sigma}$ is the effective stress defined by Equation (2.115) and the yield function $f(\sigma)$ was first discussed in the paragraphs following Equation (2.96). The Mises-Schleicher yield criterion takes into account the difference between yield strengths in tension and compression as well as the effect of the hydrostatic stress σ_{kk}. In the special case that $\sigma_C = \sigma_T$, Equation 8.36 reduces to the traditional von Mises yield criterion (Equation 2.114).

Unfortunately, there is not enough data in other multiaxial states (e.g., in torsion) to be able to determine a full yield surface at this point, and so we cannot state that the Mises-Schleicher yield criterion is the appropriate one for nanocrystalline nickel. This is an area where additional experimentation is sorely needed in other stress states, but these are difficult to come by (in part because of the paucity of bulk nanocrystalline materials). Some suggestions for yield surfaces come from simulations, but these are still too heavily constrained to be relied upon for engineering purposes with respect to yield (remembering that the simulations are typically nonconservative, predicting unrealistically high stresses).

8.11 Closing

This chapter has discussed a wide range of modeling approaches to the problem of the mechanics of nanomaterials, but the reader should recognize that this is a field in explosive growth, and much continues to be done to push the boundaries of our modeling capabilities. Certainly much remains to be done. We are not at the point, as of this writing, where we can identify specific constitutive laws for nanocrystalline materials, or specify with certainty that one particular material, made in a particular way, is better than another for a specific engineering application. We do have excellent measures of strength, however, and these indicate great promise.

It appears clear that dramatic progress in nanomaterials can be made through a coordinated effort involving processing research (for improving consistency of materials and reducing defect populations), sophisticated modeling (to tell the producers what is worth making and where it is best to commit effort and investment) and mechanical and materials characterization experiments over a wide range of length and time scales (to determine true material behavior, remembering that our intuition is not reliable over this range of scales).

8.12 Suggestions for Further Reading

1. Phillips, R.W. (2001). Crystals, Defects and Microstructures, Cambridge University Press, Cambridge.
2. Weiner, J.H. (1983). Statistical Mechanics of Elasticity. Wiley, New York.
3. Rapaport, D.C. (2004). The Art and Science of Molecular Dynamics Simulation. Cambridge University Press, Cambridge.
4. Liu, W.K., E.G. Karpov, et al. (2004). An introduction to computational nanomechanics and materials. Computational Methods in Applied Mechanics and Engineering 193: 1529–1578.
5. Curtin, W.A. and R.E. Miller (2003). Atomistic/continuum coupling in computational materials science. Modeling and Simulation in Materials Sciences and Engineering 11: R33–R68.
6. Van Swygenhoven, H. and J.R. Weertman (2006). Deformation in nanocrystalline metals. Materials Today 9(5): 24–31.
7. Liu, W.K., E.G. Karpov, et al. (2006). Nano Mechanics and Materials: Theory, Multiscale Methods and Applications. Wiley, New York.

8.13 Problems and Directions for Future Research

1. Consider the development of a molecular dynamics simulation of the simple tension problem (using, for example, LAMMPS) for a single crystal of an fcc metal – say nickel – loaded at a constant high strain rate. Find an EAM potential for nickel in the literature, and implement the parameters in your MD code. Decide what temperature you are going to use for your simulations. Next, choose which orientation, e.g., [110] to use for the tensile loading axis. Determine what simulation size you can manage with your computing system. How will you make this simulation sample representative of the larger experimental sample? Can you use periodic boundary conditions? If you do, how will the traction boundary conditions be implemented (tensile strain rate imposed along the long axis, traction-free along the sides)? What does a traction-free boundary mean for a collection of atoms?
   Construct the single crystal sample for your simulation, and ensure that you have relaxed your structure. Determine the meaning of the following terms for your simulation: thermostat and barostat. How will you impose the constant strain rate loading that you would like to apply? Which atoms will have imposed velocities? Compute the stress histories that you obtain from your simulations. How are these stresses defined? What are virial stresses? What is the volume over which you average to obtain the stresses? Do you average over a number of timesteps as well as a volume? If so, how do you decide how many timesteps to average over to compute the stress state? Did you achieve your desired uniaxial tensile stress state, and if not, what is the magnitude of the error?

What are your choices for visualizing the atomic motions? Can you distinguish atoms that are in irregular lattice positions (such as around dislocation cores)?

2. A common assumption in dislocation dynamics codes is that the force on the dislocation is proportional to the dislocation velocity (the so-called dislocation drag regime, see Figure 5.19). Using the Orowan equation (Equation 5.31) and Figure 5.19, compute the plastic strain rate at which this becomes a reasonable assumption in a metal such as lead. Note that the typical mobile dislocation density in a metal is in the range of 10^{13}–10^{15} m^{--2}. 3. Find a downloadable crystal plasticity code that you can use in conjunction with a finite element program. A common example is a "user-material subroutine" or UMAT for use in conjunction with the commercial finite element software known as ABAQUS (Simulia) and written by Huang & Kysar. Use this code to simulate the deformation of a microcompression pillar (see Chapter 3) of copper. You will need to obtain some properties for the slip systems and hardening rates in the copper from the literature.

References

Ashby, M. (1970). Deformation of plastically non-homogeneous materials. *Philosophical Magazine 21*(170), 399.

Bishop, J. F. W. and R. Hill (1951a). A theoretical derivation of the plastic properties of a polycrystalline face-centred metal. *Philosophical Magazine 42*(334), 1298–1307.

Bishop, J. F. W. and R. Hill (1951b). A theory of the plastic distortion of a polycrystalline aggregate under combined stresses. *Philosophical Magazine 42*(327), 414–427.

Born, M. and K. Huang (1954). *Dynamical Theory of the Crystal Lattices*. Oxford: Oxford University Press.

Brenner, D. W., O. A. Shenderova, J. A. Harrison, S. J. Stuart, B. Ni, and S. B. Sinnott (2002). A second-generation reactive empirical bond order (rebo) potential energy expression for hydrocarbons. *Journal of Physics-Condensed Matter 14*(4), 783–802.

Chen, M. W., E. Ma, K. J. Hemker, H. W. Sheng, Y. M. Wang, and X. M. Cheng (2003a). Deformation twinning in nanocrystalline aluminum. *Science 300*(5623), 1275–1277.

Cheng, S., J. A. Spencer, and W. W. Milligan (2003b). Strength and tension/compression asymmetry in nanostructured and ultrafine-grain metals. *Acta Materialia 51*(15), 4505–4518.

Daw, M. S. and M. I. Baskes (1984). Embedded-atom method - derivation and application to impurities, surfaces, and other defects in metals. *Physical Review B 29*(12), 6443–6453. ISI Document Delivery No.: SX735 Times Cited: 2262 Cited Reference Count: 69.

Derlet, P. M., H. Van Swygenhoven, and A. Hasnaoui (2003). Atomistic simulation of dislocation emission in nanosized grain boundaries. *Philosophical Magazine 83*(31–34), 3569–3575. Sp. Iss. SI.

Farkas, D. and W. A. Curtin (2005). Plastic deformation mechanisms in nanocrystalline columnar grain structures. *Materials Science and Engineering a-Structural Materials Properties Microstructure and Processing 412*(1–2), 316–322. Sp. Iss. SI.

Gao, H., Y. Huang, W. D. Nix, and J. W. Hutchinson (1999). Mechanism-based strain gradient plasticity - i. theory. *Journal of the Mechanics and Physics of Solids 47*(6), 1239–1263.

Gao, H. and P. Klein (1998). Numerical simulation of crack growth in an isotropic solid with randomized internal cohesive bonds. *Journal of the Mechanics and Physics of Solids 46*, 187–218.

Gurtin, M. E. and L. Anand (2008). Nanocrystalline grain boundaries that slip and separate: A gradient theory that accounts for grain-boundary stress and conditions at a triple-junction. *Journal of the Mechanics and Physics of Solids 56*(1), 184–199.

Hirth, J. and J. Lothe (1992). *Theory of Dislocations* (Second ed.). Malabar, FL: Krieger.

Huang, Y., H. Gao, W. D. Nix, and J. W. Hutchinson (2000). Mechanism-based strain gradient plasticity - ii. analysis. *Journal of the Mechanics and Physics of Solids 48*(1), 99–128.

Jiang, B. and G. J. Weng (2003). A composite model for the grain-size dependence of yield stress of nanograined materials. *Metallurgical and Materials Transactions a-Physical Metallurgy and Materials Science 34A*(3), 765–772.

Kraft, R. H., J. F. Molinari, K. T. Ramesh, and D. H. Warner (2008). Computational micromechanics of dynamic compressive loading of a brittle polycrystalline material using a distribution of grain boundary properties. *Journal of the Mechanics and Physics of Solids 56*(8), 2618–2641.

Kumar, S. and W. A. Curtin (2007). Crack interaction with microstructure. *Materials Today 10*(9), 34–44.

Liu, W., E. Karpov, and H. Park (2006). *Nano Mechanics and Materials: Theory, Multiscale Methods and Applications*. New York: Wiley.

Liu, W., E. Karpov, S. Zhang, and H. Park (2004). An introduction to computational nanomechanics and materials. *Computational Methods in Applied Mechanics and Engineering 193*, 1529–1578.

Lund, A. C. and C. A. Schuh (2005). Strength asymmetry in nanocrystalline metals under multiaxial loading. *Acta Materialia 53*(11), 3193–3205.

Miller, R. E. and E. B. Tadmor (2002). The quasicontinuum method: Overview, applications and current directions. *Journal of Computer-Aided Materials Design 9*(3), 203–239.

Mishin, Y., D. Farkas, M. J. Mehl, and D. A. Papaconstantopoulos (1999). Interatomic potentials for monoatomic metals from experimental data and ab initio calculations. *Physical Review B 59*(5), 3393–3407.

Nix, W. D. and H. J. Gao (1998). Indentation size effects in crystalline materials: A law for strain gradient plasticity. *Journal of the Mechanics and Physics of Solids 46*(3), 411–425.

Noronha, S. J. and D. Farkas (2002). Dislocation pinning effects on fracture behavior: Atomistic and dislocation dynamics simulations. *Physical Review B 66*(13).

Noronha, S. J. and D. Farkas (2004). Effect of dislocation blocking on fracture behavior of al and alpha-fe: a multiscale study. *Materials Science and Engineering a-Structural Materials Properties Microstructure and Processing 365*(1–2), 156–165.

Phillips, R. (2001). *Crystals, Defects and Microstructures*. Cambridge: Cambridge University Press.

Rapaport, D. C. (2004). *The Art and Science of Molecular Dynamics Simulation*. Cambridge: Cambridge University Press.

Sansoz, F. and J. F. Molinari (2005). Mechanical behavior of sigma tilt grain boundaries in nanoscale cu and al: A quasicontinuum study. *Acta Materialia 53*(7), 1931–1944.

Schiotz, J. and K. W. Jacobsen (2003). A maximum in the strength of nanocrystalline copper. *Science 301*(5638), 1357–1359.

Schuster, B. E., Q. Wei, H. Zhang, and K. T. Ramesh (2006). Microcompression of nanocrystalline nickel. *Applied Physics Letters 88*(10).

Shenoy, V. B., R. Miller, E. B. Tadmor, D. Rodney, R. Phillips, and M. Ortiz (1999). An adaptive finite element approach to atomic-scale mechanics - the quasicontinuum method. *Journal of the Mechanics and Physics of Solids 47*(3), 611–642.

Tadmor, E. B., M. Ortiz, and R. Phillips (1996). Quasicontinuum analysis of defects in solids. *Philosophical Magazine a-Physics of Condensed Matter Structure Defects and Mechanical Properties 73*(6), 1529–1563.

Tersoff, J. (1988). New empirical-approach for the structure and energy of covalent systems. *Physical Review B 37*(12), 6991–7000.

Troiani, H., M. Miki-Yoshida, G. Camacho-Bragado, M. Marques, A. Rubio, J. Ascencio, and M. Jose-Yacaman (2003). Direct observation of the mechanical properties of single-walled carbon nanotubes and their junctions at the atomic level. *Nanoletters 3*(6), 751–755.

Van Swygenhoven, H. and J. R. Weertman (2006). Deformation in nanocrystalline metals. *Materials Today 9*(5), 24–31.

Volokh, K. Y. and K. T. Ramesh (2006). An approach to multi-body interactions in a continuum-atomistic context: Application to analysis of tension instability in carbon nanotubes. *International Journal of Solids and Structures 43*(25–26), 7609–7627.

Wang, Y. M., S. Cheng, Q. M. Wei, E. Ma, T. G. Nieh, and A. Hamza (2004). Effects of annealing and impurities on tensile properties of electrodeposited nanocrystalline ni. *Scripta Materialia 51*(11), 1023–1028.

Warner, D. H., F. Sansoz, and J. F. Molinari (2006). Atomistic based continuum investigation of plastic deformation in nanocrystalline copper. *International Journal of Plasticity 22*(4), 754–774.

Wei, Y. J., C. Su, and L. Anand (2006). A computational study of the mechanical behavior of nanocrystalline fcc metals. *Acta Materialia 54*(12), 3177–3190.

Weiner, J. (1983). *Statistical Mechanics of Elasticity*. New York: Wiley.

Yamakov, V., D. Wolf, M. Salazar, S. R. Phillpot, and H. Gleiter (2001). Length-scale effects in the nucleation of extended dislocations in nanocrystalline al by molecular-dynamics simulation. *Acta Materialia 49*(14), 2713–2722.

Yu, M. F. (2004). Fundamental mechanical properties of carbon nanotubes: Current understanding and the related experimental studies. *Journal of Engineering Materials and Technology-Transactions of the Asme 126*(3), 271–278.

Yu, M. F., O. Lourie, M. J. Dyer, K. Moloni, T. F. Kelly, and R. S. Ruoff (2000b). Strength and breaking mechanism of multiwalled carbon nanotubes under tensile load. *Science 287*(5453), 637–640.

Zhang, H., B. E. Schuster, Q. Wei, and K. T. Ramesh (2006). The design of accurate micro-compression experiments. *Scripta Materialia 54*(2), 181–186.

Zhang, P., Y. Huang, P. H. Geubelle, P. A. Klein, and K. C. Hwang (2002). The elastic modulus of single-wall carbon nanotubes: a continuum analysis incorporating interatomic potentials. *International Journal Of Solids And Structures 39*(13–14), 3893–3906.

Zhang, P., H. Jiang, Y. Huang, P. H. Geubelle, and K. C. Hwang (2004). An atomistic-based continuum theory for carbon nanotubes: analysis of fracture nucleation. *Journal of the Mechanics and Physics of Solids 52*(5), 977–998.

Index

R

S

T